UNIVERSIDADE DO ALGARVE

Radio frequency system for remote fish monitoring in aquaculture

Tiago João Barbosa de Almeida

Dissertação

Mestrado Integrado em Engenharia Eletrónica e Telecomunicações

Trabalho efetuado sob a orientação de:

Prof. Doutor Henrique Leonel Gomes

2017

UNIVERSIDADE DO ALGARVE

Radio frequency system for remote fish monitoring in aquaculture

Tiago João Barbosa de Almeida

Dissertação

Mestrado Integrado em Engenharia Eletrónica e Telecomunicações

Trabalho efetuado sob a orientação de:

Prof. Doutor Henrique Leonel Gomes

2017

Radio frequency system for remote fish monitoring in aquaculture

Declaração de autoria de trabalho

Declaro ser o(a) autor(a) deste trabalho, que é original e inédito. Autores e trabalhos consultados estão devidamente citados no texto e constam da listagem de referências incluída.

Assinatura do candidato:_____

Agradecimentos

Eu não poderia deixar de começar por apresentar uma palavra de agradecimento às pessoas que, de forma direta ou indireta, contribuíram para o sucesso da minha dissertação. O trabalho realizado insere-se no projeto europeu *AquaExcell* 2020, que é coordenado na Universidade do Algarve pelo Prof. Adelino Canário. O trabalho realizado nesta tese insere-se especificamente na work-package 8, coordenada pelo grupo do Prof. Juan A. Montiel-Nelson do *Institute for Applied Microelectronics/EE&A, Dept. University of Las Palmas de Gran Canaria*, em Espanha.

Agradeço ao Prof. Dr. Henrique Leonel Gomes, pela oportunidade e orientação da elaboração deste trabalho que foi bastante aliciante e desafiador para mim, pondo bastante à prova as minhas capacidades de resolver problemas, indo à procura de soluções e também usando os conhecimentos que fui aprendendo ao longo do curso e também da vida. Obrigado ao Prof. Adelino Canário pela cedência do laboratório associado Centro de Ciências do Mar (CCMAR) e ao Prof. Henrique Gomes ela cedência do laboratório de Eletrónica Orgânica (Instituto de Telecomunicações) para o desenvolvimento do trabalho. Também não poderia deixar de agradecer ao Dr. Peter Hubbard pela ajuda durante os testes experimentais e ao Dr. João Reis que gentilmente cedeu o aquário usado nestes testes e ao Prof. Adelino Canário que tornou possível a realização deste trabalho.

Agradeço também aos meus colegas e também amigos da universidade pelos bons momentos proporcionados, pela amizade, força e ajuda durante o longo período que passei na universidade. Um especial obrigado ao Hélder Simões e Aldric Négrier pelo apoio constante e ajuda durante o desenvolvimento dos projetos que tinha de fazer. Sem a ajuda de todos, nada disto seria possível.

Por fim, devo agradecer aos meus pais, familiares e amigos externos à universidade que me apoiaram ao longo da minha carreira académica. Embora não saibam como me poderiam ajudar dentro da universidade, deram-me sempre força e motivação para continuar em frente para chegar a estar prestes a terminar este curso universitário.

A todos, um enorme obrigado.

Resumo

A produção de peixes em aquacultura tem vindo a crescer exponencialmente. Atualmente, aproximadamente 50% do peixe consumido é produzido mundialmente em aquacultura. Com o objetivo de maximizar o rendimento de produção de peixe, são usadas densidades populacionais relativamente elevadas em espaços confinados. As condições de produção de peixe obrigam a ter um conjunto de preocupações com a saúde e bem-estar dos peixes por razões económicas e éticas.

Em ambientes de aquacultura, é importante medir parâmetros que possam indiciar o desenvolvimento de alterações no estado de saúde dos peixes, sendo crucial para tomar medidas preventivas e impedir a propagação de doenças. Um dos indicadores mais relevantes que afeta a saúde do peixe é o *stress*. Quando submetidos a um *stress* prolongado, os peixes acabam por ficar suscetíveis a doenças, que se podem propagar rapidamente por toda a população com consequências catastróficas. É possível avaliar se um peixe está em estado de *stress* através de um conjunto de alterações fisiológicas e comportamentais, como por exemplo o aumento da hormona cortisol no sangue ou o aumento do batimento cardíaco.

O objetivo do nosso projeto é desenvolver um sistema de monitorização capaz de detetar, em tempo real, as alterações fisiológicas ou comportamentais indicadoras de *stress*. O sistema implementado é constituído por um sensor ou vários sensores colocados no peixe a nadar livremente no tanque. Os dados recolhidos são então enviados por um sistema de transmissão de dados sem fios, através de ondas rádio, para uma estação base onde ocorre a monitorização dos dados.

O consórcio onde foi realizado o nosso projeto (AquaExcell 2020) definiu que o sistema teria de ser um sistema comercial de identificação por rádio frequência (RFID) a funcionar a 134.2 kHz. Os sistemas RFID são usados vulgarmente na identificação e leitura de etiquetas de identificação eletrónica em animais ou objetos.

O sistema RFID utilizado é um sistema passivo, em que a etiqueta eletrónica colocada no peixe não tem uma bateria. A energia que a etiqueta precisa é obtida através do sinal que é enviado pela antena do leitor. É um sistema de baixo custo, confiável e com um tempo de vida relativamente longo (duração de meses).

Foi construído um sistema RFID a funcionar à frequência de 134.2 kHz usando equipamento comercial da Texas Instruments™. O trabalho envolveu a otimização da distância máxima entre a etiqueta e a antena do leitor que permite obter leituras de forma

confiável. Define-se a distância máxima como alcance de leitura. O alcance de leitura do sistema é um aspeto crucial porque as ondas eletromagnéticas são fortemente atenuadas pela água, que depende da frequência do sistema e da condutividade do meio. Tipicamente, um sistema a funcionar a 134.2 kHz tem um alcance inferior a um metro.

O alcance de leitura do sistema depende do tipo de antenas usadas quer para a etiqueta quer para o leitor, da disposição espacial das antenas, do número de antenas e da forma como estas antenas são ligadas (em paralelo, em série, etc.). A presença de interferências externas (metais na proximidade das antenas) também condicionam o alcance.

Foram realizadas experiências quer usando uma antena, quer usando duas antenas de leitura. Usando duas antenas, foi possível fazer uma monitorização em todo o volume de um tanque de água salgada de 70 cm de comprimento, 30 cm de altura e 40 cm de largura.

Palavras-chave: *Stress*, Peixe, Sistema de monitorização, Aquacultura, Identificação por Rádio-Frequência (RFID).

Abstract

Stress is a factor that influences fish welfare. Some physiological and behavioral stress responses, such as the increase of cortisol release and heart rate, are triggered in fish and can show the severity of stress in fish.

The objective of our work is to develop a system to monitor a device placed in free-swimming fish. The device has one or multiple sensors that measures parameters related with the stress or health state of the fish. The data recorded by the sensor is transmitted to a base station. Data transmission uses radio-frequency identification (RFID) technology. The tag is battery-less and receives the energy from the magnetic field provided by the base station. The system is low-cost, reliable and provides long-term monitoring.

The project has been defined to use a commercial system operating at 134.2 kHz from Texas Instruments^{TM}. The work carried out involved the optimization of the maximum distance between the tag and reader antenna to maintain a reliable communication. The maximum distance is defined as read range. The optimization of the read range is a crucial point on this thesis because radio waves are strongly attenuated underwater.

The read range is influenced by the reader power, antennas size, antennas orientation as well as the presence of the metal in the antennas proximity. These aspects were studied in detail in this thesis. Measurements of the read range of the system were performed for a system with one reader antenna (single-antenna system) and a system with two reader antennas (multi-antenna system). For a multi-antenna system, we successfully covered the volume of a water tank with 70 cm length, 30 cm height and 40 cm width.

Keywords: Stress, Fish, Monitoring system, Aquaculture, Radio-frequency identification (RFID).

Index

Index of Figures

Index of Tables

Abbreviations List

AC	Alternating Current
ADC	Analog-to-Digital Converter
AFE	Analog Front-End
ASK	Amplitude Shift Keying
DC	Direct Current
DCO	Digitally Controlled Oscillator
EEPROM	Electrically-Erasable Programmable Read-Only Memory
FDX	Full-Duplex
FSK	Frequency Shift Keying
GUI	Graphical User Interface
HDX	Half-Duplex
HF	High Frequency
I2C	Inter-Integrated Circuit
JTAG	Joint Test Action Group
LF	Low Frequency
LSB	Least Significant Bit
MCU	Microcontroller
MSB	Most Significant Bit
PPM	Pulse Position Modulation
PWM	Pulse Width Modulation
RF	Radio Frequency
RFID	Radio-f requency Identification
SIMO	Slave-Input Master-Output
SOMI	Slave-Output Master-Input
SPI	Serial Peripheral Interface
UART	Universal Asynchronous Receiver/Transmitter
UHF	Ultra High Frequency
USB	Universal Serial Bus
VLO	Very-low-power Low-frequency Oscillator

Chapter 1

INTRODUCTION

Summary

This chapter presents the main objective of the thesis and describes how the thesis is organized. It also describes the current understanding about fish welfare and some methods and techniques for measuring stress indicators and transmitting sensor data from a device to a base station.

1.1 Structure of the thesis

The thesis is organized in 5 chapters. Chapter 1 outlines the structure of the thesis, summarizes the objectives, and presents a brief description about fish welfare in aquaculture. Chapter 2 provides a review about RFID technology. Chapter 3 presents the architecture of the RFID system used on this thesis. The optimization and characterization of the RFID system is described in chapter 4 where results related to read range and other factors are presented and discussed. Finally, chapter 5 presents the relevant conclusions as well as suggestions for further work.

1.2 Objectives

The main objective of the thesis is to develop a radio frequency identification (RFID) system to transmit data from a tag located on a free-swimming fish in an aquaculture tank to a base station located outside the tank. The RFID system operates at the frequency of 134.2 kHz. The tag has sensors which monitor several parameters related with stress or the health state of the fish. The crucial point of the RFID system is to maximize the read range of the antennas to cover the largest possible volume underwater.

The work is developed as part of the European project called AQUAEXCEL2020. The objective of the project is to coordinate and improve the performance of key European aquaculture research facilities to provide adequate experimental support and innovation to the European industry. One of the project work packages aims to design, probe and implement miniaturized biosensors for the specific, individual and remote fish monitoring of parameters related to overall fish performance and welfare.

1.3 Motivation

Aquaculture is the farming of aquatic organisms in any type of aquatic environment, under human control. The aim of aquaculture is human consumption and income. Aquaculture industry has been growing fast in world food production, accounting in the present approximately 50% of global fish used for human consumption and an annual average growth rate of approximately 6% [1]. With the continued expansion of the aquaculture industry, fish welfare has become a concern in terms of fish well-being and aquaculture production [2], [3]. The definition of fish welfare has led to debate worldwide and consequently to the creation of legislations and guidelines, concerning the general status of fish welfare [4]–[7]. An individual fish is in a good state of welfare, if it is healthy, comfortable, well-nourished, safe and able to express natural behavior with the surrounding ambient. Also, avoiding negative effects such as pain, fear and stress are indicators of good fish welfare [8].

Stress is a major factor that influences fish welfare. Fish have mechanisms necessary to cope with harmful stimuli (or stressors) through physiological and behavioral stress responses [9]. Divided in three stages, primary responses evoke the release of hormones such as cortisol and adrenaline into the blood. Short-term (low duration) secondary responses are triggered immediately with metabolic changes and increased heart and ventilation rate, which make fish better able to cope with the stressor. However, if fish cannot cope with the stressor, longer-term tertiary responses evoke changes detrimental to fish welfare, including adverse changes in behavior, immune function, growth, reproduction, disease resistance and may cause mortality. Stress can evoke any of the responses, directly or indirectly, depending on the magnitude, frequency and duration of the stressor. Stressors can be physical (e.g. aquaculture practices such as handling, capture, confinement and transport), chemical (e.g. toxic heavy metals) and perceived (e.g. undesirable sounds and the presence of predators) [10].

The concern about fish welfare in aquaculture has evoked the importance to create or develop methods and techniques to measure some stress indicators. The main indicators are the concentration level of plasma cortisol, color changes in fish body, heart and ventilation rate, and changes in behavior of the fish. Monitoring welfare of farmed fish requires effective, simple, accurate, economical and practical systems [11].

Fish release cortisol into the water via gills, bile and urine [12]. Laboratorial methods such as radioimmunoassay, enzyme-linked immunosorbent assay and high-performance liquid chromatography are used to assess cortisol release rate [12]–[14]. Water samples are extracted and measured outside the tank, without disturbing the fish, being a great advantage to measure free cortisol with a non-invasive method. However, the techniques are time-consuming, technical demanding, complex, expensive and not suitable to probe individual fish.

Visual methods are ones of the least invasive methods, because fish are not required to be handled or captured. Visual changes in body color and fish behavior can be observed directly by researcher's eye or with the aid of video cameras, or indirectly by using automated image processing techniques. Stress can be quantified through body darkening (the darker is the body, the most stressed is the fish), which can be mainly observed on their skin [15]–[18] and eyes [18]–[21]. Behavioral changes are easily observed in a stressed fish. An automatic image analysis method combined with video recording was used to quantify food anticipatory behavior in fish population [22] and tracking of individual fish in two dimensions [23] and three dimensions [24]. The advantages of the visual methods and techniques are the easy implementation, high reliability and no physical contact with the fish. A potential disadvantage is related to real-time monitoring of fish because constant visual contact of fish would be required. Situations where an individual fish is located in remote zones of the tank or in highly populated environment are not suitable for visual monitoring.

Heart rate can be assessed by the operculum or directly over the heart of fish. However, heart rate is difficult to assess and requires invasive methods. Four sensors providing the least invasive methods to monitor heart rate are electrocardiogram [25]–[30], Doppler [25], pulse oximeter [27] and ultrasonography [27]. The use of the sensors has been impracticable underwater, which means fish must be captured and removed from the tank to apply the sensors and requires fish to be sedated for the surgical procedures. However, the development of a wearable, flexible and waterproof sensor applied in free-swimming fish [30] shows potential for an effective, real-time and long-term underwater monitoring and the procedure does not require anesthesia on fish. However, the device coupled to the fish body is large and difficulties come when the sensors are applied on a population. Heart rate techniques uses expensive, complex equipment which with low

portability. Also, in order to assess heart rate, fish need to be handled and captured from the environment.

The ventilation rate can be assessed manually by measuring the opercula beat rate of fish, which is easily measured by visually observing the operculum and manually counting the beats per minute [31]. However, the method is only possible in smaller environments and larger fish. Furthermore, the automatic assessment of the ventilation rate provides the possibility to monitor free-swimming fish through low-cost and reliable sensors such as the electromyogram [32], [33] and accelerometers [34], [35]. The ventilation rate assessment is non-invasive, inexpensive and does not require sophisticated equipment to monitor free-swimming fish. However, ventilation rate does not reflect the stress level, only shows whether fish are stressed or not.

The sensor is integrated in a tag with an antenna to transmit the measured data remotely through telemetry techniques. The term telemetry is defined as the wireless transmission of data acquired by single or multiple sensors, from a transmitter to a receiver placed at some distance away. The transmitter is usually an electronic tag attached to the fish, containing the sensing circuitry coupled with an antenna. Electronic tags can be either active, where tags require an internal battery, or passive, where tags require energy from an external source, in order to power their circuits. There are five common electronic tags used in telemetry, radio tag, acoustic tag, data storage tag, pop-up satellite archival tag and passive integrated transponder [36]. The tags are relatively expensive, but in many cases, some of the collected types of data cannot be provided by other methods. The most suitable tag is the one which lasts longer, the cheaper and smaller one with a variety of sensors and a long read range.

The proposed method for the system of this thesis is the passive integrated transponder, more specifically the RFID tag, which is very popular among the tags commercially available. The feature of the RFID tag having no battery is the key, which dramatically reduces the cost and size of the tag and provides the possibility to monitor fish of all sizes for over a year. Also, since the aquaculture tank is a relatively small system, the proposed system is highly suitable. All efforts to optimize the system are necessary in order to transmit continuously sensor data in any spatial point in the aquaculture tank at any moment, providing so the real-time system.

Chapter 2

UNDERWATER RFID TELEMETRY

Summary

This chapter provides a review about radio frequency identification (RFID) technology used in PIT tags. The fundamental elements which compose a RFID system are described in detail as well as some factors contributing to a better performance of the system. A review about the application of RFID systems underwater is also provided.

2.1 Introduction

Radio frequency identification (RFID) is a wireless technology which uses radio frequency (RF) signals for communication between the device attached to objects or animals (including humans), and a receiving equipment placed at a distance away. RFID technology does not require the transmitter to be in direct contact or in line-of-sight with a receiver in order to transmit data. Comparing with conventional methods of identification such as bar-code and optical character recognition systems, RFID technology provides several advantages. Higher read range, identification of devices in remote locations, reliable reading in harsh environments, faster data transmission and the possibility of reading multiple devices at the same time are some of the advantages [37]. RFID technology provides a wide range of applications such as access control, electronic toll collection and animal identification, tracking and sensing [38].

2.2 Architecture of the RFID system

A RFID system is composed of three fundamental elements, the tag, the reader and the computer (also called as host computer). The reader interrogates a tag by transmitting a RF signal and waits for tag response. The reader receives the tag signal and sends the information to the host computer for further processing. The communication between reader and tag is made via two antennas, each antenna attached to either reader or tag. Figure 2.1 shows a schematic diagram of a typical RFID system.

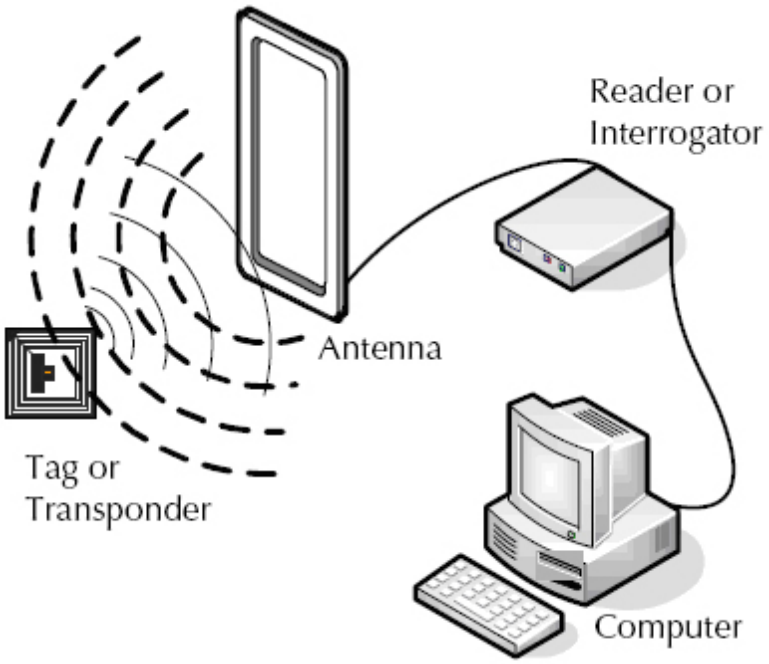

Fig. 2.1 – Schematic diagram of the RFID system [39].

2.2.1 **Tags**

The RFID tag is a data carrier device which contains a chip and an antenna. The chip processes received information by demodulating a RF signal and storing the data in memory. For data transmission, the chip modulates a backscatter RF signal with other information already stored in memory to the reader. The antenna is used for transmitting and receiving the RF signal and also collects energy from the reader [40]. Tags have a wide variety of sizes, shapes and protective housings, including circular plastic disks, rectangular smart cards or cylindrical fiber glass as shown in figure 2.2.

Fig. 2.2 – Photograph of different types of RFID tags, developed by Texas Instruments™ [41].

RFID tags can be active, passive or semi-passive. Active tags have a battery and can transmit RF signals to the reader using a far-field antenna. Passive tags do not have battery and can collect energy transmitted by an interrogation of the RFID reader through a near-field antenna and transmits a backscatter RF signal to the reader using the obtained energy. Passive tags are smaller, lighter, cheaper and more long-lasting than active tags. However, passive tags have a shorter transmission range comparing with active tags. Semi-passive tag contains an internal battery like an active tag to be used for measuring sensor data in the tag. In order to conserve battery life, some semi-passive tags act as passive tags by waiting for an interrogation of the reader to transmit back data. Semi-passive tags have the middle transmission range, size and cost, but may have the worst battery lifetime [38].

2.2.2 **Readers**

The RFID reader is an equipment which reliably reads the RF signal of tags within the range and communicates the results to the host computer. The reader interrogates the tag by transmitting a modulated RF signal with enough energy to activate the tag chip, perform data processing and transmit back data stored in the chip. The reader receives the backscatter RF signal from the tags and examines the tag data [40].

RFID readers comprise two functional blocks, the RF module and the control module. The RF module provides energy to the tags using RF field and performs the modulation/demodulation of the RF signal to/from the tag. The control module communicates and executes the commands sent by the host computer, codes and decodes the signal and have communication control with tags [38]. The two modules are represented in figure 2.3.

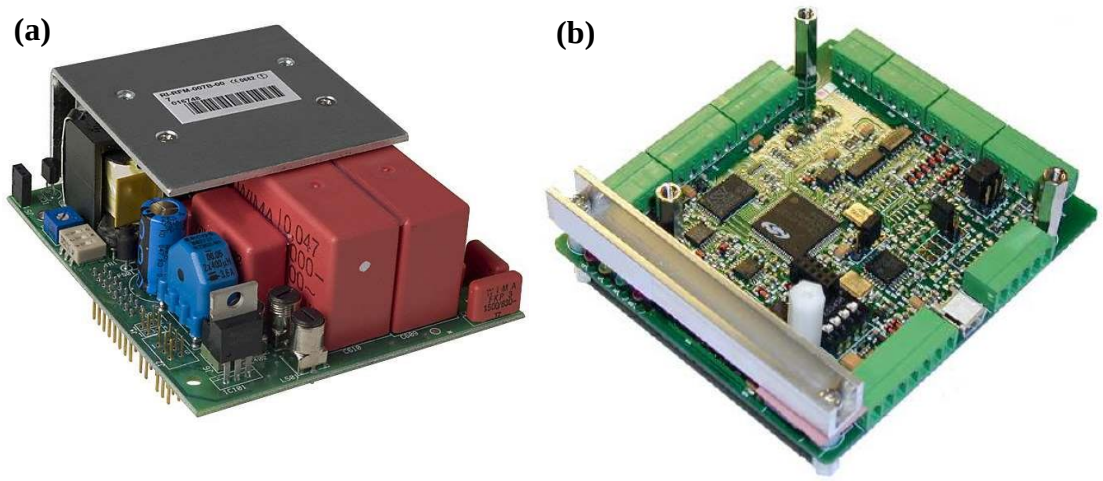

Fig. 2.3 – Photographs of the individual modules of a RFID reader, developed by Texas Instruments™. (a) RF module [42] (b) Control module [43].

RFID readers can be fixed or mobile. Fixed readers are placed in a specific interrogation zone which can be deeply controlled, allowing a highly defined reading area for when tags go in and out of the interrogation zone. Mobile readers provides dynamic reading in various locations although the reading area is lower and not highly defined. Mobile readers can be hand-held or mounted on carts or vehicles [40].

2.2.3 **Host computer**

The host computer provides an interface between the RFID reader and the user, being useful for processing and monitoring data collected by the reader. The RFID system, along with all hardware elements, comprises several software elements. Two important software elements are the firmware and the application. The firmware is a software with control operations and basic functions to be performed in the reader and the tag. The firmware is composed and uploaded inside the microcontroller of the reader or the tag by the host computer and may be upgraded to fix errors, add new functionalities

and improve stability. The application is a program with a set of instructions designed for the host computer to perform specific operations for the user, such as accessing, analyzing and monitoring data collected by the reader. Data can be accessed directly from the reader or from a database where data was previously stored. A graphical user interface (GUI) application allows users to interact directly with the RFID system [44].

2.2.4 **Antennas**

Both tag and reader have an antenna. The shape of the antenna may be squared, rectangle, circular, ellipse, hexagonal, or spiral. The size of the antenna usually depends on the wavelength. For a large wavelength, a true antenna emitting low-frequency radio waves is difficult to build. Alternatively, smaller sized loop antennas resonating at the frequency of interest are widely used and is basically a wire winded around, making a coil [45]. Figure 2.4 represents the different loop antennas with varied sizes and shapes.

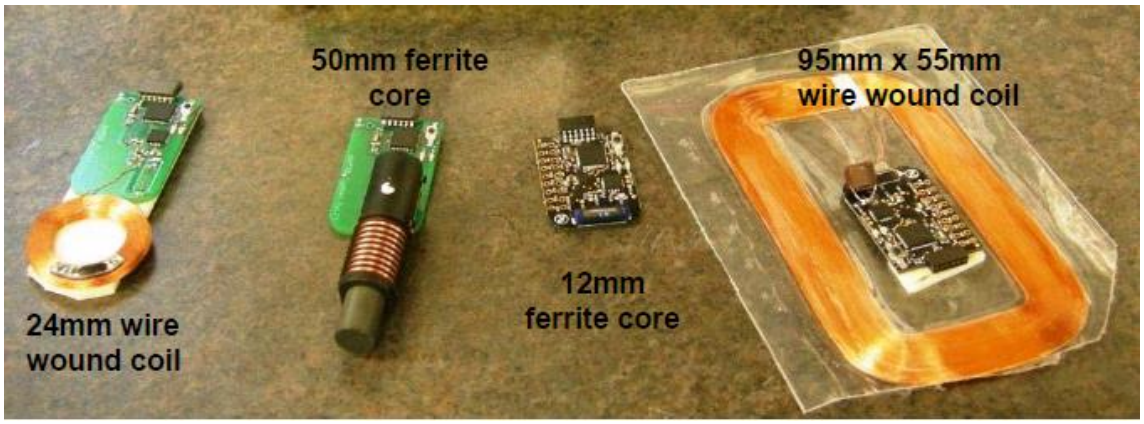

Fig. 2.4 – Photographs of different loop antennas in shape and size for tags, developed by Texas Instruments™ [41].

There are two types of loop antennas, gate antennas and stick antennas. A typical gate antenna is a rectangular or circular loop antenna which provides larger magnetic field than stick antennas, having higher read range. However, the strength of the magnetic field is weaker, mainly close to the antenna. The gate antenna is normally applied in pass-through arrangements for applications such as anti-theft retail store and animal identification in livestock. Stick antennas are generally smaller loop antennas, which are winded around a ferrite rod with magnetic properties, increasing the strength of the magnetic field in the vicinity of the antenna. Stick antennas are used in close-range systems, for applications such as animal or object identification using mobile reader or antenna [46]. Gate and stick antennas with varied sizes are represented in figure 2.5.

Fig. 2.5 – Photograph of three gate loop antennas of different sizes behind two stick loop antennas of the reader, developed by Texas Instruments™ [46].

The communication between reader and tag antennas is mainly done through methods of energy coupling. Inductive coupling is one method, which involves the reader antenna generating a magnetic field, produced by alternating current (AC) flowing through reader antenna. The strength of the magnetic field varies in time, resonating at the frequency of interest. When the time-varying magnetic field is passing through the tag antenna, an AC voltage is induced across the tag antenna terminals, which is rectified and filtered to get the direct current (DC) voltage. The DC voltage is stored in a capacitor to be used to activate the chip and sensors of the tag when the voltage reaches a certain level. The activation and successive transmission of the backscatter RF signal from the tag to the reader depends on the read range of the system. Read range is considered to be the maximum distance between reader and tag antennas to reliably communicate with each other [47]. The principle of inductive coupling is represented in figure 2.6.

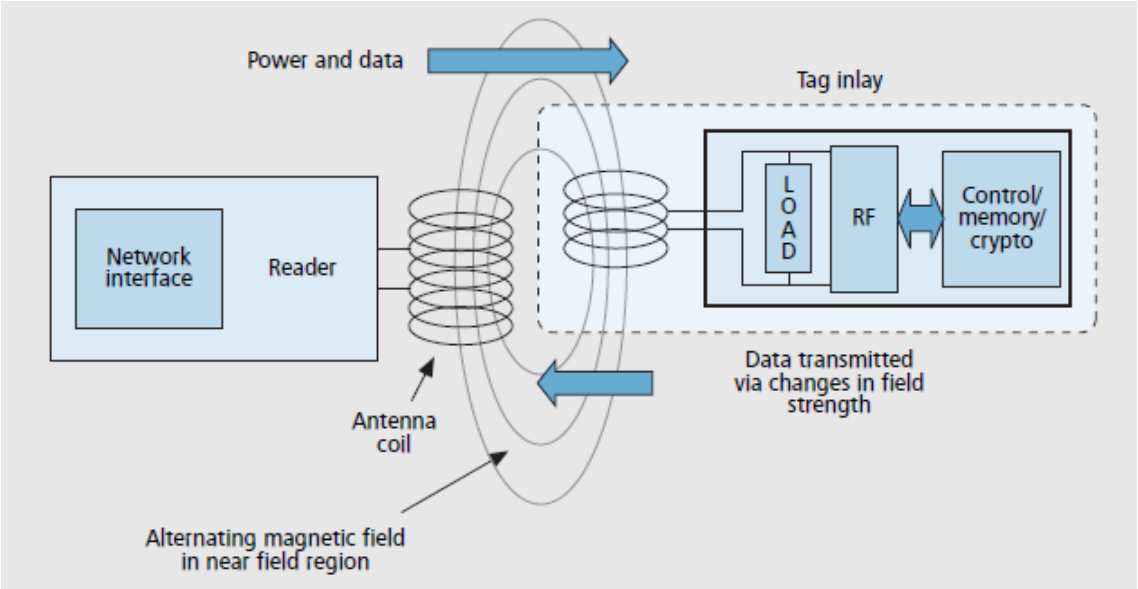

Fig. 2.6 – Principle of inductive coupling between reader and tag antennas [47].

A great advantage for inductive coupling is magnetic field does not require line-of-sight, because the flux lines cross most of the common materials. However, the strength of the magnetic field on tag is attenuated sharply over distance away from the reader as $1/r^3$, where r is the distance between the reader and the tag. Also, inductive coupling requires large antennas and does not provide a well-defined reading area. The coupling between tag and reader is not uniform in all locations inside the area.

Loop antennas use inductive coupling between reader and tag, detecting RF signals in various different frequencies. Equation 2.1 calculates the strength of the magnetic field at a spatial point z from a circular loop antenna [45].

$$B_z = \frac{\mu_0 I N a^2}{2\sqrt{(a^2 + r^2)^3}} \qquad (2.1)$$

In equation 2.1, B_z is the strength of the magnetic field at a specific point z in Webers per square meter (Wb/m^2), μ_0 is the absolute magnetic permeability of the vacuum ($4\pi*10^{-7}$) in Henrys per meter (H/m), I is the AC current flowing through the antenna in Amperes (A), N is the number of loops of the antenna, a is the radius of the loop in meters (m) and r is the radial distance in meters (m) between the center of the loop and the spatial point where magnetic field is determined. According to equation 2.1, the strength of the magnetic field is directly proportional to the AC current of the transmitting antenna, but falls off rapidly over distance away from the antenna.

To maximize energy transfer between the reader and the tag, LC (inductance-capacitance) resonance circuits in the reader and also in the tag are required. The resonance frequency of the system need to be tuned for both circuits by changing the inductance and capacitance to the desired values [48]. Figure 2.7 represents the LC circuit of reader and tag.

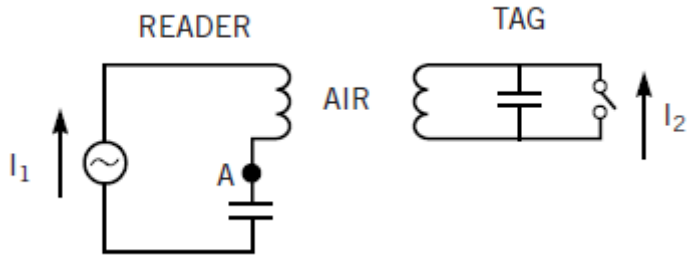

Fig. 2.7 – LC circuits of reader and tag. The inductor is the antenna itself and the capacitor is connected in series or in parallel to the antenna. The reader has the capacitor in series with the antenna for maximizing current through the antenna. The tag has the capacitor in parallel with the antenna for maximizing induced voltage in the tag antenna [48].

Inductance is mainly influenced by size, shape, number of loop turns and wire length of the antenna, among other factors. Capacitance is influenced just by an equivalent circuit of capacitors in the antenna terminals. Equation 2.2 calculates the resonance frequency for both reader and tag LC circuits [46].

$$f_0 = \frac{1}{2\pi\sqrt{LC}} \qquad (2.2)$$

In equation 2.2, f_0 is the resonance frequency in Hertz (Hz), L is the inductance in Henrys (H) and C is the capacitance in Faradays (F).

The system amplifies oscillations within a particular bandwidth centered by the resonance frequency, while reducing oscillations at the other frequencies outside the bandwidth. The efficiency of the system is determined by quality factor Q, a parameter of the antenna which characterizes the rate of stored energy relative to the dissipated energy of the resonance circuit. A high Q antenna provides way higher output RF power than low Q antennas, for the same input power, thus high Q antenna provides better efficiency and higher read range [46]. Equation 2.3 calculates the quality factor of the antenna.

$$Q = \frac{f_0}{B} \qquad (2.3)$$

In equation 2.3, Q is the quality factor, f_0 is the resonance frequency in Hertz (Hz) and B is the bandwidth in Hertz (Hz). According to equation 2.3, a high Q antenna provides lower bandwidth than low Q antennas, filtering more undesirable signals and noise, although being less tolerant to detuning. Figure 2.8 represents the RF output power of two antennas with different quality factor [46].

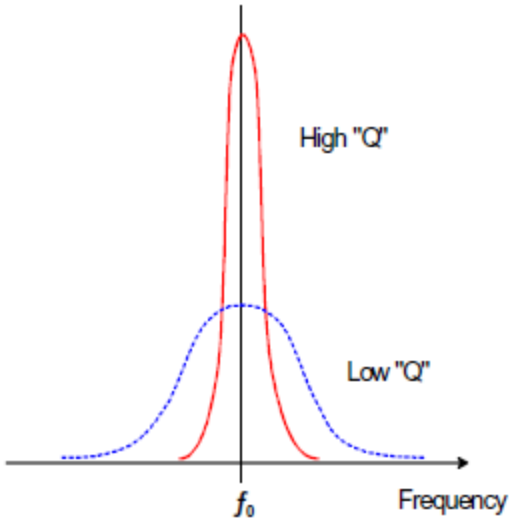

Fig. 2.8 – The RF output power of a high Q antenna is compared with the RF output power of a low Q antenna. The parameter f_0 is the resonance frequency of the system [46].

Equation 2.4 calculates the quality factor of the antenna in terms of resistance and inductance [46].

$$Q = \frac{2\pi f_0 L}{R} \qquad (2.4)$$

In equation 2.4, Q is the quality factor, f_0 is the resonance frequency in Hertz (Hz), L is the inductance in Henrys (H) and R is the resistance of the antenna in Ohms (Ω). According to equation 2.4, the quality factor is inversely proportional to the resistance of the antenna. The type of wire determines the resistance of the antenna and consequently the quality factor. A type of cable with low resistance used to build a high Q antenna is litze wire, which uses multiple insulated wire strands twisted as close together as possible and then is used silk to cover the wire strands. For low Q antennas, the insulated transformer wire with high resistance is used [46].

The induced AC voltage across the antenna is also a product of the quality factor of the antenna. Equation 2.5 calculates the induced voltage in the tuned antenna [45].

$$V_0 = 2\pi f_0 NSQB_0 \cos \propto \qquad (2.5)$$

In equation 2.5, V_0 is the induced AC voltage in the antenna terminals in Volts (V), f_0 is the resonance frequency of the system in Hertz (Hz), N is the number of loops of the antenna, S is the area of the loop antenna in square meters (m^2), Q is the quality factor of the antenna, B_0 is the strength of the magnetic field in Webers per square meter (W/m^2) at the point where the receiver antenna is located and α is the angle of the antenna relative to the receiving magnetic field flux lines. According to equation 2.5, the induced AC voltage across the tag antenna terminals is dependent on the strength of the magnetic field generated by the AC current which flows through the reader antenna. A tuned large high Q reader antenna increases the induced AC voltage across the tag antenna terminals, which increases read range.

2.2.5 **RFID operating frequencies**

RFID systems operate in several frequency bands, ranging between low frequency (LF), high frequency (HF), ultra high frequency (UHF) and microwaves.

LF systems operate between 100 and 500 kHz, being generally operated at 125 kHz in applications such as access and inventory control, and vehicle immobilizers, and 134.2 kHz in animal identification and tracking. One great advantage about LF systems is the low interference with materials present around the system such as water, metals and electrical power sources. LF systems have short read range, large antennas, low cost, small read rate and have poor ability to detect multiple tags [38].

HF systems operate between 10 and 15 MHz, being generally operated at 13.56 MHz in applications such as access and library control, items and case tracking, and smart-cards. The antennas are smaller than in LF systems and have good ability to detect multiple tags. Also, the cost, read range and read rate of the HF systems are higher than in LF systems. However, HF systems has some interference issues, mainly with metal [38].

UHF systems operate between 0.4 and 1 GHz, being generally operated at 433 MHz for active tags and 860-960 MHz for passive tags. UHF systems uses shorter

antennas than in LF and HF systems in applications such as electronic toll collection and case, pallet and container tracking. Due to their larger bandwidth, UHF systems provides a high read range, high read rate and great ability to read multiple tags. However, line-of-sight is required for the communication between reader and tags. Also, UHF systems are expensive and have interference issues with materials in close proximity such as metal and water [38].

Microwave systems operate between 2.4 and 6.8 GHz, being generally operated at 2.45 GHz using passive tags and 5.8 GHz using active tags. Microwave systems are used in applications such as electronic toll collection and case, pallet and container tracking and are also used by systems such as Bluetooth and Wi-Fi. Microwave systems have basically the same characteristics as UHF systems, only provide the fastest read rate and the longest read range, although the cost is higher due to the use of active tags [38].

2.2.6 **RF communication protocols**

The RF communication protocol provides a way of communication between the reader and tag in order to transfer reliably data. The two most used protocols are Full-Duplex (FDX) and Half-Duplex (HDX) protocols.

Full-Duplex (FDX) is a communication protocol able to have data travelling bi-directionally at the same time. The reader interrogates the tag by sending energy and data, and the tag responds back while being powered by the RF field still activated by the reader [49]. The typical modulation used on FDX is amplitude shift keying (ASK), as shown in figure 2.9.

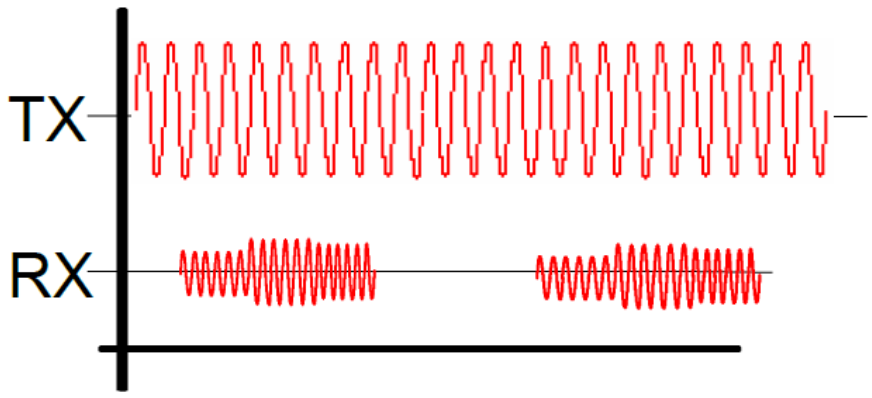

Fig. 2.9 – FDX operation. The TX is the reader and the RX is the tag. In ASK, the reader transmit a continuous RF signal and the tag sends an amplitude modulated signal. A high envelope is a binary code ‘1’ and a low envelope is a binary code ‘0’ [49].

The advantages of using FDX is the fast data transmission rate, where tag may transmit immediately continuous data and can be read more quickly and more often. However, the disadvantages of FDX are the high susceptibility to atmospheric noise due to the use of ASK, in which the noise may influence the amplitude of the signal and transmission of data is not highly reliable. Also, there are first read issues where FDX systems have to make multiple reads and compare the results [49].

Half-Duplex (HDX) is a communication protocol able to have data travelling bidirectionally. However, the communication does not travel in both directions at the same time. Instead, the reader interrogates the tag by sending energy and data, and the tag only responds back when the reader deactivates the RF field, after a pre-defined period. While waiting to transmit data, the tag stores the energy in a capacitor to be used later [49]. The typical modulation used on HDX is frequency shift keying (FSK), as shown in figure 2.10.

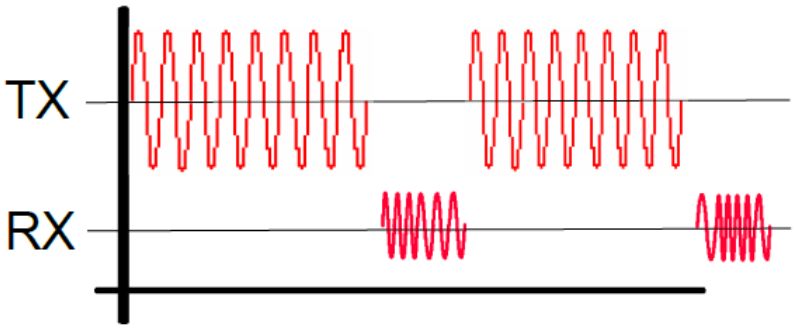

Fig. 2.10 – HDX operation. The TX is the reader and the RX is the tag. In FSK, the reader transmits a periodic RF signal and the tag sends a frequency modulated signal. The tag sends 0's nearly in the resonance frequency and 1's in a slightly lower frequency [49].

The advantage of using HDX is the low susceptibility to atmospheric noise because HDX tags use FSK which is not influenced by signal amplitude, being less sensible to noise. Besides, during tag transmission period there is no interference from reader RF field. Therefore, HDX tags are usually large tags with increased read range. Also, HDX reader only have to read a tag once, because 16-bit checksum validates the data and ensures the read is good. Also, HDX reader requires less power. However, the disadvantage of the HDX is slow data transmission rate, because the tag cannot transmit data immediately while the reader RF field is still activated. The period of the RF field

time can be shorten in order to increase the tag read rate, but the tag may not get enough energy to transmit data, decreasing reliability [49].

2.2.7 Factors affecting the read range

For inductive coupling systems, the read range depends on several factors. One of the critical aspects of the read range is the size of the reader and tag antennas. The larger is the antenna, the higher is the read range. However, when antennas get too large, they may collect more noise and the performance may decrease, which can have shorter read range than smaller antennas [46]. Also, increasing the size of the antenna may introduce difficulties to balance the LC circuits with extreme values. Other factor increasing read range is the RF power of the reader, where increased power may increase RF field and does not result in increased noise. However, there are limitations about the increase of both antenna size and RF power of the reader due to regulatory issues in order to operate without interferences with other systems [50].

One factor which reduces the read range is the environmental noise generated by power sources such as inverters, switched-mode power supplies and electric motors. The increased noise implies the tag to get closer to the reader antenna in order to be detected. Other factor is the used communication protocol, where FDX provides shorter read range than HDX due to high susceptibility to noise provided by ASK. Also, the presence of metals near the system may detune the resonance frequency, by changing the inductance of the antenna and thus reducing read range [50]. Figure 2.11 represents the detrimental effect of the presence of metal on the RF field of the reader antenna.

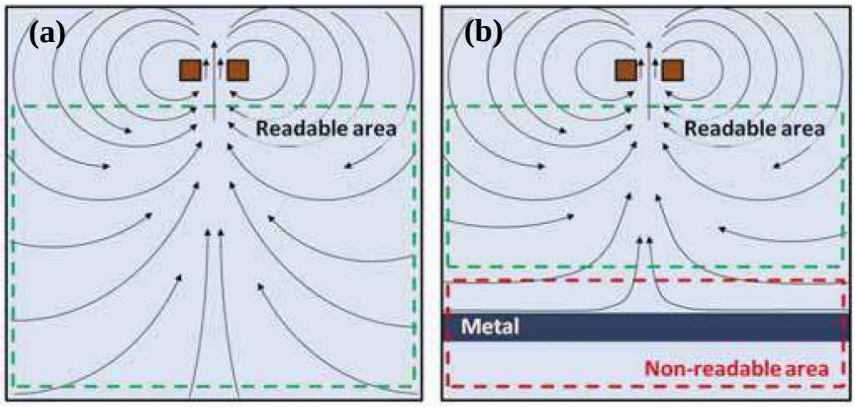

Fig. 2.11 – Detrimental effect of the presence of metal on magnetic field [51]. (a) The magnetic field is produced by a wire in an environment without metals. (b) The lines of the magnetic field are distorted by the presence of metal, causing a non-readable area.

At last, the presence of the reading holes is another factor which reduces the read range of the system. Reading holes are areas within the reader RF field where communication between antennas is not possible, due to tag orientation (the angle of the tag antenna relative to the plane of the reader antenna). For example, at a specific point within the RF field, an “in-parallel” tag (the antenna is in parallel relative to the reader antenna) may be detected by the reader, while an “in-perpendicular” tag (the antenna is in perpendicular relative to the reader antenna) may not be detected, being positioned into a reading hole. There are possibilities for a tag to be relatively close to the reader antenna in some orientations and still not be read [50]. Figure 2.12 represents the magnetic field pattern of the reader antenna.

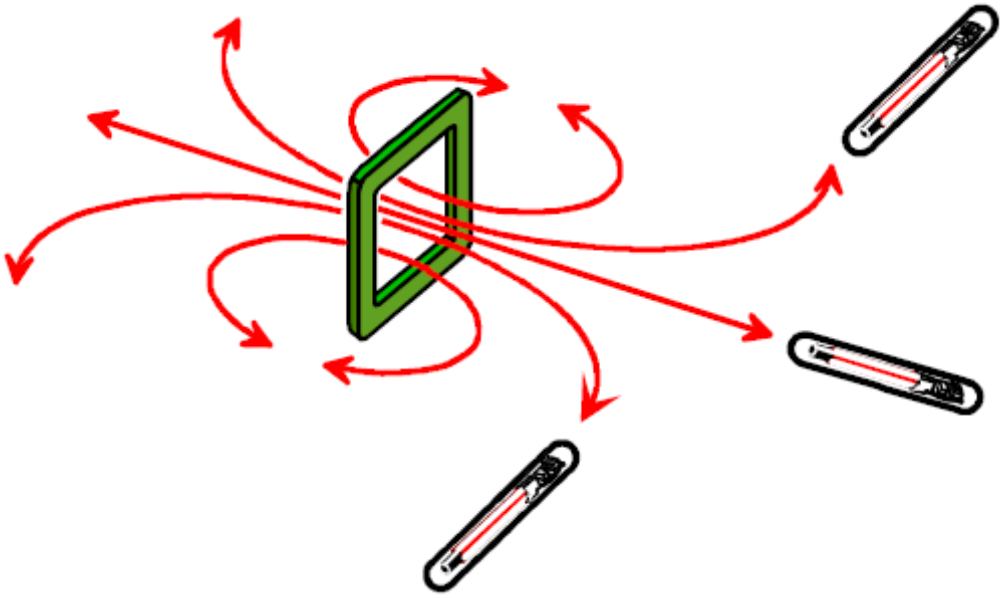

Fig. 2.12 – Magnetic field lines of the reader antenna. The reader antenna couples with two “in-perpendicular” tags and one “in-parallel” tag in different positions. The maximum distance of the read range is obtained with the “in-parallel” tag antenna [46].

Reading holes change position, depending on the tag orientation. Figure 2.13 represents the readout pattern of the system for different tag orientations.

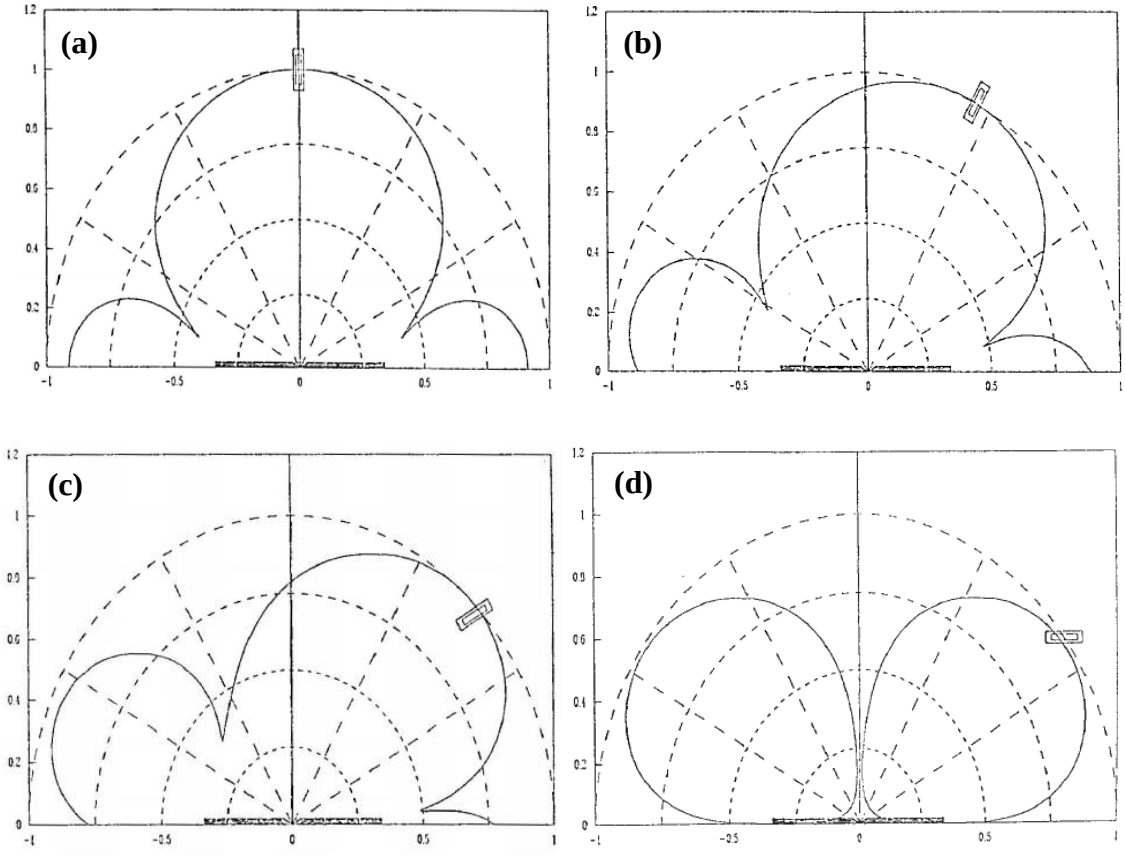

Fig. 2.13 – Readout pattern of the system for the different tag orientation angles [52]. (a) 0º tag orientation ("in-parallel" tag). (b) 30º tag orientation. (c) 60º tag orientation. (d) 90º tag orientation ("in-perpendicular" tag).

Other way to increase the read range is using two or more gate antennas on reader, making a multi-antenna system. When the two antennas are connected in parallel or in series, the reader interprets them as a single antenna. The magnetic field distribution changes and assures better transfer of energy between the loops. There are two antenna connections for the multi-antenna system, when antennas are connected in phase ("in-phase" connection) and when antennas are connected "out-of-phase" ("out-of-phase" connection) [46].

When two antennas are connected in phase, the currents in the two antennas are flowing in the same direction, resulting in the cancellation of the magnetic field in the x-axis in the region between the two antennas [53]. This connection generates a certain pattern of the magnetic field lines between antennas as represented in figure 2.14.

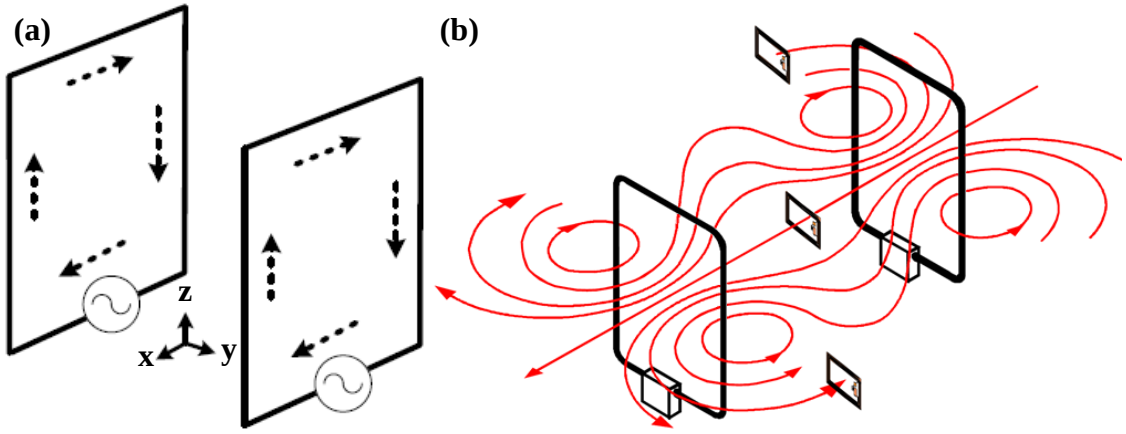

Fig. 2.14 – "In-phase" connection. (a) Opposing gate antennas whose respective currents are flowing in the same direction (adapted from [53]). (b) Resulting magnetic field pattern, easily detecting three "in-parallel" tags in the field [46].

When two antennas are connected "out-of-phase", the currents in the two antennas are flowing in the opposite direction, resulting in the cancellation of the magnetic field in the y-axis in the region between the two antennas [53]. This connection generates a different pattern of the magnetic field lines between antennas relative to the "in-phase" connection, as represented in figure 2.15.

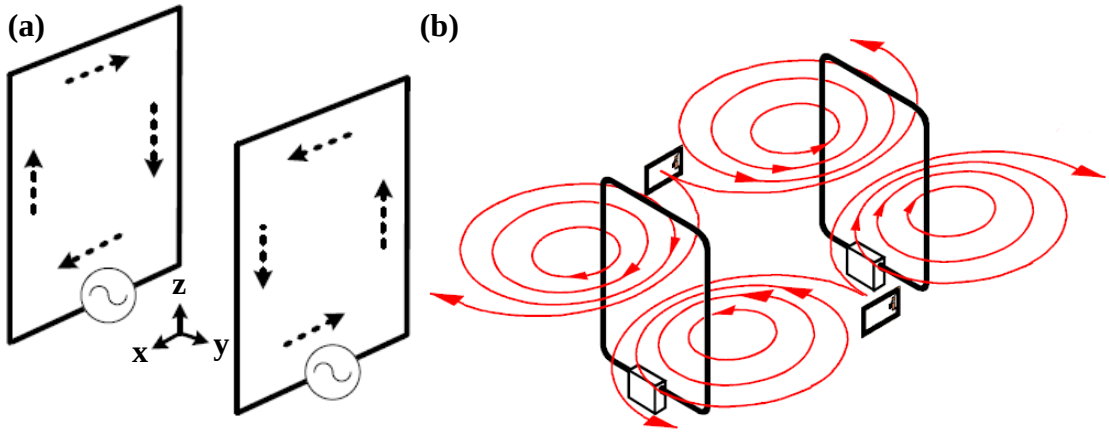

Fig. 2.15 – "Out-of-phase" configuration. (a) Opposing gate antennas whose respective currents are flowing in opposite directions (adapted from [53]). (b) Resulting magnetic field pattern, detecting two "in-perpendicular" tags [46].

The two gate antennas designed for pass-through arrangement are separated by a distance. If the distance is too large, the strength of the magnetic field in the middle region may be too weak to activate the tag [54]. However, if the distance is too close, mutual coupling between two or more reader antennas would occur, which may interfere on the system and decrease read range. There are two options to minimize mutual coupling.

First, placing the antennas "in-perpendicular" to each other, the magnetic field patterns would not overlap to each other, but rather cross, having no interference. Second, the "nulling-out" technique can be applied, which is an optimization technique to measure the optimal distance between the reader antennas where mutual coupling is nullified. The technique proceeds by connecting one antenna to the system, working as a single-antenna system and connecting the other antenna to an oscilloscope to measure the induced voltage. Moving away the second antenna until the induced voltage by the system with the first antenna is nullified, gives the optimal distance [50].

2.3 Underwater communication

The biggest issues to overcome when using RFID systems in aquatic environments are the severe effects of radio waves when travelling underwater. However, the transmission of radio signals underwater is possible and the underwater travel distance of radio waves depends mainly on two factors, the conductivity of the water and the frequency of the radio wave. Salinity affects the conductivity of the water. The more saline is the water, the shorter is the travel distance of radio waves underwater. At saltwater, the conductivity ranges from around 2 S/m to around 6 S/m, where average conductivity is normally considered about 4 S/m. At freshwater, the conductivity ranges from around 0.003 S/m to around 0.3 S/m, where average conductivity is normally considered about 0.15 S/m [55].

Skin depth is a measure of how deep electromagnetic waves can penetrate into a material, being defined as the depth at which the intensity of the radiation inside the material falls to 1/e (about 37%) of its original value at the surface [55]. Equation 2.6 calculates the skin depth of the electromagnetic wave.

$$\delta = \frac{1}{\sqrt{\pi f \mu \sigma}} \ (m) \qquad (2.6)$$

In equation 2.6, f is the frequency of the electromagnetic wave in Hertz (Hz), μ is the absolute magnetic permeability of the vacuum ($4\pi*10^{-7}$ H/m) in Henrys per meter (H/m) and σ is the conductivity of the water in Siemens per meter (S/m). According to equation 2.6, the lower are both frequency and conductivity, the higher is the skin depth [55].

Table 2.1 represents the theoretical values of the skin depth calculated for one representative value of each operating RF range (LF, HF, UHF, microwave) and average conductivity of freshwater and saltwater, respectively.

Table 2.1 – Theoretical results of the skin depth.

RF range	Frequency	Freshwater conductivity (0.15 S/m)	Saltwater conductivity (4 S/m)
LF	134.2 kHz	3.55 m	69 cm
HF	13.56 MHz	35 cm	6.8 cm
UHF	960 MHz	4.1 cm	8.1 mm
Microwave	2.45 GHz	2.6 cm	5.1 mm

For LF range, the skin depth for freshwater conductivity is a great result for long-range applications implemented underwater and even the skin depth for saltwater conductivity is still a considerable result to implement a LF system underwater.

For HF range, the skin depth for freshwater conductivity is a reasonable result for RFID systems implemented in small aquatic environments. However, the skin depth for saltwater conductivity is small, which can be implemented some close-range applications.

For UHF and microwave ranges, the skin depth for freshwater conductivity are relatively smaller than for the HF range, which can be used in close-range applications. However, the skin depth for saltwater conductivity is extremely small, which can be used in contact-only applications with the antenna of the device placed on the water surface.

In conclusion, theoretical results suggest several solutions when RFID is required for underwater applications. However, the values obtained for the skin depth are ideal values and essentially represent an upper bound. In most cases, the system present practical read range values considerably lower. To obtain reliable results in underwater applications, the chosen operating frequency should be as low as possible. Therefore, LF RFID systems are the most suitable to be implemented underwater.

2.4 Practical underwater applications using RFID systems

Practical applications for tracking objects and animals underwater has been implemented. LF systems has been used to track fish and pebbles in aquariums, rivers and oceans.

The first application is a 134.2 kHz LF RFID system applied in aquariums where tagged fish approaching the antenna placed outside are identified and all information from its species is displayed on the screen. The application was placed in saltwater and

managed to achieve a read range up to 22 cm. The read range is relatively low due to the high conductivity of the water, so the biologists expected to increase the read range by changing the position or the design of the antenna. The biologists tried to put the antenna inside the tank, using a pipe waterproof made of polyvinyl chloride. The biologists also tried multiple antenna shapes, including circular (60 cm diameter), rectangular (30 cm * 120 cm) and also a vertical straight line [55]. Figure 2.16 represents a demonstration of the implemented system with a circular antenna placed near the aquarium.

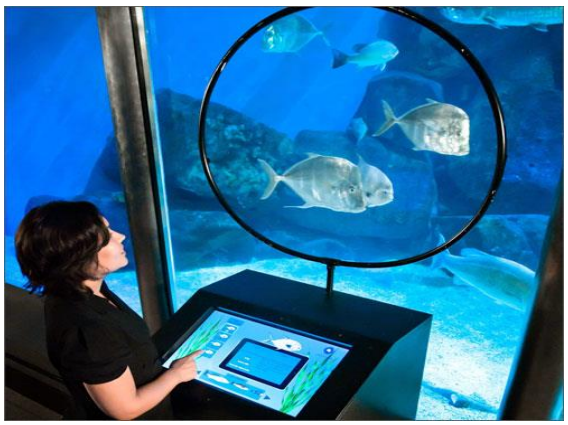

Fig. 2.16 – Animal tracking in an aquarium, using a circular antenna [55].

Another application is a 125 kHz LF RFID system applied on a gravel beach where tagged pebbles were identified for the monitoring of coastal dynamics. One of the goals of the application was to achieve the largest read range possible in saltwater [55]. The tagged "Smart Pebble" and the respective identification operations underwater are represented in figure 2.17.

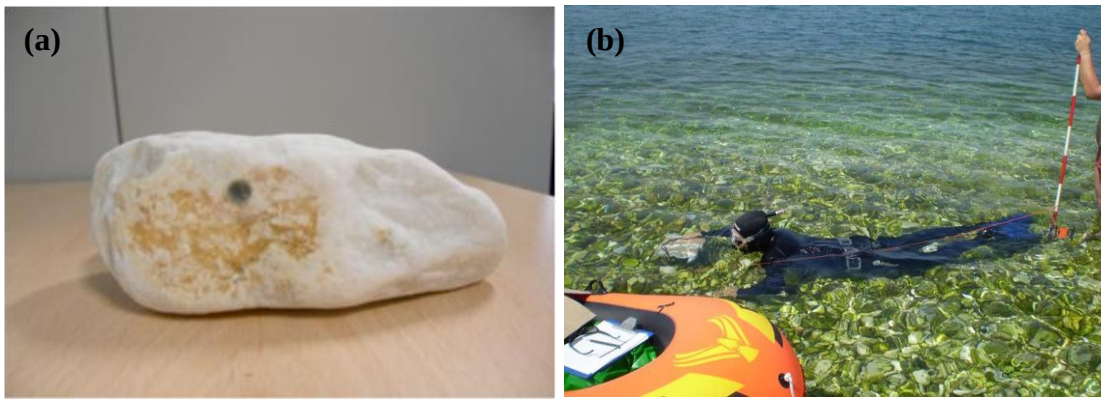

Fig. 2.17 – Environmental tracking of a coastal dynamics [55]. (a) A "Smart Pebble". On its surface is possible to notice a dark hole housing the tag. (b) A moment of the identification operations.

The geologists first tested different tag types such as plastic discs and fiber glass cylinders in laboratory environment, which tried to simulate as much as possible the real environmental conditions [55]. Table 2.2 represents the read range values for different types of tags under ideal conditions (outside water) and real conditions (underwater).

Table 2.2 – Read ranges of different LF tags [55].

Tag housing	Ideal conditions	Real conditions
Transparent disc	50 cm	38 cm
Long glass cylinder (34 mm)	65 cm	56 cm
Short glass cylinder (14 mm)	42 cm	36 cm

Results from saltwater are great results, comparing with ideal results outside saltwater. The results are in accordance with the theoretical analysis, where the achieved read range is lower than the theoretical skin depth of LF systems in saltwater (69 cm), which acts then as an upper bound. This solution has been implemented on different beaches, where the effective use of the system has achieved great results, comparing with the results measured in the laboratorial tests. The tags placed inside the pebbles were located even from distances higher than 50 cm [55].

Achieving a great read range underwater is possible and is influenced mainly by the following factors, low frequency and low conductivity (134.2 kHz and freshwater, respectively), using RF communication protocol that uses frequency modulation (HDX), large size antennas (for tag and reader), high RF power and using multiple antennas on the system. Also, some factors which may decrease the read range such as the presence of nearby metals and reading holes to the RF field should be also taken into account. This system may provide long-term, low-cost and battery-less circuit that can be implemented underwater, giving the opportunity to measure fish stress indicators in real time that may minimize fish welfare concerns.

Chapter 3

RFID SYSTEM FOR SENSING APPLICATION

Summary

This chapter describes the implementation of a RFID system operating at 134.2 kHz to read temperature from a tag located underwater. The entire system uses commercial equipment from Texas Instruments™. Main hardware and software elements of the system are described, as well as the interfaces between some of the elements.

3.1 Introduction

The RFID system of this thesis was implemented using commercial equipment manufactured by Texas Instruments™. The evaluation kit EZ430-TMS37157 includes a RFID system operating at 134.2 kHz for wireless sensing applications at short distances. The kit includes a stationary reader (RI-ACC-ADR2) with integrated RF chip (TMS3705), a control chip (TMS37F158) and a small pluggable low *Q* circular loop antenna. Also, the kit includes a tag with integrated analog front-end (AFE) (TMS37157) and microcontroller (MCU) (MSP430F2274) with an internal temperature sensor. The communication between reader and host computer is made via Universal Serial Bus (USB) interface. Therefore, a USB cable and a pluggable small auxiliary module (daughter board) with a serial to USB converter are also included in the kit, supplying 5 V from the host computer to the reader. A cable with a DC power plug pin is also provided in order to attach an external power supply with voltage up to 12 V to the reader, which increases read range. Although the system is passive, the kit includes a battery board comprising of two AAA sized cells which can be attached to the tag, which only powers its MCU and sensor, turning the tag into a semi-passive tag. Other component of the kit is a USB debugging interface (EZ430-RF), which is used to debug and upload the firmware from the host computer to the MCU of the tag, through Spy-Bi-Wire interface [56].

To extend the read range of the system, a high power RF module (RI-RFM-007b) and two high *Q* gate antennas (RI-ANT-G01E) with an inductance of 27 µH were obtained. The RF module can be used in combination with the ADR2 reader from the kit. Small modifications on the hardware were performed by removing the RF circuitry

(including TMS3705 RF chip) in order to use the ADR2 reader only as a control module, which controls the high power RF module [106]. Besides, uploading an updated firmware to the MCU of the ADR2 reader using a different debugger tool (MSP-FET) was required. Both modules were powered by a linear power supply with 12 V to the control module and a range from 7 to 24 V to the RF module. The circular loop antenna of the kit was replaced by the gate antennas. Figure 3.1 represents the schematic diagram of the implemented RFID system.

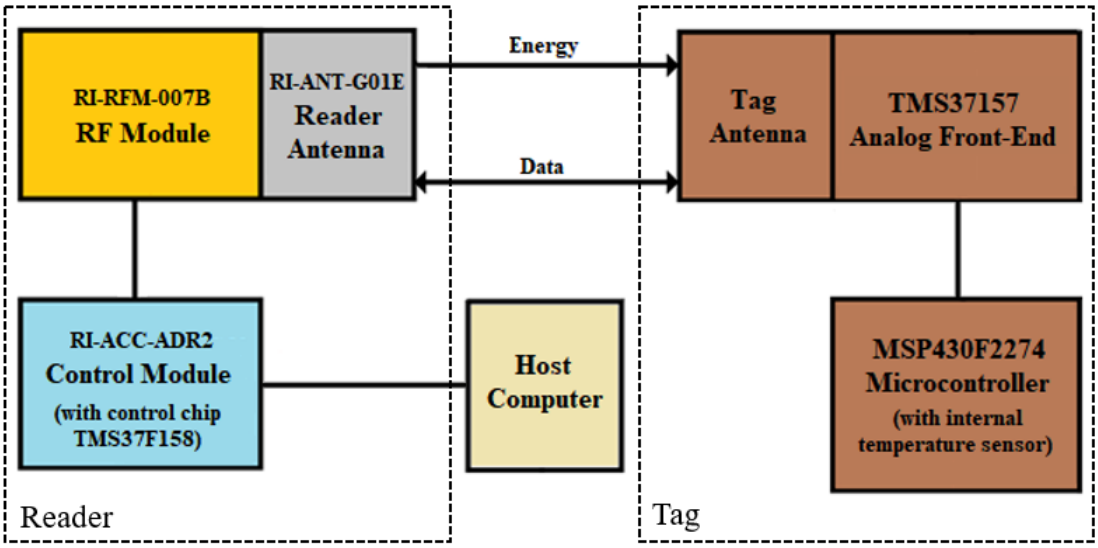

Fig. 3.1 – Schematic diagram of the implemented RFID system.

3.2 Hardware description of the RFID system

This section describes each element which composes our RFID system. Fundamental components of each element, such as the respective MCUs, AFEs and antennas of the tag and the reader, and also the host computer are also described.

3.2.1 Tag

The tag provides a communication interface with the reader over RF field resonating at 134.2 kHz. The TMS37157 AFE, along with the tag antenna, communicates with the reader by using HDX communication protocol, which allows a maximum performance and highest noise immunity between tag and reader. Also, the AFE communicates with the MCU, providing data to the electrically-erasable programmable read-only memory (EEPROM), where data may be stored or accessed. The energy collected by the tag antenna is stored in a capacitor to be used later. The tag features two

LEDs for visual feedback, a push button for user feedback and an internal temperature sensor inside the MCU. The passive tag may supply external modules and components (sensors, switches, LEDs, etc.) over the RF field [56].

3.2.1.1. MSP430F2274 microcontroller

The MSP430F2274 is a 16-bit MCU from the 2xx family of the ultra-low-power MSP430™ family of chips from Texas Instruments™. The supply voltage for the MCU ranges from 1.8 V to 3.6 V. The MCU is capable of operating at frequencies up to 16 MHz and also contains an internal very-low-power low-frequency oscillator (VLO) operating at 12 kHz at room temperature. The MCU offers 32KB program memory, 256 bytes of flash memory and 1 KB of random access memory. The MCU has two 16-bit timers, each with three capture/compare registers. The digitally controlled oscillator (DCO) wakes-up the MCU from low-power mode to active mode in less than 1 µs. The chip contains two universal serial communication interface modules which may support three different communication protocols. One module supports universal asynchronous receiver/transmitter (UART) and serial peripheral interface (SPI), whereas the other supports SPI and inter-integrated circuit ((I^{2}C). A 10-bit analog-to-digital converter (ADC) with internal reference supports conversion rates of up to 200 kbps [57]. The configuration pins of the MSP430F2274 unit are represented in figure 3.2.

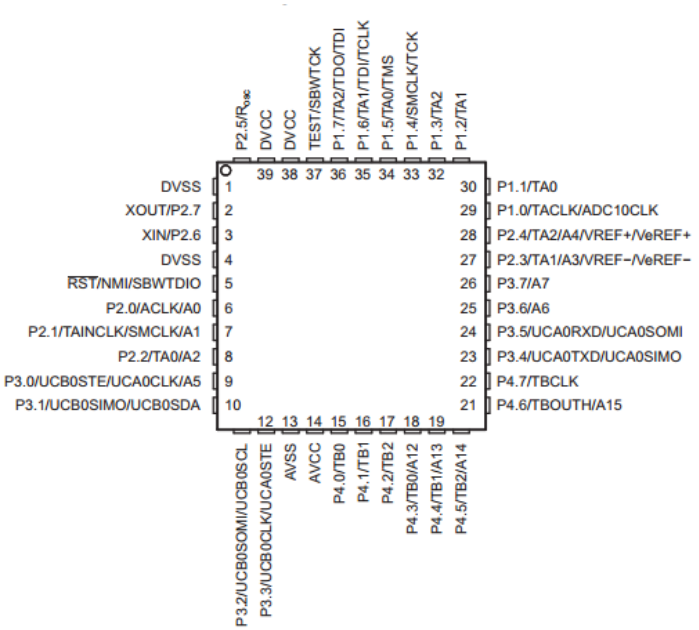

Fig. 3.2 – 40-Pin configuration of the MSP430F2274 unit [57].

3.2.1.2. TMS37157 analog front-end

The TMS37157 is a dual interface passive AFE. The TMS37157 allows the tag to communicate with the reader via RF field and also to communicate with the MSP430F2274 MCU via 3-wire SPI interface. The supply voltage for the AFE ranges from 2 V to 3.6 V. The AFE offers 121 bytes of programmable EEPROM memory, which can be accessed and altered over RF field without battery or through SPI interface by a MCU if a battery is connected [58]. The configuration pins of the TMS37157 unit are represented in figure 3.3.

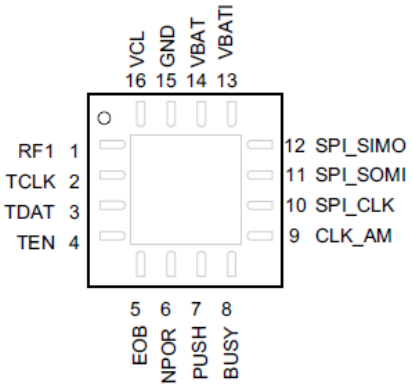

Fig. 3.3 – 16-pin configuration of the TMS37157 unit [58].

3.2.1.3. Tag antenna

The tag antenna is a XY-axis coil winded around a 12 mm ferrite core, which connects to the AFE. The tag antenna provides an inductance of 2.66 mH. A tuning LC circuit is required to achieve a resonance frequency of 134.2 kHz, whose capacitance is about 530 pF. Since there are no commercial available capacitors with standard values of 530 pF, we must use a combination of capacitors in series and in parallel to tune the antenna to the required value. The LC circuit of the tag generally contains a tuning capacitance value of 470 pF and a trimming circuit with a set of different capacitors. The automatic trimming of the LC circuit is usually performed with software assistance, which saves in memory the trim settings in order to switch on only the required capacitors in order to tune the resonance frequency of interest [58].

3.2.2 **Reader**

The reader provides an interface with the tag over RF field resonating at 134.2 kHz. The high power RF module (RI-RFM-007b) is used to drive the gate antennas, to send modulated data to the antenna and to detect and demodulate the response of the tag. The TMS37F158 control chip interfaces between the host computer and the RF module, by executing the commands sent by host computer and coding/decoding the signal to/from RF module. The ADR2 reader features two LEDs for visual feedback and a push button for user feedback. The control chip, along with the gate antenna, communicates with the reader by using HDX communication protocol.

3.2.2.1. TMS37F158 control chip

The TMS37F158 is a 16-bit MCU plus AFE integrated in a control chip from Texas Instruments™. The supply voltage for the chip ranges from 2 V to 3.6 V. The MCU is a 16-bit reduced instruction set computing based on MSP430F123 from the 1xx family of the ultra-low-power MSP430™ chips from Texas Instruments™. The MCU is capable of operating at frequencies up to 8 MHz. The control chip offers 8 KB program memory, 256 bytes of flash memory and random access memory, and 124 bytes of programmable EEPROM memory. The chip has one 16-bit timer, with three capture/compare registers. The DCO wakes-up the MCU from low-power mode in less than 6 µs. The AFE is a LF immobilizer interface which offers a high-level of security through its hardware encryption and mutual authentication with 80-bit security key length. The immobilizer interface is always accessible and operates without the need for a battery [59]. The configuration pins of the TMS37F158 unit are represented in figure 3.4.

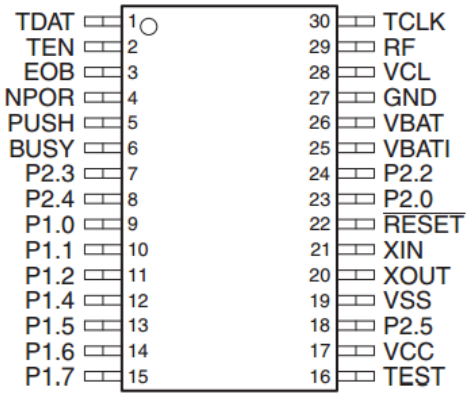

Fig. 3.4 – 30-pin configuration of the TMS37F158 unit [59].

3.2.2.2. RI-RFM-007B RF module

The RI-RFM-007B module combines with a control module and an antenna to form the reader. The RF module drives antennas with total inductance ranges from 26.0 µH to 27.9 µH, containing a capacitive tuning to resonance frequency. The supply voltage for the RF module ranges from 7 V to 24 V. The RF module contains all the analog functions to transmit a signal to a tag, to demodulate the received signal and to send the demodulated data together with clock signal to a control module. Also, the RF module has a protection circuit from damage and malfunction, which sharply limits the transmitter power output if an over-current situation or over-temperature environment exists. The allowed ranges of current and temperature are, respectively, below 1.7 A and -25º C up to +70º C [59].

3.2.2.3. RI-ANT-G01E antenna

The reader antenna is a gate antenna which connects to the RF module to generate the RF field. The gate antenna provides an inductance of 27 µH [60]. A tuning LC circuit is required to achieve a resonance frequency at 134.2 kHz, whose tuning capacitance is about 52 nF. The LC circuit of the reader is generally a set of fixed capacitors with total capacitance value of about 47 nF and a trimming circuit with a set of different capacitors. The trimming of the LC circuit cannot be done automatically, so the trimming capacitors are manually set by jumpers in order to tune to the resonance frequency of interest [42].

3.2.3 Host computer

The host computer is connected to the control module, using an USB interface. The host computer provides the software elements for processing and monitoring data collected by the reader. Also, the host computer uses programming software to develop the firmware and the application codes.

3.3 Communication interfaces between devices

Most interfaces use bidirectional serial communication protocols such as SPI and UART, transmitting data serially bit by bit. SPI is synchronous because a dedicated clock signal to transmit data is required. Generally, the master generates and transmits the clock signal along with data to the slave in order to synchronize communication between two devices. On the other hand, UART is asynchronous because independent clocks on each

device are used to transmit data, requiring both devices to have the same baud-rate, which is typically 9600 bps, in order to communicate with each other. Because the baud-rate is defined in software, the speed of transmission of UART is much lower than in SPI, which relies on hardware.

In this section, four different interfaces using different communication protocols are described. The RFID system and respective interface connections are represented in figure 3.5.

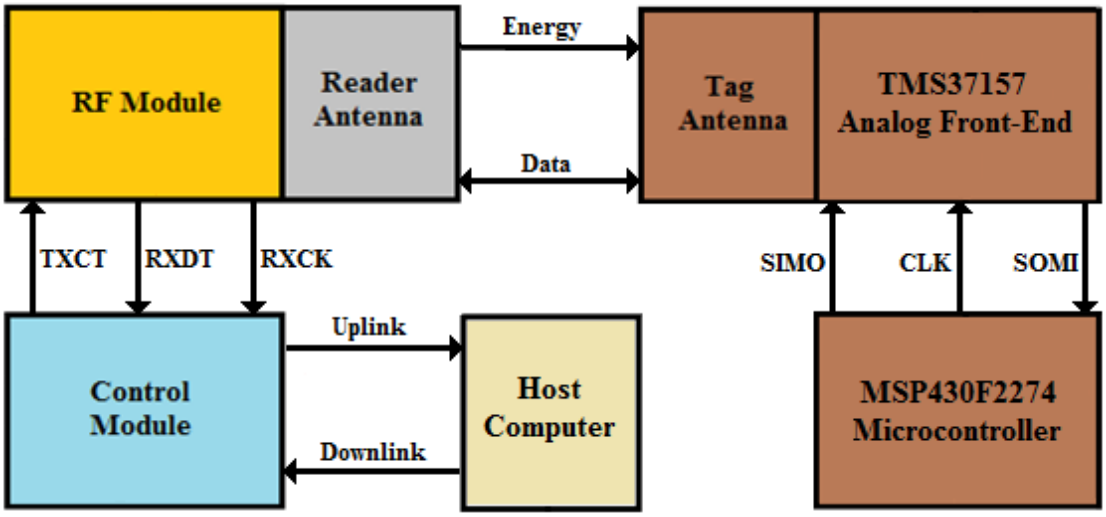

Fig. 3.5 – Schematic diagram of the communication between the elements which integrate the RFID system.

3.3.1 **Interface between AFE and MCU of the tag**

Both MCU and the AFE of the tag are connected to each other through a 3-wire SPI interface. The MCU with the clock sources is designed as the master and the AFE is designed as the slave. The slave-input master-output (SIMO) transmits data along with the clock signal from the MCU to the AFE, whereas the slave-output master-input (SOMI) transmits synchronized data from the AFE to the MCU. To wake up and access to the MCU, a BUSY routine is performed, indicating the availability to communicate data between the two devices. To trim the LC circuit of the tag to 134.2 kHz, a PUSH routine is performed, if a new antenna is connected to the tag. CLKA/M provides clock signals derived from the LC circuit to the MCU, which can be used as a time reference or for trimming measurements. Figure 3.6 shows the interface between MCU and AFE.

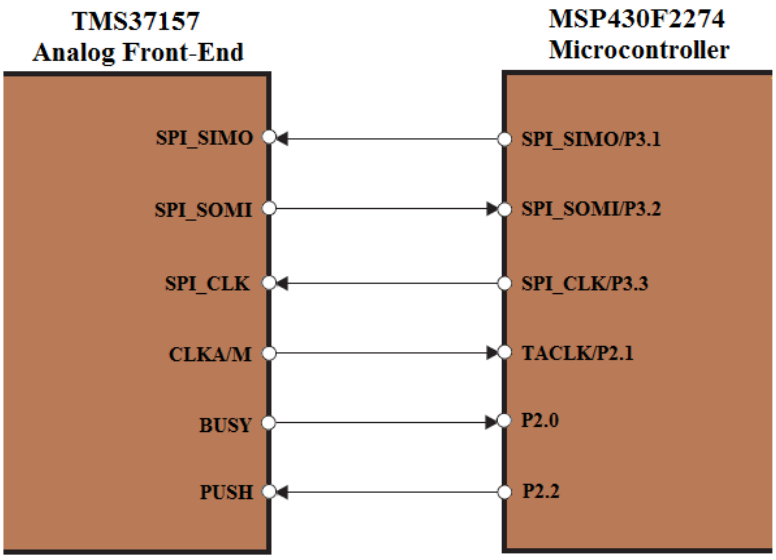

Fig. 3.6 – Interface between the AFE and the MCU of the tag (adapted from [61]).

3.3.2 Interface between control module and RF module

The communication protocol of the interface between control module and RF module is derived from SPI protocol. For the coding of the transmitting data, the control module may use pulse width modulation (PWM) or pulse position modulation (PPM) over TXCT pin. However, the clock signal is not required on transmission, since the modulated data contain pulses with different fixed pre-defined timings for low bit and high bit, respectively [62]. The control module currently uses PPM to interface with the RF module. For the decoding of receiving data, the demodulated data uses the relationship of the signals between the RXDAT and RXCLK pins to transmit data back to the control module. The signal RXCLK is the reference clock signal to decode the RXDAT data stream. The moment RXCLK signal changes from LOW to HIGH during each data bit, current LOW or HIGH state of the RXDAT signal corresponds to a low bit or high bit, respectively. The data stream always starts with the least significant bit (LSB) and ends with the most significant bit (MSB). Figure 3.7 shows the interface between the control module and the RF module of the reader.

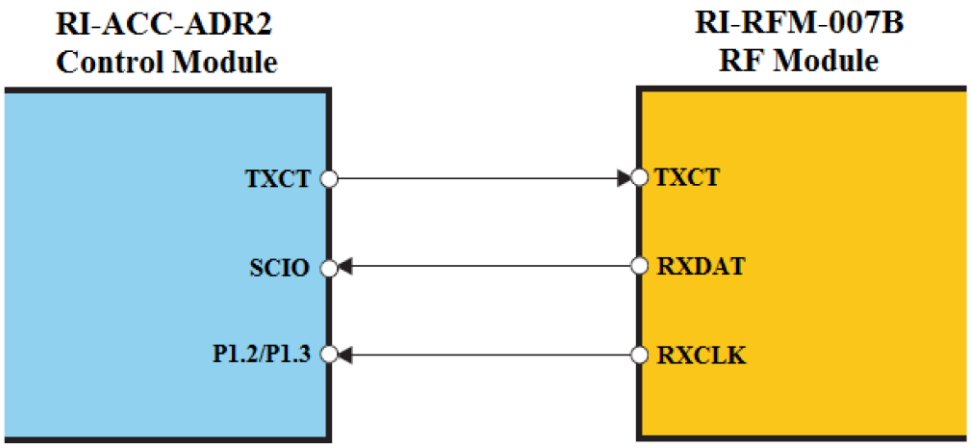

Fig. 3.7 – Interface between the control module and the RF module of the reader (adapted from [43]).

3.3.3 Interface between reader and tag antennas

Modulated data and energy are transferred between reader and tag antennas, over RF field. For transmission of data from reader to tag, the RF module modulates data using PWM and the RF field generated by the reader antenna is amplitude modulated. The generated RF field depends on the pulse width ratio or duty cycle, which can be changed between 0% and 50% for the RF module. When using ratios smaller than 50%, the RF module works in a less efficient way, leading to an increased power dissipation and thus to higher temperature increase, and the strength of the magnetic field decreases for charging the tag. The RF module is typically operating at 50% duty cycle [42]. An example of the pulse width cycle with different ratios is provided in figure 3.8.

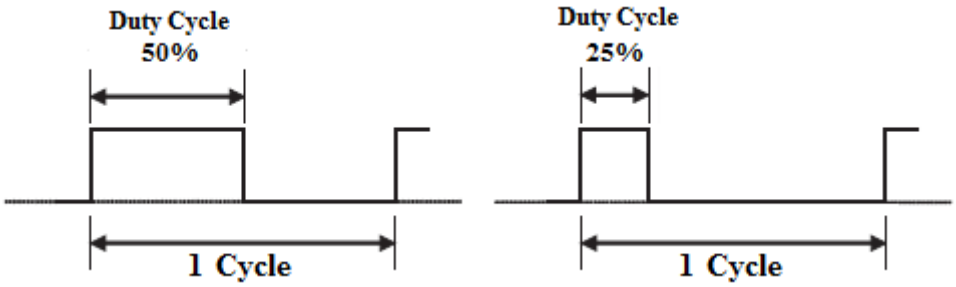

Fig. 3.8 – Example of a pulse width cycle (adapted from [42]). (a) Pulse width ratio of 50%. (b) Pulse width ratio of 25%.

For transmission of data from tag to reader, the tag sends a FSK signal with typical high and low bit frequencies of 123.2 kHz and 134.2 kHz, respectively. The high and low

bits have different durations due to one bit being equivalent to 16 cycles of the frequency. An example of the high bit and low bit modulated in FSK is provided in figure 3.9.

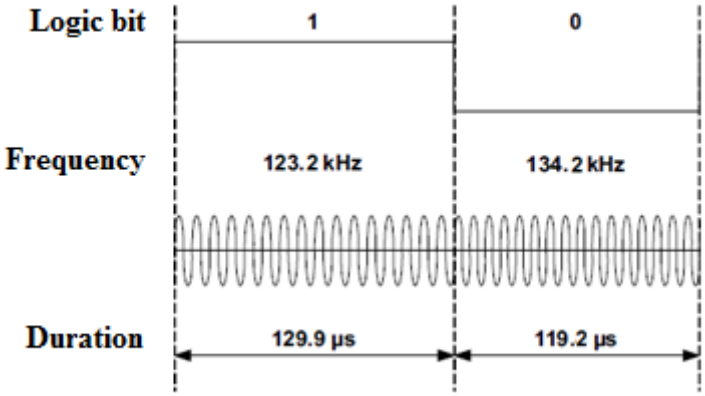

Fig. 3.9 – Example of high bit and low bit modulated in FSK, respectively. The time required for transmitting a high bit and a low bit are slightly different due to slightly difference between modulation frequencies (adapted from [58]).

3.3.4 **Interface between host computer and control module**

The daughter board implements a USB to serial UART interface which emulates a COM port in the operating system (host computer). The typical COM port settings are necessary for communication between the host computer and the control module:

- Bits per second: 9600
- Data bits: 8
- Parity: none
- Stop bits: 1
- Flow control: none

The settings allow the user to transmit and receive serial data over a terminal window at a fixed baud-rate of 9600 bps with no flow control. The data is transmitted/received using a telegram with a variety of fields, corresponding to specific portions of data relative to the telegram. The downlink protocol defines the transmitting telegram and the uplink protocol defines the receiving telegram of the host computer [62]. Two of the most important commands of the application are the battery charge and the MSP access, which are used for the downlink and uplink telegrams.

3.3.4.1. Downlink protocol

The reader sends a telegram with the corresponding command to the tag, starting with the LSB and ending with the MSB. Figure 3.10 provides the downlink protocol structure to initiate a tag command.

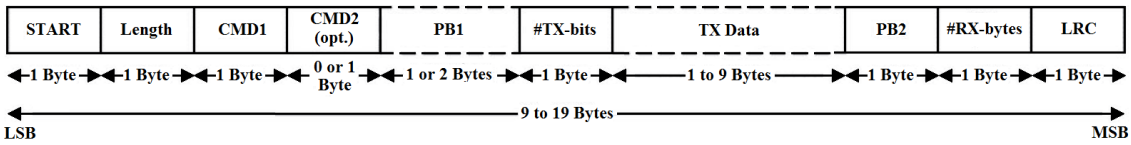

Fig. 3.10 – Downlink protocol structure.

Each byte represents two hexadecimal numbers, being an easier way to represent the information for the users. Table 3.1 provides the explanation of each field on the telegram.

Table 3.1 – Downlink telegram description.

Field	Description
Start	The start byte determines the beginning of the telegram. The start byte is always the hexadecimal number 1 (0x01)
Length	The length byte represents the number of bytes of the whole telegram (except start byte, length and LRC fields).
CMD1	The first command byte provides the instructions to the reader which defines the telegram. Each corresponding bit of the field represents a different instruction, which may define the type of modulation used (PPM or PWM), the existence of a CMD2 in the telegram and also the existence of an additional byte for PB1.
CMD2	The second command byte provides additional instructions to the reader which defines the telegram. The second command byte is usually applied if the telegram is a battery charge command, when the magnetic field must stay on after PB2 and no response is expected.
PB1	The first power burst represents the time in milliseconds to charge the storage capacitor of the tag, which can be extended up to 2 bytes. For 1 byte, the maximum of the power burst is 256 ms. For 2 bytes, the maximum is 4096 ms or approximately 4 seconds.
#TX-bits	The number of data bits transmitted to the tag.
TX Data	Transmitted data, providing instructions and additional information to the tag.
PB2	The second power burst represents the time in ms to charge the storage capacitor of the tag and is normally used for a MSP access command, which requires more energy to activate the MCU and sensors.
#RX-bytes	The number of bytes the tag send back to the reader, which is usually 10 bytes the reader expects to receive (0x0A).
LRC	The longitudinal redundancy check (LRC) calculates a byte over the whole telegram so the reader checks if the transmitted data does not contain errors. The start byte is not included for the calculations.

3.3.4.2. Uplink protocol

The reader sends a different telegram with the corresponding data back to the host computer, regardless of whether or not a tag was in range, starting with the LSB and ending with the MSB. Figure 3.11 provides the uplink protocol structure containing the tag data.

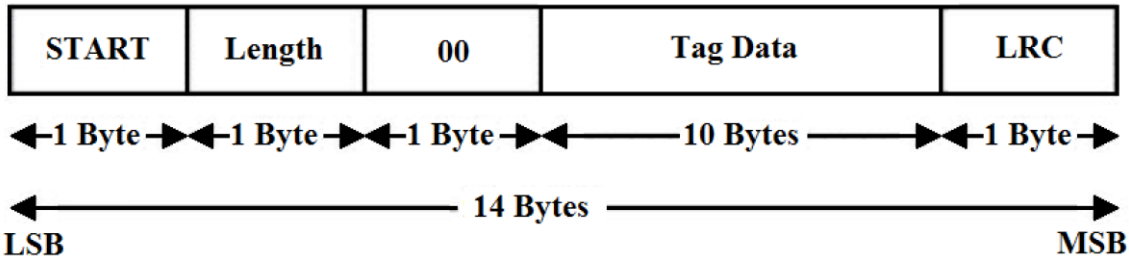

Fig. 3.11 – Uplink protocol structure.

As in downlink protocol, each byte represents two hexadecimal numbers. Table 3.2 provides the explanation of each field on the telegram.

Table 3.2 – Uplink telegram description

Field	Description
Start	The start byte determines the beginning of the telegram. The start byte is always the hexadecimal number 1 (0x01)
Length	The length byte represents the number of bytes of the whole telegram (except start byte, length and LRC fields), being usually 11 bytes (0x0b).
00	Fixed byte, which is always the hexadecimal number 0 (0x00)
Tag Data	Received data from tag, which usually begins with 0x7E. If no tag was detected by the reader or a battery charge command was performed, the reader responds to the host computer by setting the whole Tag Data (10 bytes) to 0 (0x00).
LRC	The LRC is calculated by the reader over all bytes of the incoming or outgoing telegram so the user can calculate the LRC over the data and compare with the received LRC for error detection. The start byte is not included for the calculations.

3.3.4.3. Example of a telegram: battery charge command

Battery charge command is used to activate the RF field of the reader in order to power the MCU of the tag and the attached system battery. When the command is received by the tag, the AFE applies a voltage of about 3.4 V to VBAT pin which leads to the MCU. The charge current depends on the antenna and RF field strength of the reader. The RF field has to remain on after transmitting the telegram. The tag does not answer to a battery charge command, which does not provide a typical uplink structure.

The charging of the battery is only ended once the next command is transmitted by the reader to the AFE of the tag. Figure 3.12 represents an example of the battery charge command for the downlink protocol structure.

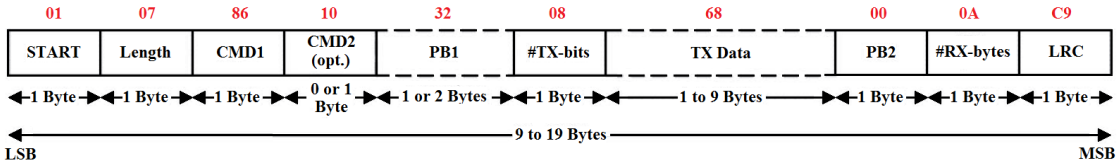

Fig. 3.12 – Example of a structured battery charge command. Every field contains one byte each. The battery charge command is designated as the code 0x68 on TX Data.

3.3.4.4. Example telegram: MSP access command

MSP access command allows the MCU to access the memory of the AFE (EEPROM) and execute a program written on its memory. The MSP access command is mainly used only to transfer data over the RF field directly to the MCU and back to the reader. Figure 3.13 represents an example of the MSP access command for the downlink structure.

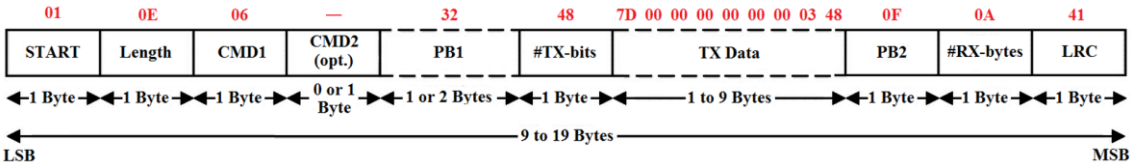

Fig. 3.13 – Example of a structured MSP access command. Every field contains one byte, except CMD2 which contains no bytes and TX Data which contains nine bytes. The MSP access command is designated as the first byte 0x7D on TX Data, along with a set of arbitrary values (0x00). Finally two bytes for a block check character (BCC) checksum in the end of the field (0x03 for MSB of BCC and 0x48 for LSB of BCC).

Contrary to what happens to the battery charge command, the tag answers to a MSP access command, always providing six bytes of data to the reader. Figure 3.14 represents an example of the MSP access command for the uplink structure.

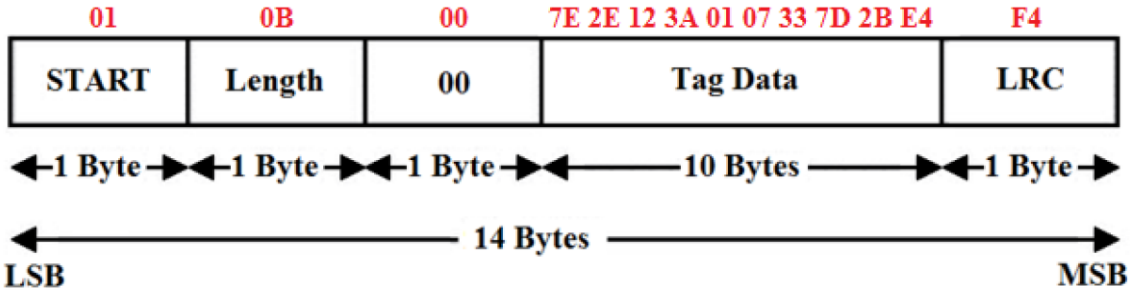

Fig. 3.14 – Example of a structured received response. Every field contains one byte each, except Tag Data which contains 10 bytes. It starts by the first byte (0x7E), following 6 bytes corresponding to sensor data. Next, 0x7D byte corresponds to the MSP access command which was previously sent to the tag and the following two bytes corresponds to a 16-bit BCC checksum.

3.4 Software development

The software is a fundamental part on the RFID system. In order to provide sensor data to the host computer, two firmware programs must be uploaded, one for the reader and the other for the tag. Also, an application program for the host computer must be used for post-processing, data monitoring and data storage.

3.4.1 Firmware

The source code to perform all the necessary functions are written in C and programmed into the MCUs of the tag and the reader. For programming, debugging and uploading the firmware to the MCUs of the reader and tag is required a debugging interface and a software application supporting debugging functionality. The EZ430-RF debugger tool was used to compile and debug the firmware to the MCU of the tag, through Spy-Bi-Wire interface. However, the control module only supports a 4-wire Joint Test Action Group (JTAG) interface (the Spy-Bi-Wire interface of the EZ430-RF corresponds to the 2-wire JTAG). Therefore, a MSP-FET debugger tool with 4-wire JTAG compatibility is used for the control module [63]. The software program used was Code Composer Studio version 6.1.3, which is an integrated development environment to develop software for Texas Instruments™ MCUs. The software provides the writing environment, builds the code, debugs with the help of a debugger tool and upload the firmware to the MCU. Figure 3.15 represents a screenshot of the environment provided by the program.

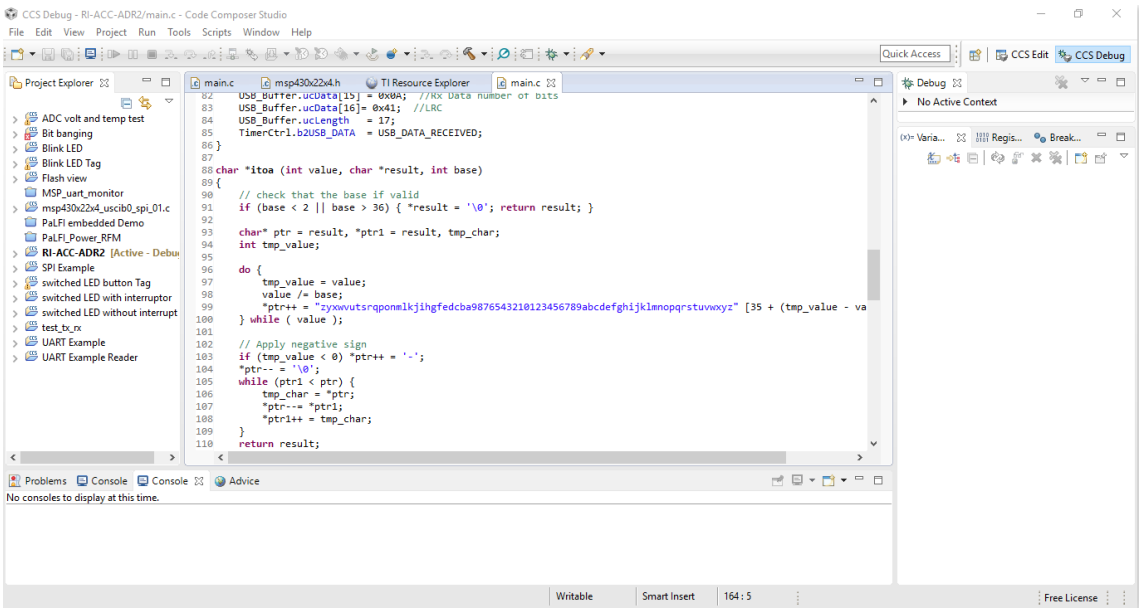

Fig. 3.15 – Screenshot of the work environment of the Code Composer Studio™ software program.

The source codes of the firmware for both reader and tag MCUs were based on the source codes provided by the Texas Instruments™ [56]. The codes were modified and implemented for the sensing application of this thesis.

3.4.1.1. Tag firmware

The tag firmware was modified in order to send sensor data to the host computer. After reset and initialization of the MCU (including ports, timers and SPI), the main program enables two interrupts (BUSY and PUSH interrupts) and enters in low-power mode, waiting for a PUSH button interrupt or a BUSY interrupt. When the PUSH button is pressed, the PUSH pin is set HIGH and a routine is performed to trim the resonance frequency. When the AFE receives an MSP access command, the BUSY pin is set HIGH and also the VBATI pin is set HIGH in order to wake up the MCU. When the AFE resets BUSY, a routine is performed to execute an application program written on memory. The AFE waits until the MCU processes the routine and sends six bytes of data back to the AFE. The RF field of the reader has to stay on, supplying energy to the AFE. When the reader switches off the RF field, the AFE sends the data back to the reader.

The application program written on memory is used to get data from the internal temperature sensor of the MCU and the program needs to be developed for our application. Figure 3.16 provides a flow diagram of the BUSY interrupt service routine. The main program and the PUSH interrupt service routine were not modified [61].

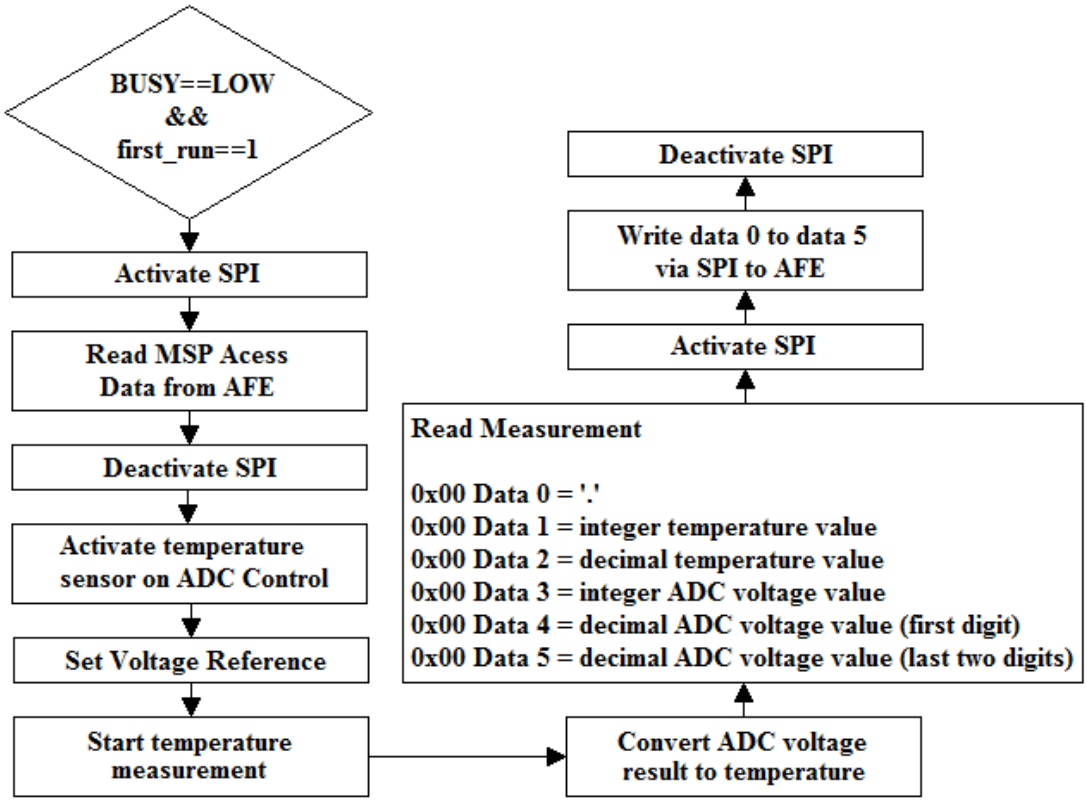

Fig. 3.16 – Flow diagram of the modified BUSY interrupt service routine.

3.4.1.2. Reader firmware

The reader firmware was modified in order to receive sensor data to the host computer every 1 second. After reset and initialization of the MCU, the main program enables a PUSH button interrupt and sets HIGH the state of a LED on the daughter board, turning on the LED and meaning the system is in standby mode. After pressing the push button, the state of the LED toggles from HIGH to LOW, turning off the LED, meaning the system is in active mode. Thus, a battery charge is sent first and then a MSP access command after 1 second to the tag. Then, the reader receives data from the tag and checks if the first byte is a period character, meaning sensor data was received. After check, the

reader sends temperature and ADC voltage to the host computer, each result ending with a newline character, which works as a separator of data. The process is repeated continuously, until the push button is pressed and stops the process, entering in standby mode again. Figure 3.17 provides a flow diagram of the main program.

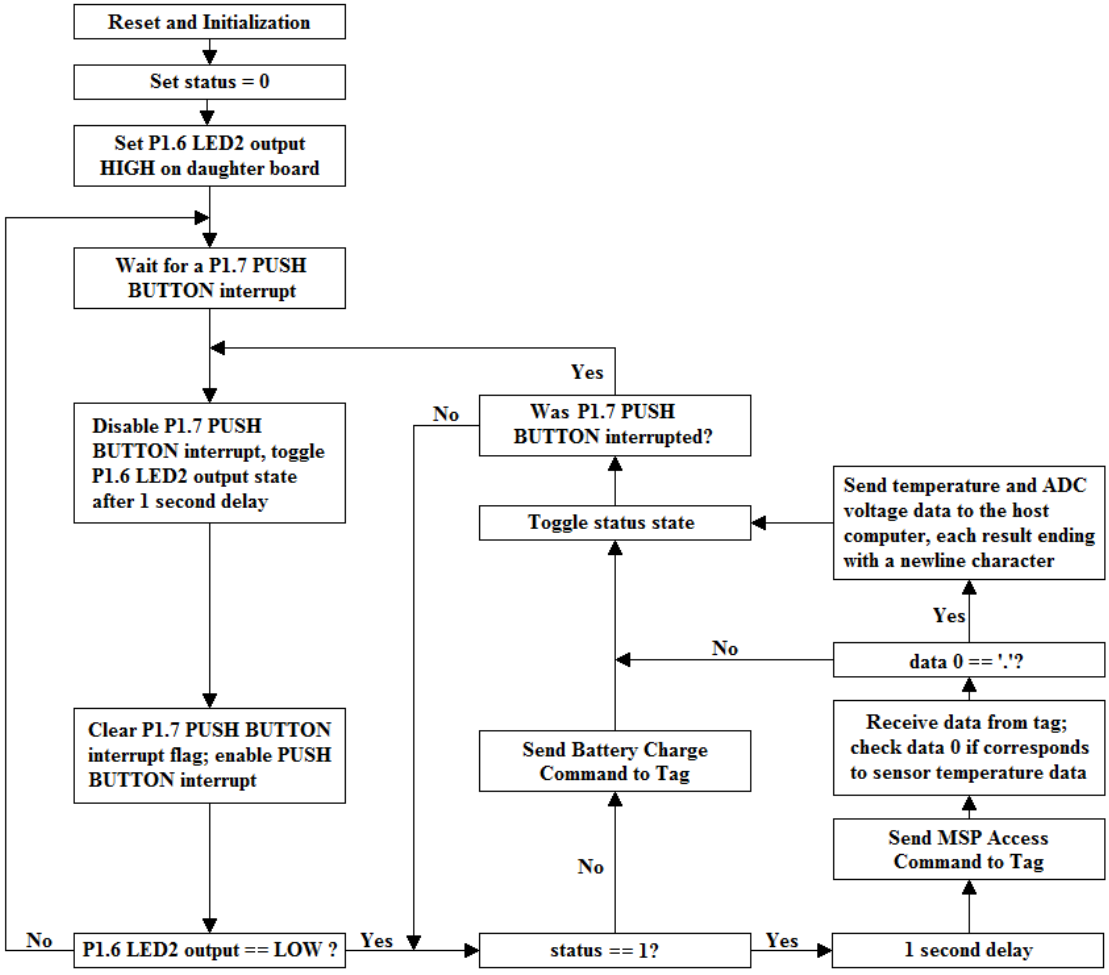

Fig. 3.17 – Flow diagram of the modified main program.

3.4.2 **Application**

The kit provides a GUI application which can be installed in the host computer. The application have some basic functions such as flashing an LED using RF power, performing read/write functions from/to the non-volatile EEPROM memory on the AFE, charging and checking the tag storing capacitor and accessing to the tag MCU. Figure 3.18 provides a screenshot of the GUI application environment provided by Texas Instruments™.

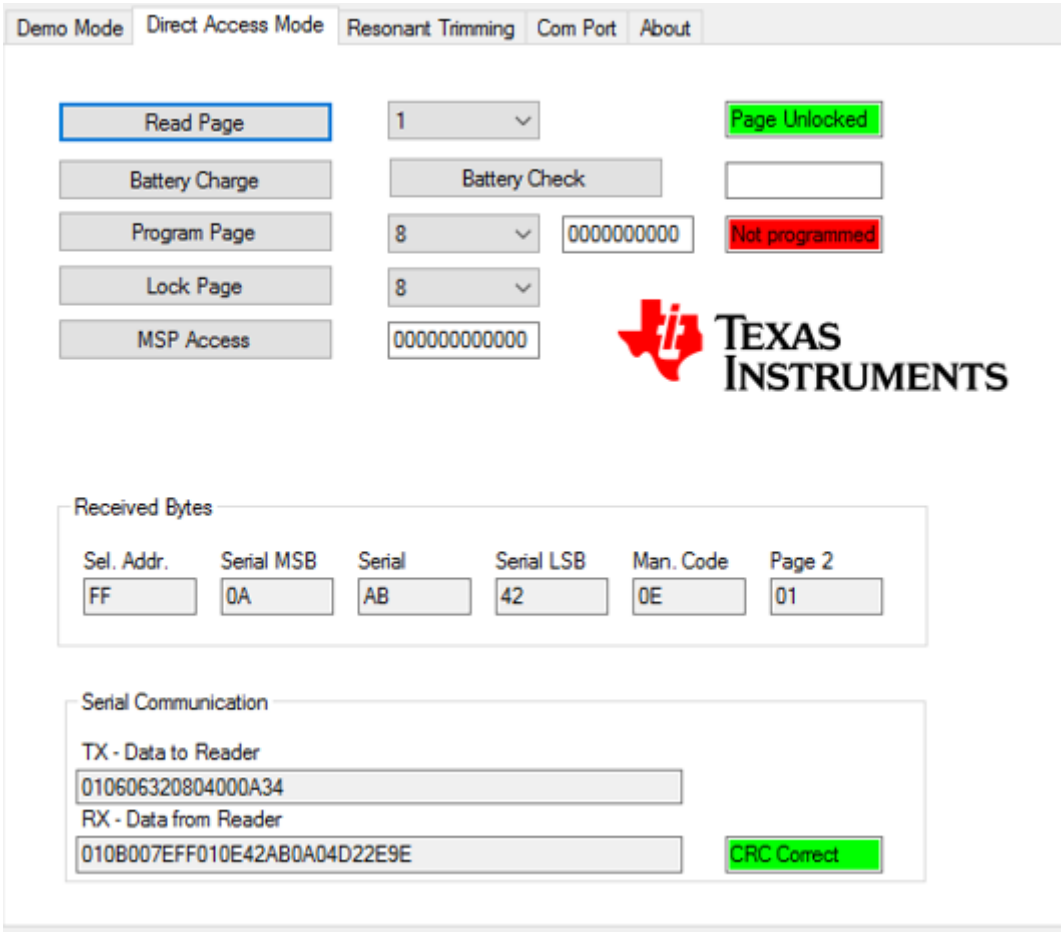

Fig. 3.18 – Screenshot of the work environment of the GUI RFID application provided by Texas Instruments™.

Despite all the features, the GUI application does not provide a function to automatically detect and monitor sensor data. Therefore, an application was developed to get sensor data from reader, displaying the temperature and ADC voltage on a console, plotting the temperature data as a function of the number of samples and storing the data in a file for later usage. The code was programmed using MATLAB® 8.3, where a console is available for monitoring data. After reset and initialization of the software program, a COM port was established with UART serial connection with baud-rate of 9600 bps to communicate with the reader. A text file (.txt extension) is created with the name containing the current date and time in the folder of the program. Then, the first data byte is obtained and the program checks if the byte is a newline character. If the byte is not a newline character, the byte is saved in a temporary memory and gets the next data byte, otherwise all the data bytes relative to the temperature of a single measurement were received. Right after, four fields are printed to the console and also stored in the text file,

the sample number, current data, current time and temperature measurement. Then, the data bytes from the ADC voltage are received and the process is the same, printing an extra field of the ADC voltage result for the same measurement. All the process is repeated as long as the reader is in active mode and transmitting sensor data to the host computer. Figure 3.19 provides the flow diagram of the application.

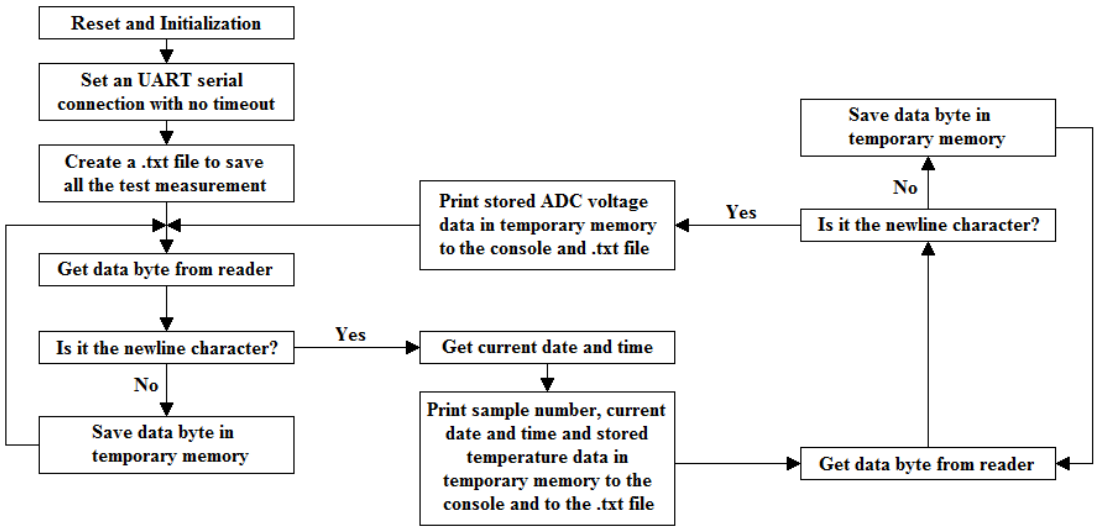

Fig. 3.19 – Flow diagram of the application.

To finish monitoring and data storage, a command is required to close the execution of the program, which runs indefinitely. After interrupting the program, the text file is saved, containing exactly all the information in the console about the data monitoring. Figure 3.20 represents a typical output of the application on the console.

Sample 1	2016-09-24	16:48:33	Temperature=19.41 °C	Voltage=1.756 V
Sample 2	2016-09-24	16:48:34	Temperature=19.41 °C	Voltage=1.756 V
Sample 3	2016-09-24	16:48:35	Temperature=19.41 °C	Voltage=1.756 V
Sample 4	2016-09-24	16:48:36	Temperature=19.41 °C	Voltage=1.756 V
Sample 5	2016-09-24	16:48:37	Temperature=19.82 °C	Voltage=1.759 V
Sample 6	2016-09-24	16:48:38	Temperature=19.82 °C	Voltage=1.759 V
Sample 7	2016-09-24	16:48:39	Temperature=19.41 °C	Voltage=1.756 V
Sample 8	2016-09-24	16:48:41	Temperature=19.82 °C	Voltage=1.759 V
Sample 9	2016-09-24	16:48:42	Temperature=19.82 °C	Voltage=1.759 V
Sample 10	2016-09-24	16:48:43	Temperature=19.41 °C	Voltage=1.756 V
Sample 11	2016-09-24	16:48:44	Temperature=19.82 °C	Voltage=1.759 V
Sample 12	2016-09-24	16:48:45	Temperature=19.41 °C	Voltage=1.756 V
Sample 13	2016-09-24	16:48:46	Temperature=19.82 °C	Voltage=1.759 V
Sample 14	2016-09-24	16:48:47	Temperature=19.82 °C	Voltage=1.759 V
Sample 15	2016-09-24	16:48:48	Temperature=19.41 °C	Voltage=1.756 V
Sample 16	2016-09-24	16:48:49	Temperature=19.41 °C	Voltage=1.756 V
Sample 17	2016-09-24	16:48:50	Temperature=19.82 °C	Voltage=1.759 V
Sample 18	2016-09-24	16:48:51	Temperature=19.82 °C	Voltage=1.759 V
Sample 19	2016-09-24	16:48:52	Temperature=19.41 °C	Voltage=1.756 V
Sample 20	2016-09-24	16:48:53	Temperature=19.41 °C	Voltage=1.756 V
Sample 21	2016-09-24	16:48:54	Temperature=20.24 °C	Voltage=1.761 V
Sample 22	2016-09-24	16:48:55	Temperature=19.41 °C	Voltage=1.756 V
Sample 23	2016-09-24	16:48:56	Temperature=19.82 °C	Voltage=1.759 V
Sample 24	2016-09-24	16:48:57	Temperature=19.41 °C	Voltage=1.756 V
Sample 25	2016-09-24	16:48:58	Temperature=19.41 °C	Voltage=1.756 V
Sample 26	2016-09-24	16:48:59	Temperature=19.82 °C	Voltage=1.759 V
Sample 27	2016-09-24	16:49:00	Temperature=19.41 °C	Voltage=1.756 V
Sample 28	2016-09-24	16:49:01	Temperature=19.41 °C	Voltage=1.756 V

Fig. 3.20 – Example of an output on the console where 28 measurements were taken in 28 seconds, displaying the temperature values and respective ADC voltage.

After closing the program, a plot with the acquired temperature values are displayed as a function of the sample number as represented in figure 3.21. The measurements in figure 3.21 were taken in a different date and time relative to the measurements on figure 3.20.

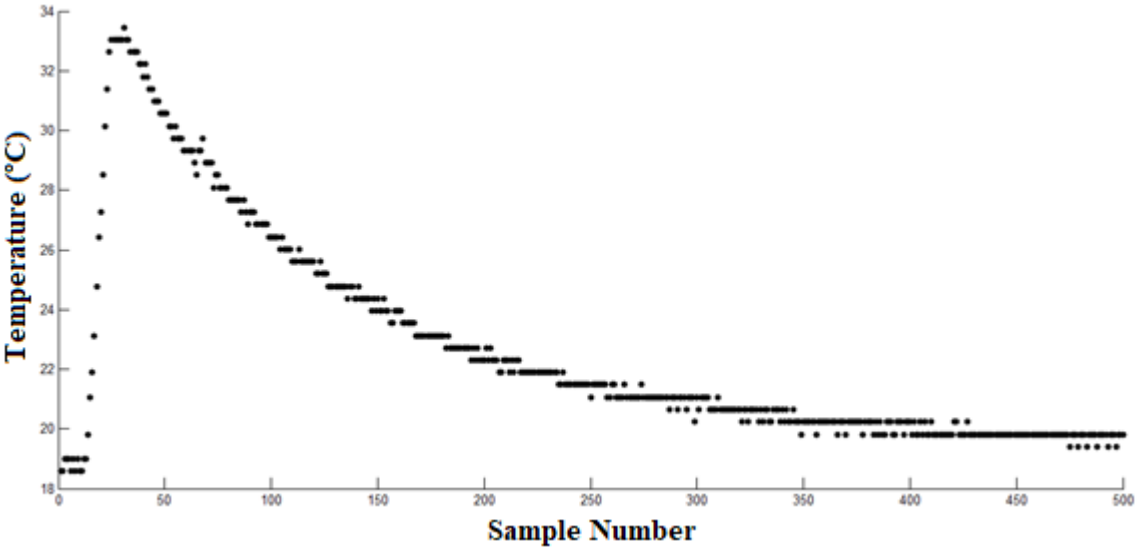

Fig. 3.21 – Example of a graphic of temperature as a function of the sample number (total of 500 samples were acquired).

The development of the sensing application to transmit remotely temperature data has been done successfully. The optimization of the RFID system to achieve the largest read range underwater in order to transmit the sensor data from the tag placed underwater to the reader outside water is important for this application.

Chapter 4

EXPERIMENTAL WORK

Summary

This chapter describes the experimental work carried out in the thesis. The different parts of the RFID system were characterized, including the two large reader antennas and a high power RF module. The read range of the RFID system is evaluated in air as well as underwater. Different spatial configurations for the reader antennas were tested. The system was optimized to cover the entire volume of a water tank with the dimensions of 30 cm height, 70 cm length and 40 cm width. The detrimental effects on the performance of the system caused by metallic elements in the proximity of the antennas are also described.

4.1 Introduction

The schematic diagram of the mounted RFID system is represented in figure 5.1. The diagram calls the attention for three parameters, the read range *d*, the tuning capacitance *C* and the DC current *i* provided to the RF module. The larger the current *i*, the higher the magnetic field, thus the longer is the read range *d*. For a fixed inductance of the reader antenna, a variable capacitor in RF module is important for tuning correctly the LC circuit.

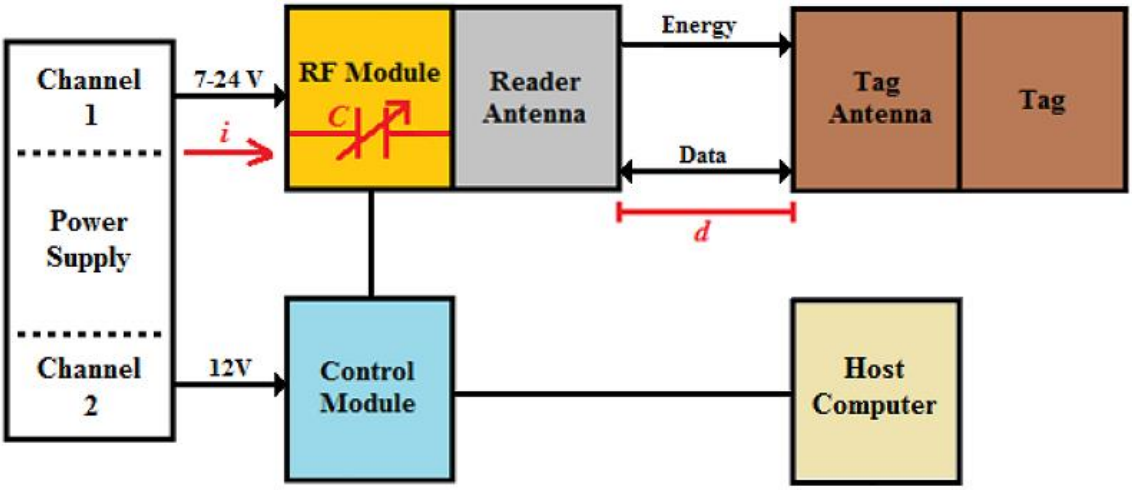

Fig. 4.1 – Block diagram of the implemented RFID system. It is represented the three parameters which influence the communication distance between reader and tag. The DC current *i* is flowing to the RF module, the maximum distance *d* between reader and tag antennas and the tuning capacitance *C*.

We measure how *d* depends on *i* and *C*. The current *i* was measured with an ammeter connected in series in the positive pole of power supply to the RF module. The distance *d* was measured by using a ruler placed between reader and tag antennas. The capacitance *C* was measured using an LCR meter (Fluke PM6306).

The system was first tested in air using one gate antenna (single-antenna system) and later using two gate antennas (multi-antenna system). Once the multi-antenna system was optimized, the system was evaluated to perform readings in a water tank with the dimensions of 30 cm height, 70 cm length and 40 cm width. The tag placed underwater was encapsulated.

4.2 Characterization of RF components

In this section, the different parts of our RFID system are electrically characterized. Detrimental effects which detune the antennas caused by the presence of metallic elements in the proximity of the RF field or additional extended cables connected to the reader antenna are also presented and discussed.

4.2.1 **Characterization of the RF module**

The reader must be tuned to the frequency of 134.2 kHz. This is achieved by using a configuration of fixed capacitors and additional trimming capacitors in the RF module which can be set by jumpers. The tuning capacitance is achieved when the antenna drives the maximum DC current from the power supply, meaning the reader is tuned. The graphic of the DC current as function of the capacitance is represented in figure 4.2.

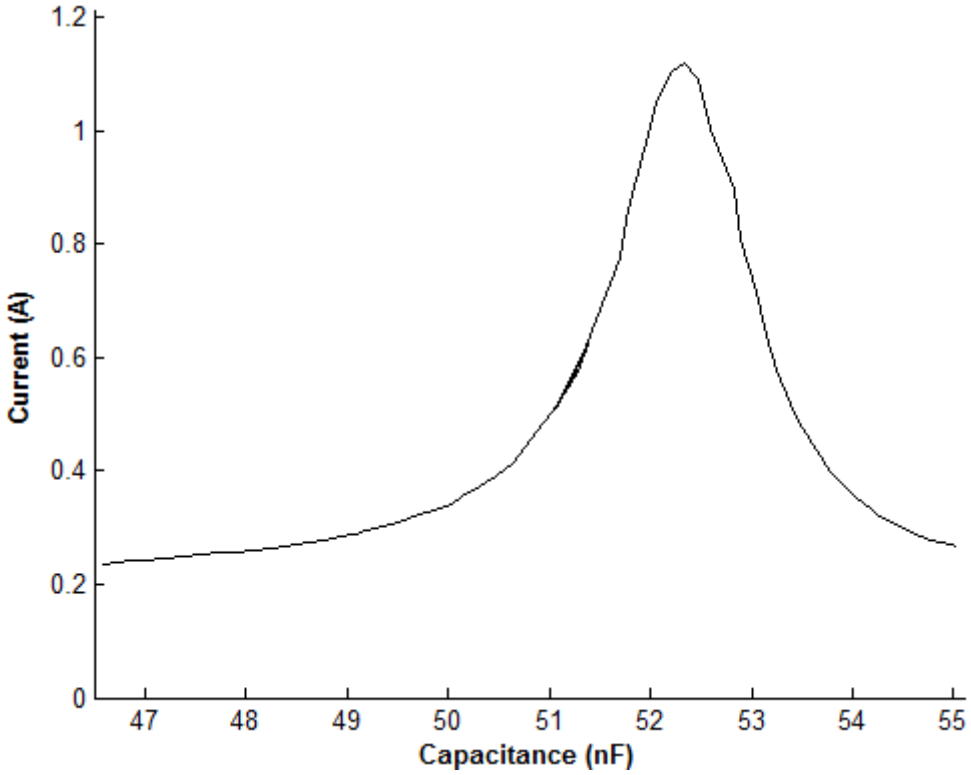

Fig. 4.2 – The variation of the DC current provided by the RF module as function of the capacitance.

Figure 4.2 shows a typical bell-shaped curve of the current versus capacitance. The peak current value of 1.12 A corresponds to a capacitance value of 52.33 nF to balance the circuit and get the maximum performance of the antenna. The measured tuning capacitance value is slightly different from the theoretical value of 52.09 nF estimated using equation 2.2 and 27 µH of inductance.

4.2.2 **Characterization of the gate antenna**

The antenna performance depends on the inductance *L*, resistance *R* and quality factor *Q*. We measured the antenna parameters as function of the frequency. The frequency responses of the inductance, resistance and quality factor of the antenna are represented in figures 4.3, 4.4 and 4.5, respectively.

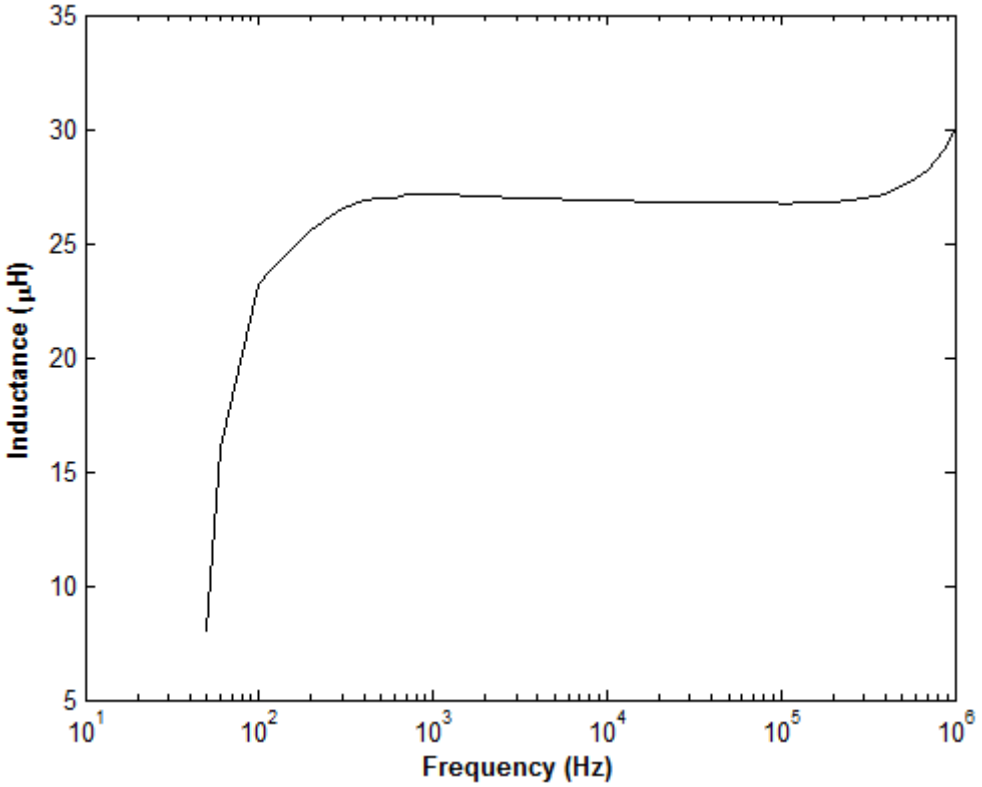

Fig. 4.3 – Frequency response of the antenna inductance.

Figure 4.3 shows the frequency dependence of the antenna inductance *L*. For low frequencies, *L* is low but increases rapidly with frequencies up to 1 kHz, reaching a plateau of approximately 27 μH for frequencies above 1 kHz. This value is in agreement with the typical value in datasheet of the gate antenna [46].

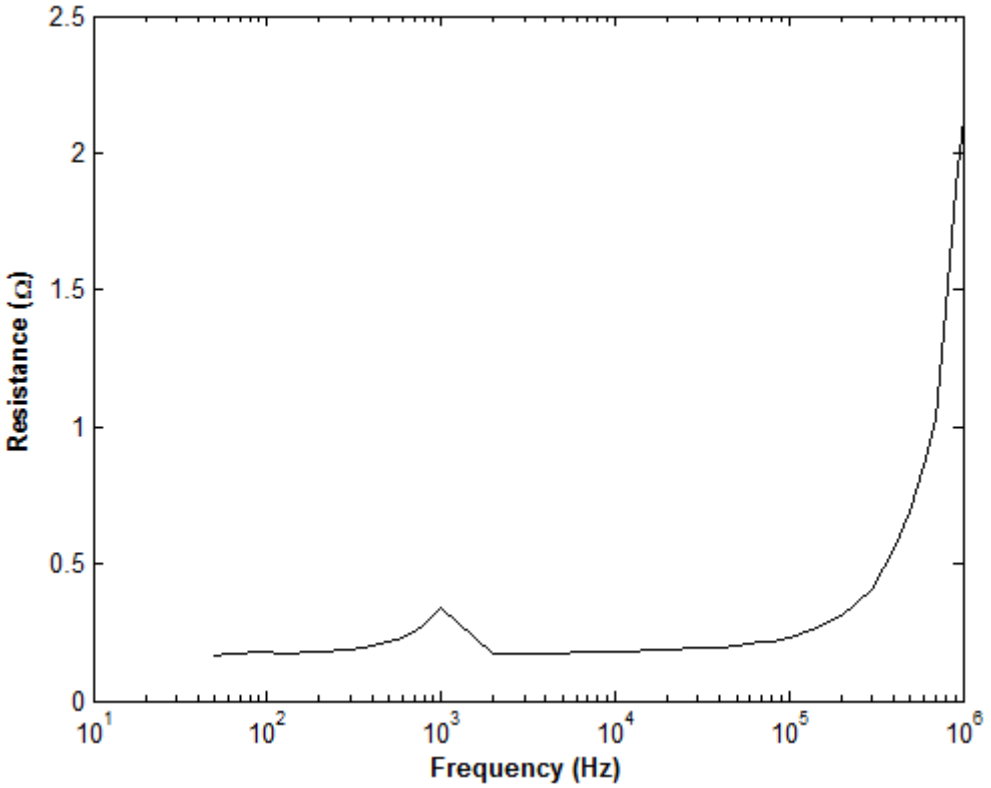

Fig. 4.4 – Frequency response of the antenna resistance.

Figure 4.4 shows the frequency dependence of the antenna resistance *R*. For low frequencies, *R* is low with values approximately 0.2 Ω. For frequencies above 100 kHz, *R* increases rapidly, reaching approximately 2 Ω. At the frequency of 134.2 kHz, *R* is nearly 0.25 Ω, slightly higher than a typical value of nearly 0.23 Ω estimated using equation 2.4, 27 μH of inductance and a typical quality factor value of 100 on the basis of the information provided on the product datasheets [46].

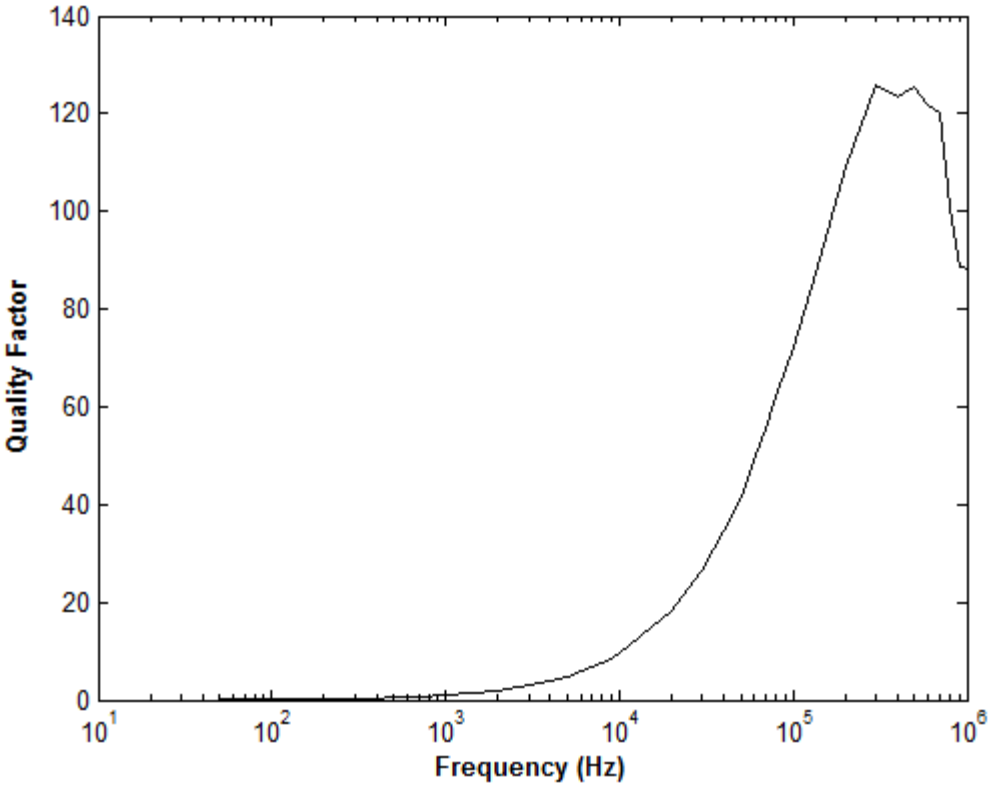

Fig. 4.5 – Frequency response of the quality factor of the antenna.

Figure 4.5 shows the frequency dependence of the antenna quality factor *Q*. For low frequencies, *Q* is low but increases rapidly with frequency up to 200 kHz, reaching a maximum value of approximately 130. At 134.2 kHz, *Q* is 87.5, a lower value than the one expected on the basis of the information provided on the product datasheets [46].

4.2.2.1. Parasitic effects caused by additional wires

The high *Q* gate antenna of the reader is composed of a special cable with low resistance called litz wire. Antennas are well described by LC equivalent circuits. Figure 4.6 shows the equivalent circuit of our antenna at the frequency of 134.2 kHz.

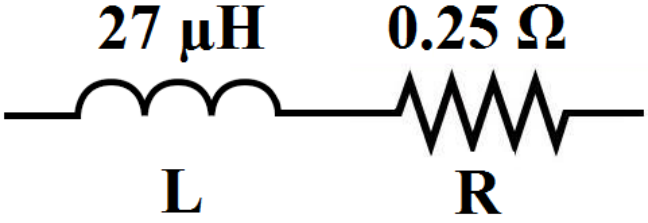

Fig. 4.6 – Equivalent circuit of the reader antenna. The resistance and inductance of the reader antenna were measured for a frequency of 134.2 kHz.

One of the factors which changes the inductance and resistance of the antenna is the length of the external connecting cable. The high *Q* antenna integrates a one-meter length antenna cable, which allows the antenna loop to be separated from the RF module and the longer the cable, the greater the losses introduced to the antenna, which can detune the LC circuit. Typically, for every meter length of added cable, the total inductance value of the antenna increases by approximately 0.5 µH [46]. Along with the one-meter length cable integrated in the gate antenna, one additional one-meter length cable was connected to the gate antenna. Unfortunately, adding extra cables also adds extra resistance and *Q* drops, decreasing the performance of the system. Figure 4.7 represents the equivalent circuit of the antenna connected with an extra one-meter length cable.

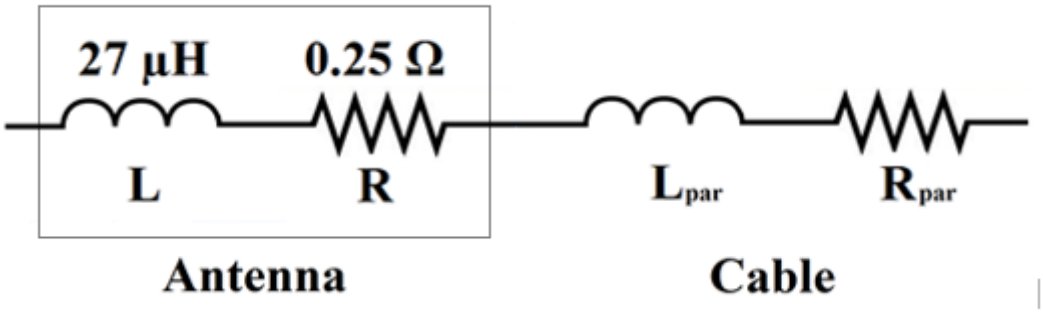

Fig. 4.7 – Equivalent circuit of the reader antenna connected in series with a one-meter length cable. The resistance and inductance of the reader antenna were measured for a frequency of 134.2 kHz.

An increase of 0.5 µH in the inductance is enough to detune the resonance frequency. Figure 4.8 compares the supply DC current as function of the capacitance of the gate antenna (with additional one-meter length cable), with the current of the standard (without extra cable) gate antenna.

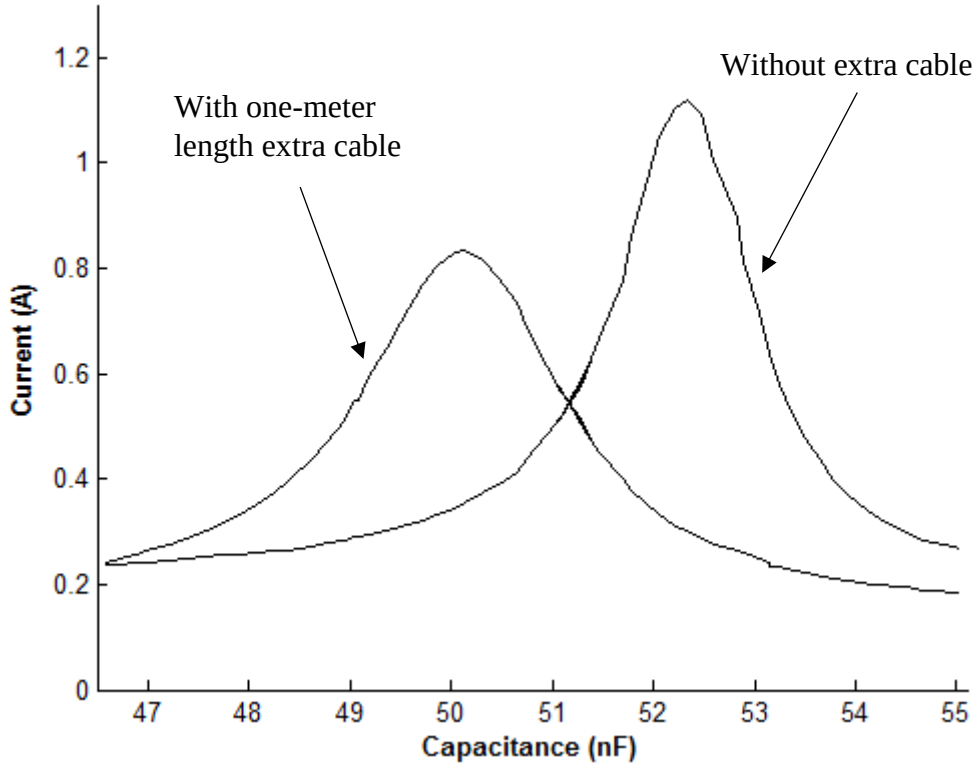

Fig. 4.8 – The magnitude of the supply DC current versus capacitance tuning of the RF module, with and without extra cable added in the terminals of the antenna.

Figure 4.8 shows the changes in the supply DC current provided to the antenna when an additional cable is added. The presence of an additional cable forces the resonance peak in current to move for lower capacitance values. In addition, the current magnitude decreases about 25%. Therefore, adding a one-meter cable to the antenna detunes the system and decrease the read range.

4.2.2.2. Parasitic effects caused by nearby metals

The presence of a nearby metal also affects the gate antenna. The metal acts as an antenna by absorbing and reflecting the energy of the magnetic field generated by the antenna, reducing the read range of the antenna. Figure 4.9 represents how the antenna supply DC current changes as the antenna moves away from a metal plate placed in a position parallel to the antenna.

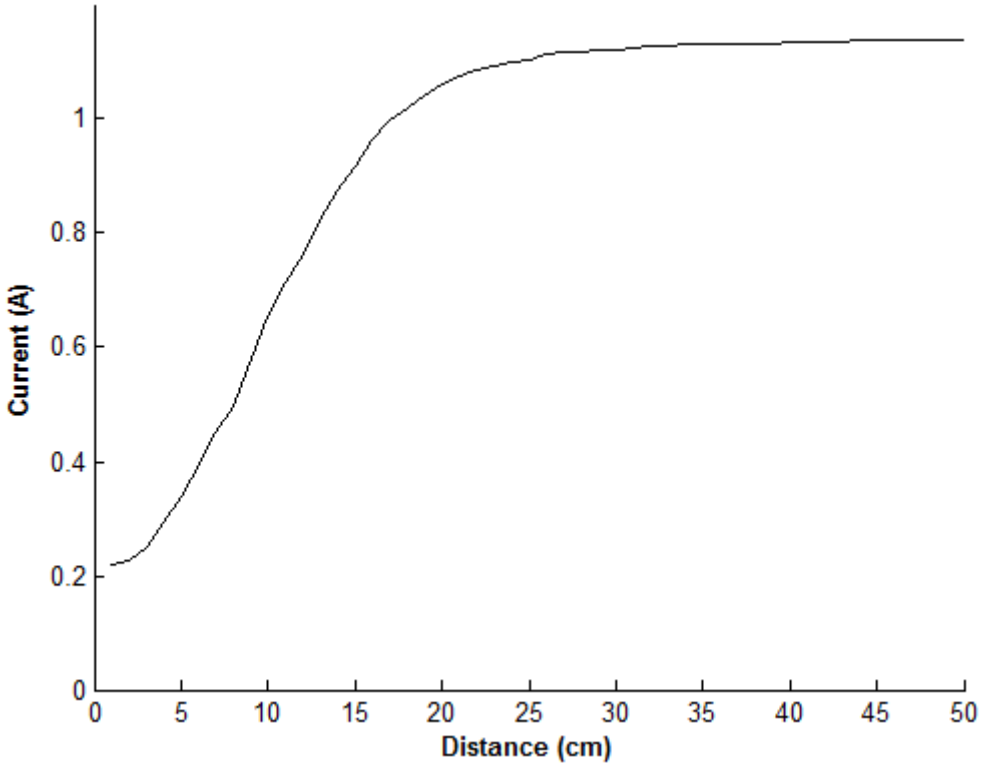

Fig. 4.9 – The influence of a metal plate in the vicinity of a reader antenna. The shorter the distance between the metal plate and the antenna the lower is the supply DC current.

Figure 4.9 shows the dependence of the antenna current *i* as function of the distance to an interfering parasitic metal plate. When the metal plate is 1 cm away, *i* is 0.22 A. As the metal moves away from the antenna, *i* increases. After a distance of 30 cm between the parasitic metal plate and antenna, the influence of the metal on *i* becomes null.

The variation of the antenna inductance, resistance and quality factor with the distance to a parasitic metal plate are shown in figures 4.10, 4.11 and 4.12, respectively.

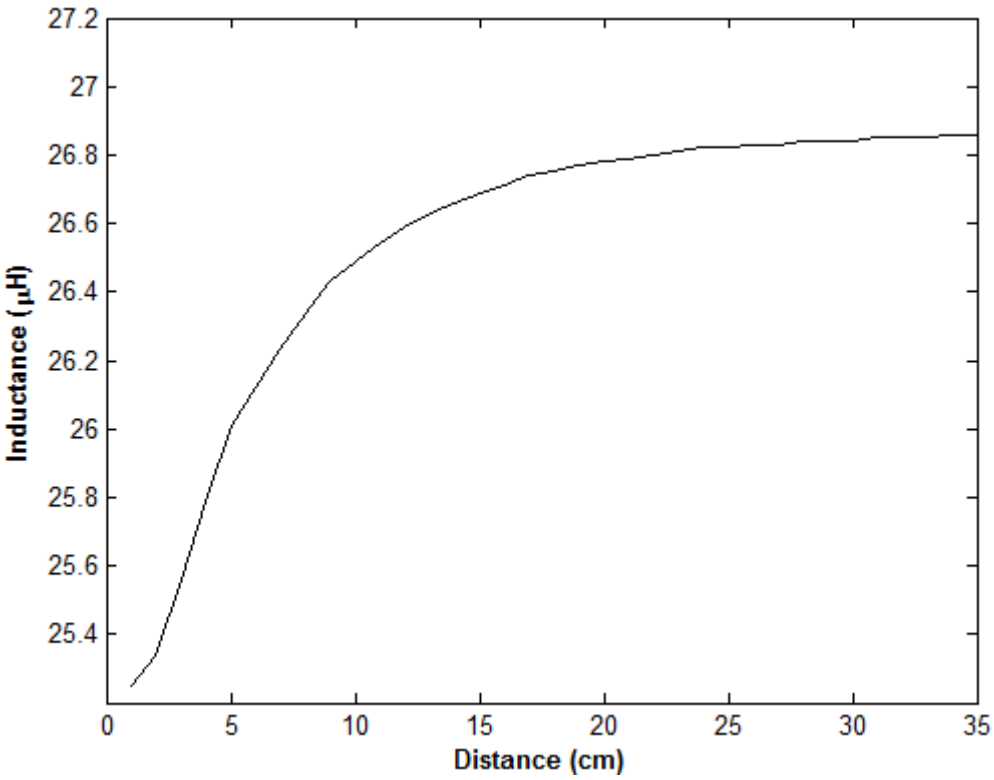

Fig. 4.10 – Antenna inductance as function of the distance between a parasitic metal plate and the antenna.

Figure 4.10 shows the dependence of the antenna inductance *L* as function of the distance to an interfering parasitic metal plate. When the metal plate is 1 cm away, *L* is 25.25 µH, which is lower than the nominal value of 27 µH. As the metal moves away from the antenna, *L* increases and it will approach the value of 27 µH. After a distance of 30 cm between the parasitic metal plate and antenna, the influence of the metal on *L* becomes null.

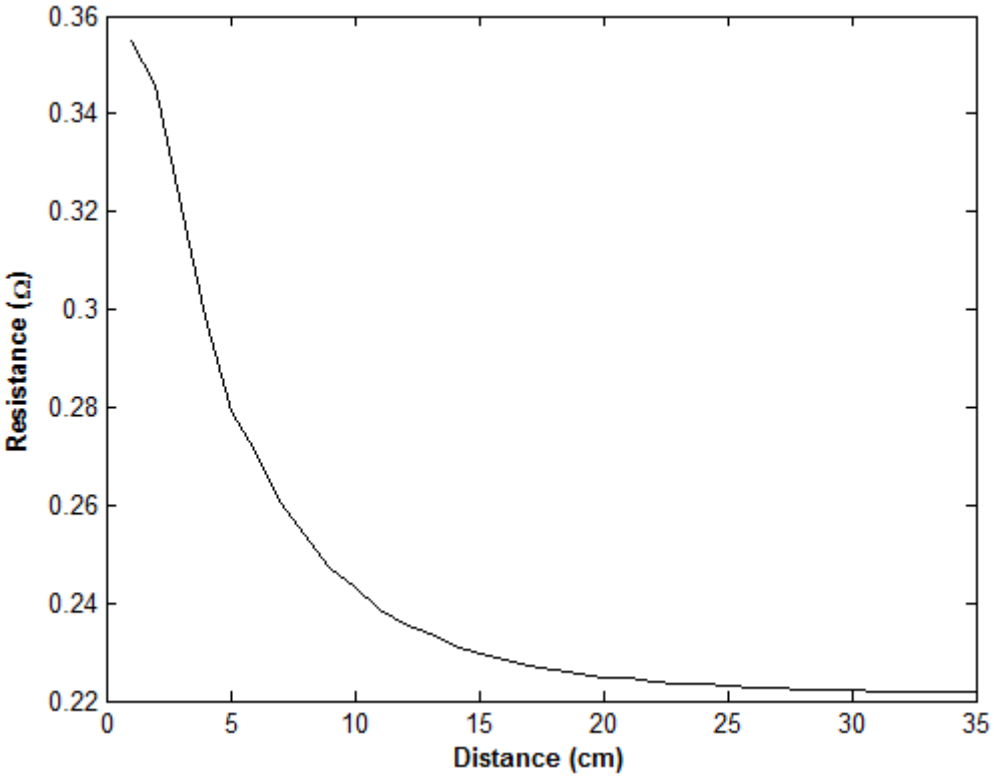

Fig. 4.11 – Antenna resistance as function of the distance between a parasitic metal plate and the antenna.

Figure 4.11 shows the dependence of the antenna resistance *R* as function of the distance to an interfering parasitic metal plate. When the metal plate is 1 cm away, *R* is 0.36 Ω, which is higher than the nominal value of 0.23 Ω. As the metal moves away from the antenna, *R* decreases. After a distance of 30 cm between the parasitic metal plate and antenna, the influence of the metal on *R* becomes null.

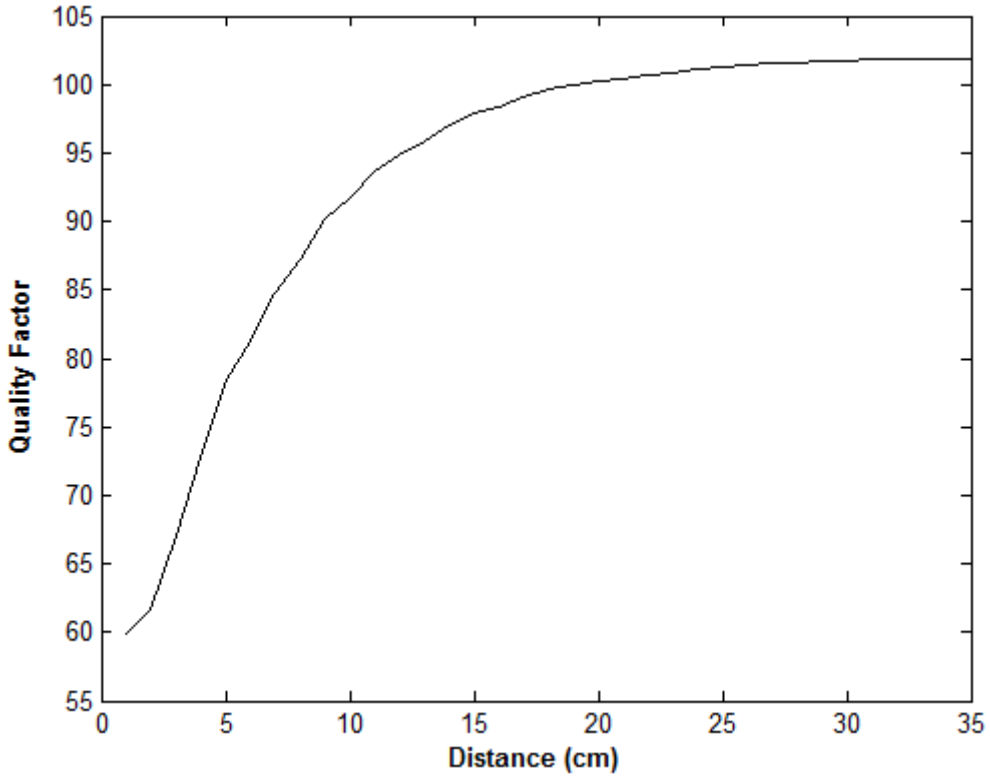

Fig. 4.12 – Antenna quality factor as function of the distance between a parasitic metal plate and the antenna.

Figure 4.12 shows the dependence of the antenna quality factor *Q* as function of the distance to an interfering parasitic metal plate. When the metal plate is 1 cm away, *Q* is 60, which is lower than the nominal value of 100. As the metal moves away from the antenna, the *Q* increases. After a distance of 30 cm between the parasitic metal plate and antenna, the influence of the metal on antenna resistance becomes null.

In summary, the presence of nearby metals degrades the characteristics of the antenna. A distance of 30 cm is considered a safe distance between a parasitic metal and the gate antenna.

4.3 Read range measurement using single-antenna system

One of the most important factors in a communication system is the read range where two devices can reliably communicate to each other. Maximizing the read range is important to make an efficient system when the device must be detected for large distances.

4.3.1 Characterization of the mutual coupling between two antennas

Mutual coupling is the interaction between multiple antennas. Noise and undesirable signals can be received by external systems through mutual coupling, which degrades the performance of the system. Mutual coupling can be avoided if the antennas are placed in perpendicular to each other or by "nulling-out" technique. The induced AC voltage can be measured using an oscilloscope connected to a receiving reader gate antenna while our RFID system is performing normally. Figure 4.13 represents the schematic diagram used of a simulation between two antennas mutually coupled.

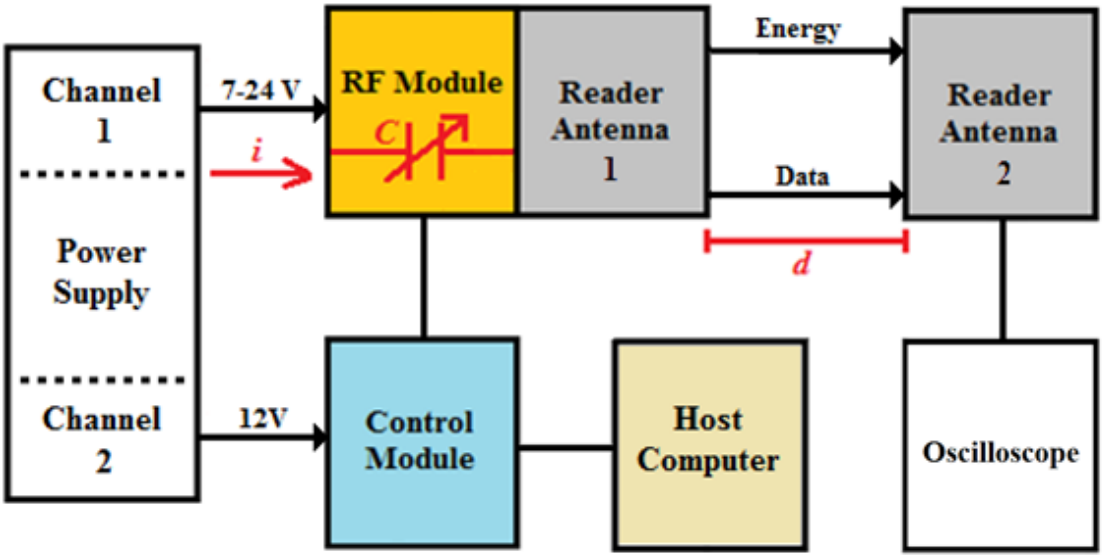

Fig. 4.13 – Schematic diagram to perform the measurements of the induced voltage.

The induced voltage to the receiving reader antenna falls off with the distance away from the reader as $1/d^3$ where d is the distance between antennas. Induced voltage was first measured when antennas were placed in parallel to each other and then when antennas were placed in perpendicular to each other. The induced AC voltage value

measured in the oscilloscope is the peak voltage of the received signal in the antenna. Figure 4.14 represents the induced AC peak voltage as function of the distance obtained from the “nulling-out” technique for “in-parallel” and “in-perpendicular” antennas with different input DC currents.

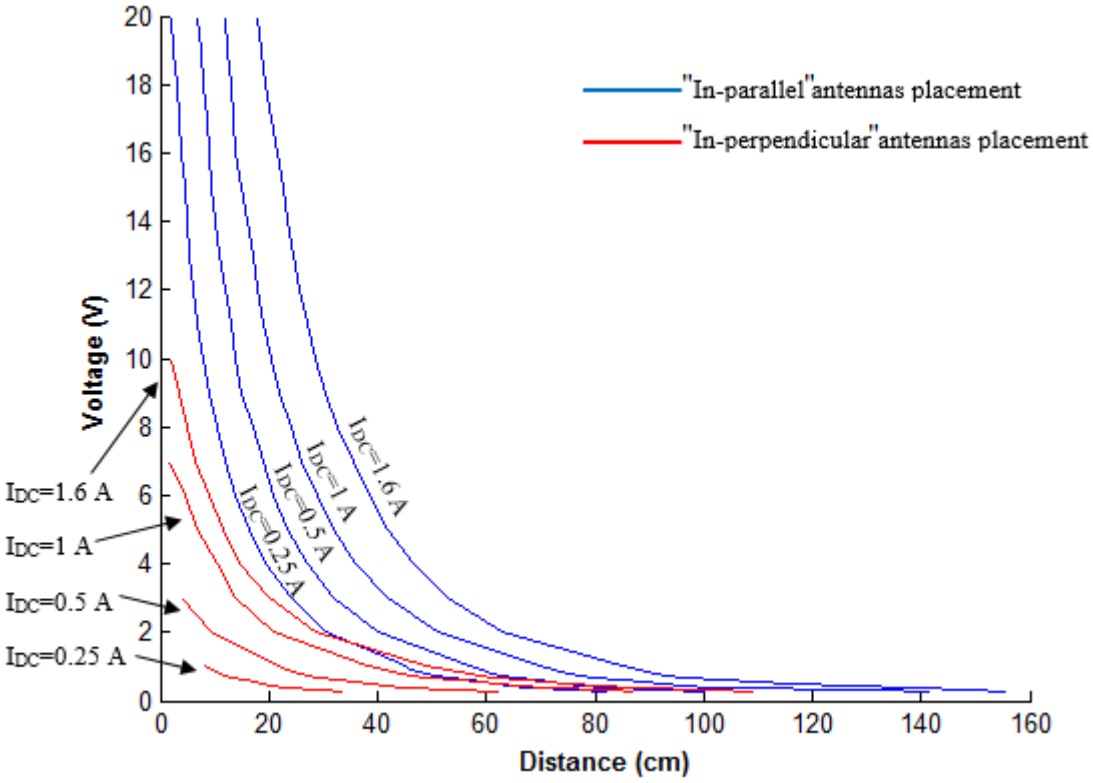

Fig. 4.14 – Measurement of the induced voltage of the receiving reader antenna as a function of distance between antennas.

Figure 4.14 shows the rapid decay of the peak voltage in antenna through distance. The blue curves represent the two antennas placed in parallel and the red curves represent the antennas placed in perpendicular to each other. Each curve is determined with different DC supply current values in the RFID system. The higher the current, the higher is the induced voltage in the second antenna. After a distance of 70 cm, all curves have peak voltages under 3 V. This value is less than the voltage required to power up the tag. The blue curve with the lowest current (250 mA) provides higher induced voltage than the red curve with the highest current (1600 mA) up to a distance of 30 cm. The mutual coupling is greatly reduced with both antennas perpendicular to each other.

4.3.2 **Measurements of the read range in air**

Since the magnetic field lines are circular, the magnetic field does not couple equally with the tag in all locations. Thus, a map of the area covered by the reader antenna is important. Three specific locations of the tag in the magnetic field were defined. These locations are shown in figure 4.15.

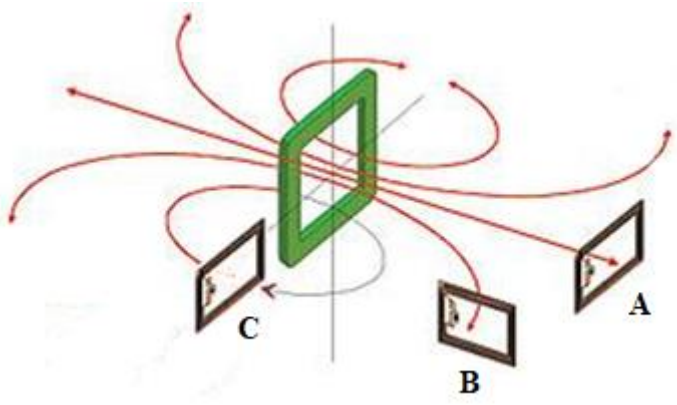

Fig. 4.15 – Magnetic field flux lines generated by the reader antenna. Three specific locations in the magnetic field pattern were defined. In location **A**, the straight line detects an "in-parallel" tag. In location **B,** the longest curved line detects an "in-perpendicular" tag. In location **C**, the shortest curved line detects an "in-parallel" tag (adapted from [46]).

Figure 4.16 represents a typical readout pattern of the system whose areas represent the read range map of "in-parallel" tags and "in-perpendicular" tags.

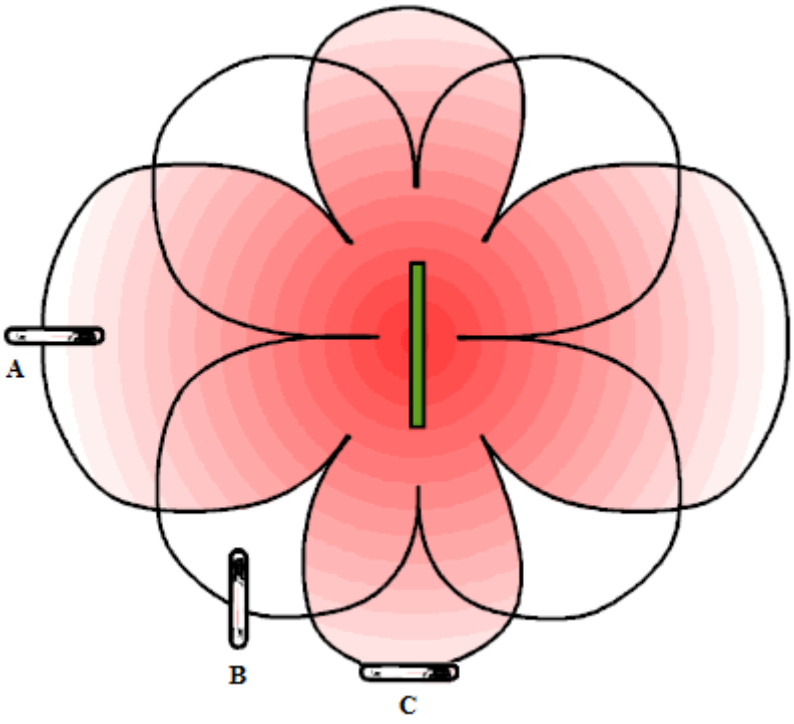

Fig. 4.16 – Readout pattern of the magnetic field generated by the reader antenna. **A, B** and **C** are pre-selected locations of the tag antennas with specific orientation, exactly the same points as described in the figure 4.16 (adapted from [46]).

The red area shown in figure 4.16 represents all the reading area with "in-parallel" tags and the overlapped area represents all the reading area with "in-perpendicular" tags. The LC circuit of the reader is tuned in order to cover the largest reading area around the antenna. Figure 4.17 shows the read range as function of the capacitance for the three locations set in figure 4.16.

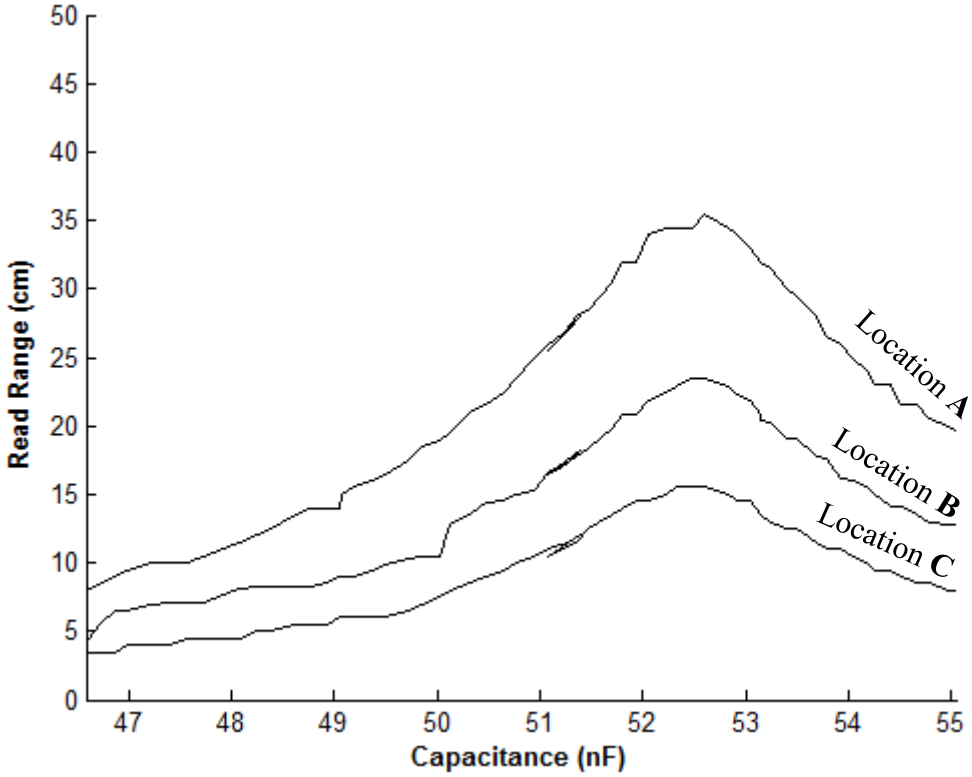

Fig. 4.17 – Read range as function of the capacitance for the three pre-selected locations.

Figure 4.17 shows the curves of the three pre-selected locations as expected with different read range values for each tuning capacitance. Location **A** is the one which provides the highest read range peak value of 35.5 cm. Location **C** is the one which provides the lowest read range peak value of nearly 15.5 cm. Location **B** provides the read range peak value of 23.41 cm. The three curves are not shifted to each other, having the respective peak values at 52.33 nF.

Figure 4.18 represents the measured read range in a noisy environment and also in a relatively free noise environment only for location A. We define as noisy environment when the surrounding area in the proximity of the antennas has metallic elements and electrical power sources.

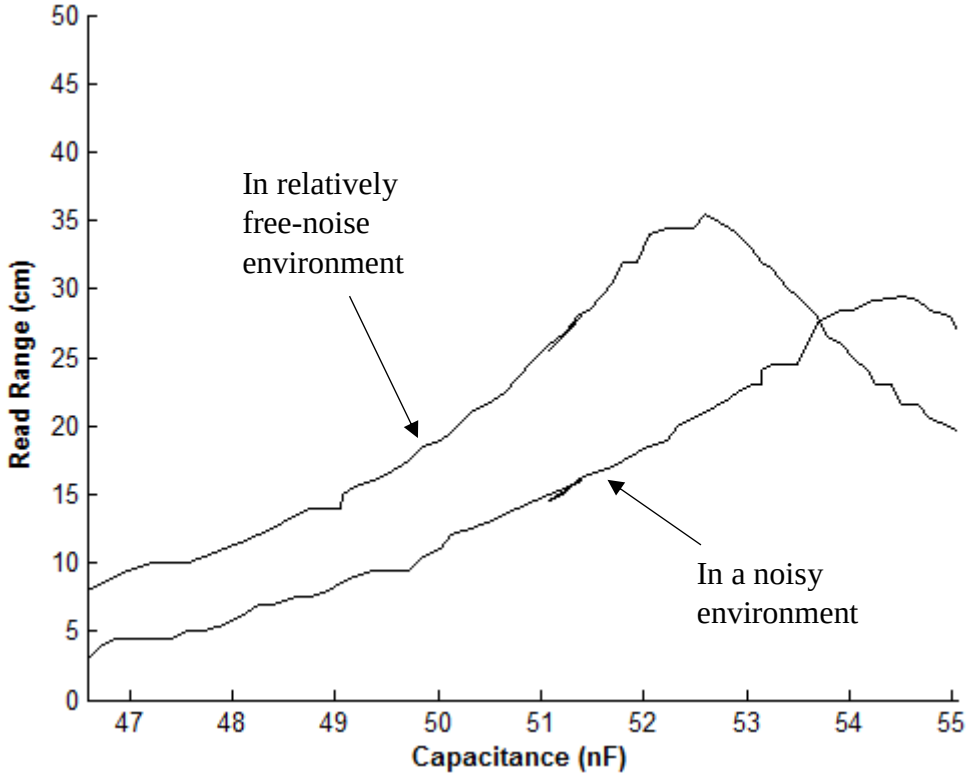

Fig. 4.18 – The effect of parasitic elements (metals and power supplies) in the RFID system cover area.

Figure 4.18 shows that the presence of parasitic disturbing elements such as nearby metal and electrical power sources detunes the system. For the tuning capacitance value of 52.33 nF, the read range can be reduced by 15 cm when parasitic elements are located in the surroundings.

To overcome the issues relative to the noise from surrounding environment, the increasing of the reader power is necessary. Until now, the RFID system was powered by 12V, but power can be increased up to 24V. Normally, when the voltage doubles, the DC current also doubles. Until now, a peak value of 1.1A with 12V was achieved by the tuned system. By increasing the voltage up to 24V, the DC current should double to 2.2 A. However, due to RF module circuit protection, which only supports until 1.7 A input DC current value. When current surpasses 1.7A, the protection circuit shorts the current back

to ground. The bell shaped curve of the current supply cannot be traced perfectly, but the maximum read range is obtained with 1.7 A, providing so the maximum performance of the single-antenna system. Figure 4.19 shows the maximum read range values achieved for 12 V and 24 V and also in noisy environment and relatively free-noise environment for high *Q* antenna. Also, figure 4.19 represents the maximum read range values for a low *Q* antenna firstly tested at 5 V and 12 V, using the kit EZ430-TMS37157.

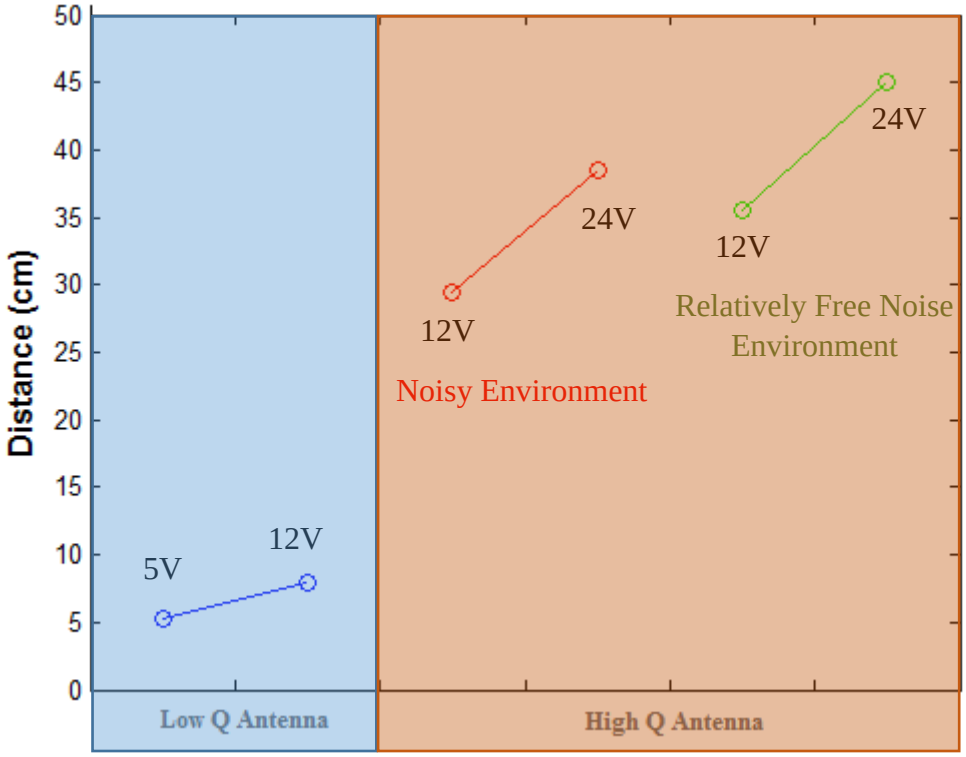

Fig. 4.19 – Maximum read range values obtained by measurement in tuned system for low *Q* antenna and high *Q* antenna.

Figure 4.19 shows a great increase of the read range for high *Q* antennas, comparing with low *Q* antennas, for the same input voltage (12 V). In high *Q* antennas, the relatively free noise environment provides a better increase of the read range than the noisy environment, for the same input voltage (12 V and 24 V). Using just one antenna, a read range value of 45 cm was achieved in air, being a reasonable value for monitoring fish in aquaculture tanks.

4.4 Read range measurement using multi-antenna system

If the read range provided by a single-antenna system is not enough, one of the best techniques to greatly increase read range is to implement one additional antenna to the reader, making a multi-antenna system. The RFID system has two antennas connected to the RF module, being interpreted as a single antenna with changed inductance. The changing of the inductance depends on the antennas configuration on the RF module. A series connection of the antennas has a lower inductance in respect to a parallel connection.

For the single-antenna system, a 27-µH gate antenna is connected to the RF module with a tuning capacitance of approximately 52 nF to resonate at 134.2 kHz. For multi-antenna antenna, if two gate antennas are connected in series (“in-series” antennas), the inductance doubles to 54 µH whereas if connected in parallel (“in-parallel” antennas), the inductance divides in half to 13.5 µH. In order to resonate at 134.2 kHz, for “in-series” antennas, the tuning capacitance should divide in half to about 26 nF whereas for “in-parallel” antennas, the tuning capacitance should double to about 104 nF. The trimming capacitors does not cover the new tuning capacitance values of the multi-antenna system with the actual fixed capacitors, therefore a new configuration of fixed capacitors is needed. Basically, a new equivalent circuit of fixed capacitors with total capacitance of approximately 52 nF is added in series or in parallel to the LC circuit, depending on the configuration of the antennas. Only two capacitors are added with respective values of 3.3 nF and 47 nF. The 3.3 nF capacitor is connected in parallel to the LC circuit for both configurations, whereas the 47 nF is connected in series for “in-series” antennas and in parallel for “in-parallel” antennas. Figure 4.20 represents a schematic diagram of the modified LC circuit with the new external capacitors.

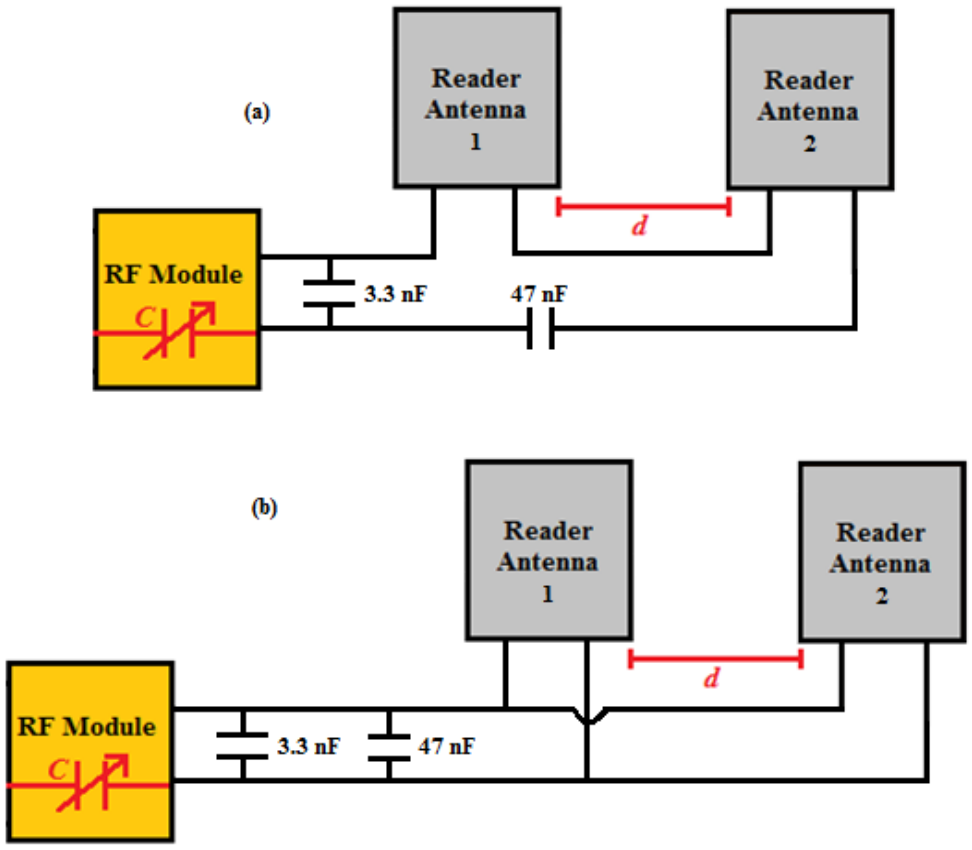

Fig. 4.20 – Modified LC circuit with additional fixed capacitors. (a) "In-series" antennas, (b) "In-parallel" antennas.

Multi-antenna systems provides two antenna connections. An "in-phase" connection and "out-of-phase" connection, each connection generates a different magnetic field pattern, depending if the current of each antenna are flowing in the same direction or in opposed directions. There are two options to change from "in-phase" connection to "out-of-phase" connection and vice-versa, by simply turn one of the antennas 180º or by swapping over the pair of connectors of one antenna connected to the RF module.

4.4.1 **Tuning of the LC circuit**

Figures 4.21 and 4.22 demonstrate the antenna supply current as function of capacitance for the different four possible antennas configurations, when the connection is in phase or out of phase, in the case both antennas are connected in series and in parallel, respectively.

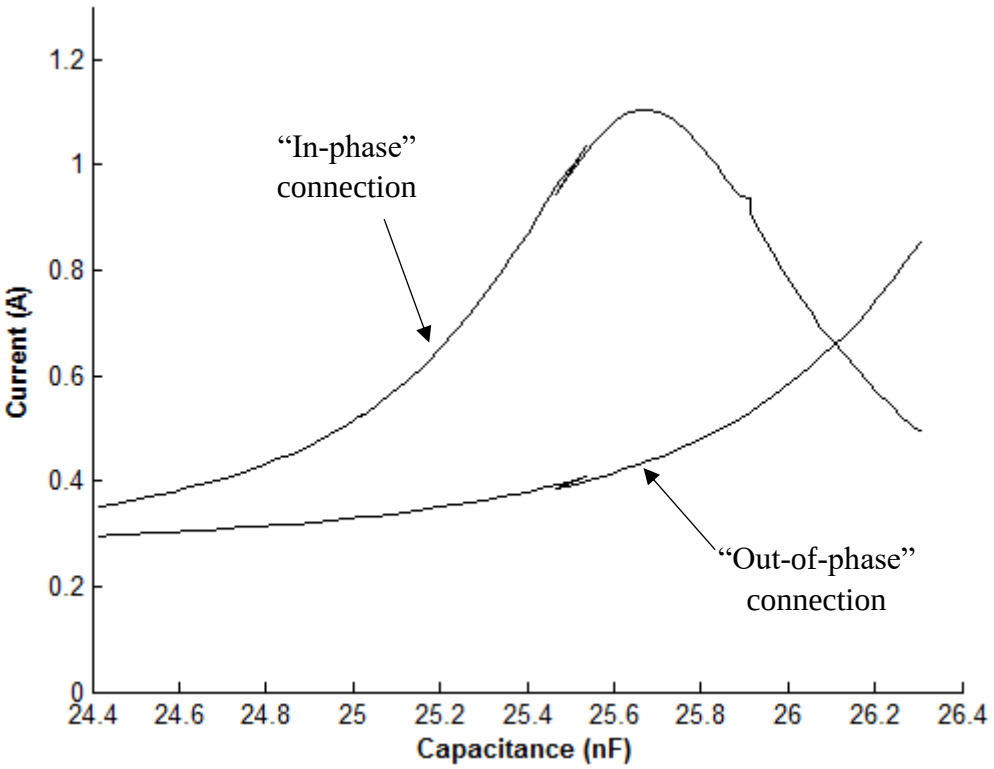

Fig. 4.21 – Antenna supply current as function of the capacitance tuning of the RF module, with "in-phase" and "out-of-phase" connections of the "in-series" antennas.

Figure 4.21 shows a bell shaped curve for "in-phase" connection with peak value of 1.12 A, for a tuning capacitance value of 25.65 nF. For "out-of-phase" connection, an exponential curve is shown in figure 4.21. The capacitance range is left shifted relative to the peak point where the LC circuit should be tuned for the configuration, therefore a perfect bell shaped curve could not be represented.

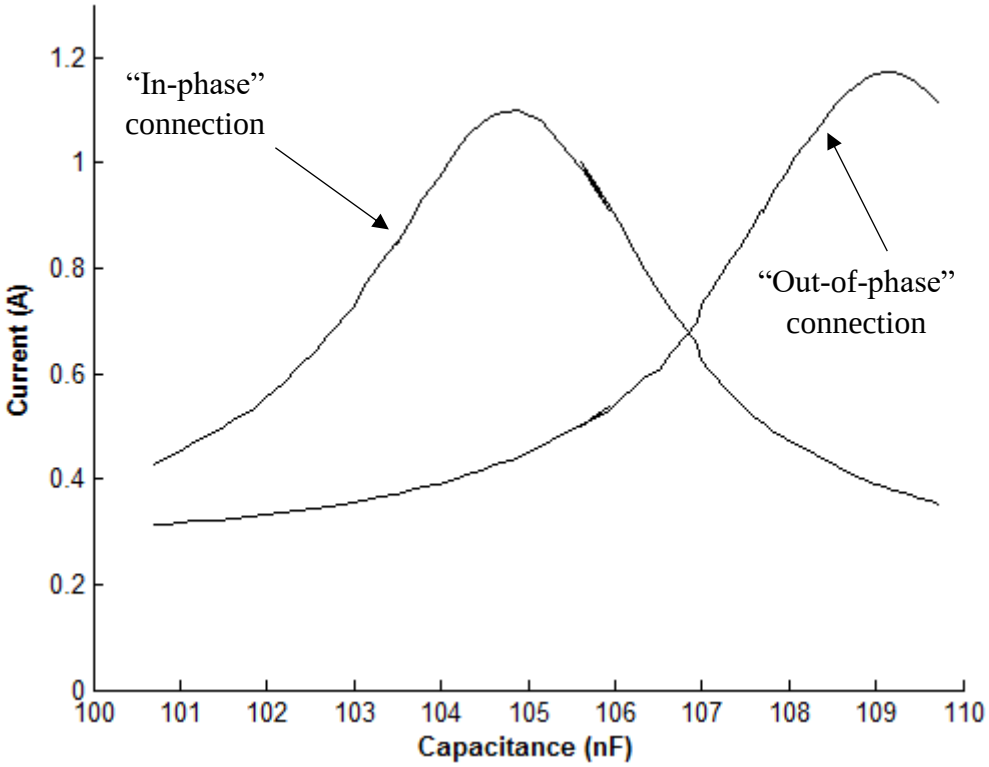

Fig. 4.22 – Antenna supply current as function of the capacitance tuning of the RF module, with "in-phase" and "out-of-phase" connections of the "in-parallel" antennas.

Figure 4.22 shows a bell shaped curve for "in-phase" connection with peak value of 1.1 A, for a tuning capacitance value of 104.87 nF. For "out-of-phase" connection, the capacitance range is left shifted relative to the peak point where the LC circuit should be tuned for the configuration, therefore a perfect bell shaped curve could not be observed. However, the peak point could be still observed with a value of 1.17 A, for a tuning capacitance value of 109.08 nF.

According to figures 4.21 and 4.22, for a specific configuration of antennas, both "in-phase" and "out-of-phase" connections are detuned relatively to each other which means both connections provides different inductance values to the LC circuit. However, changing the trimming capacitance values does not cover the tuning of the LC circuit for all four configurations. However, there are other ways to tune the antenna without changing the capacitance. One way is changing the inductance by adding interference sources such as metal near antennas or extra cables to the antenna terminals, although the performance of the system may decrease. Other way is using the mutual coupling of the reader antennas by moving further or closer the antennas relative to each other. Figure

4.23 represents the antenna supply current as a function of the distance starting at 10 cm up to 80 cm of the four configurations for a constant trimming capacitance value.

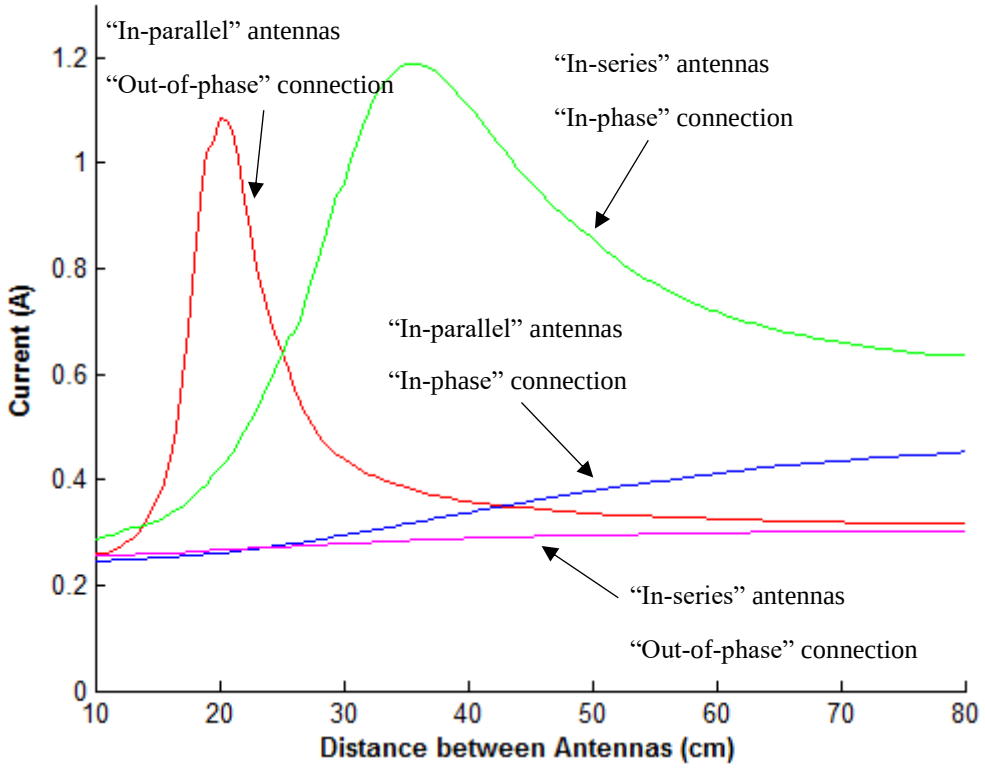

Fig. 4.23 – Antenna supply current as function of the distance (between antennas) for four configurations.

Figure 4.23 shows, for a constant trimming capacitance value, only two configurations are possible to be tuned, the "in-series" antennas with "in-phase" connection and the "in-parallel" antennas with "out-of-phase" connection. The "in-phase" connection provides higher current than "out-of-phase" connection, obtaining a peak value of 1.19 A at 16 cm distance and a value of 1.09 A at 20 cm distance, respectively. For maximum performance of the system, the current value of approximately 1.2 A becomes the maximum DC current for two-antenna system, never reaching the RF module limit value of 1.7 A.

Figures 4.21, 4.22 and 4.23 show that tuning both antennas is possible by manipulating two variables, the tuning capacitance and distance between antennas. To provide a greater flexibility for the LC circuit, both the variables must be manipulated, individually, one after other. Fixing a variable and changing the other may tune the LC circuit only for two configurations.

4.4.2 **Measurement of the read range in air**

For each configuration of the multi-antenna system, the read range can be measured for the best performance. There are two cases the read range can be determined, when the antennas are mutual coupled or not. For antennas not mutually coupled, each antenna works independently as a single antenna. For the measurements of the single-antenna system, the maximum read range achieved was 45 cm. However, the measurements were obtained only for half magnetic field. Therefore, the best read range of the antennas not mutually coupled is the double of the maximum read range obtained by the measurements of a single-antenna system multiplied by the number of antennas. For the two-antenna system, the maximum read range possible to achieve is 180 cm, being an excellent read range for low frequency in air.

For mutually coupled antennas, the aim is not to obtain the highest read range but rather to cover the widest volume between the areas of the antennas. The aim for the next experiences is to obtain the minimum DC supply current values required to cover three new pre-selected locations, meaning the entire volume between the areas of the antennas is covered. Figure 4.24 shows the new pre-selected points of the tags in the volume between the areas of the antennas.

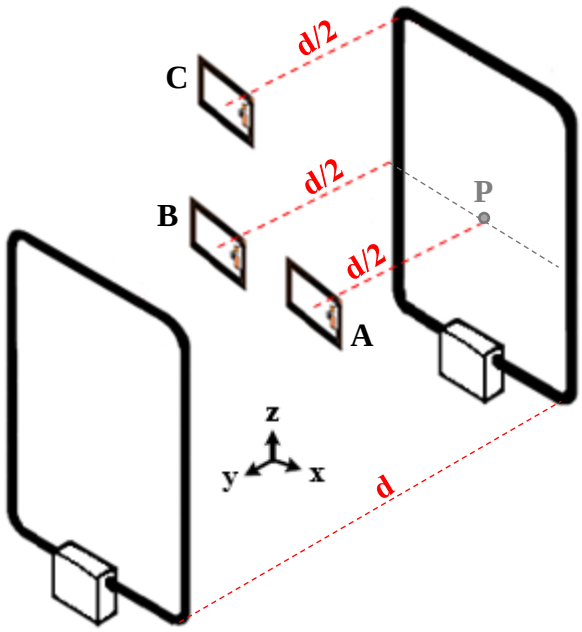

Fig. 4.24 – Pre-selected locations of the tags inside the volume between the areas of the antennas. Point **P** is the centered point of the gate antenna. Location **A** provides the furthest read range relative to the y-axis. Location **B** provides the furthest read range relative to the x-axis. Location **C** provides the furthest read range relative to the z-axis, covering all the volume between the areas of the reader antennas.

Figures 4.25, 4.26 and 4.27, provide the minimum antenna supply current dependence with the distance between antennas (starting at 20 cm up to 70 cm), relative to the "in-phase" connection, for "in-parallel" tags detected at locations **A**, **B** and **C**, respectively. Figures 4.28 and 4.29 provide the minimum antenna supply current dependence with the distance between antennas, relative to the "out-of-phase" connection, for "in-perpendicular" tags located at locations **B** and **C**, respectively. For "out-of-phase" connection, the location **A** is not measured since the magnetic field pattern does not reach the centered zone.

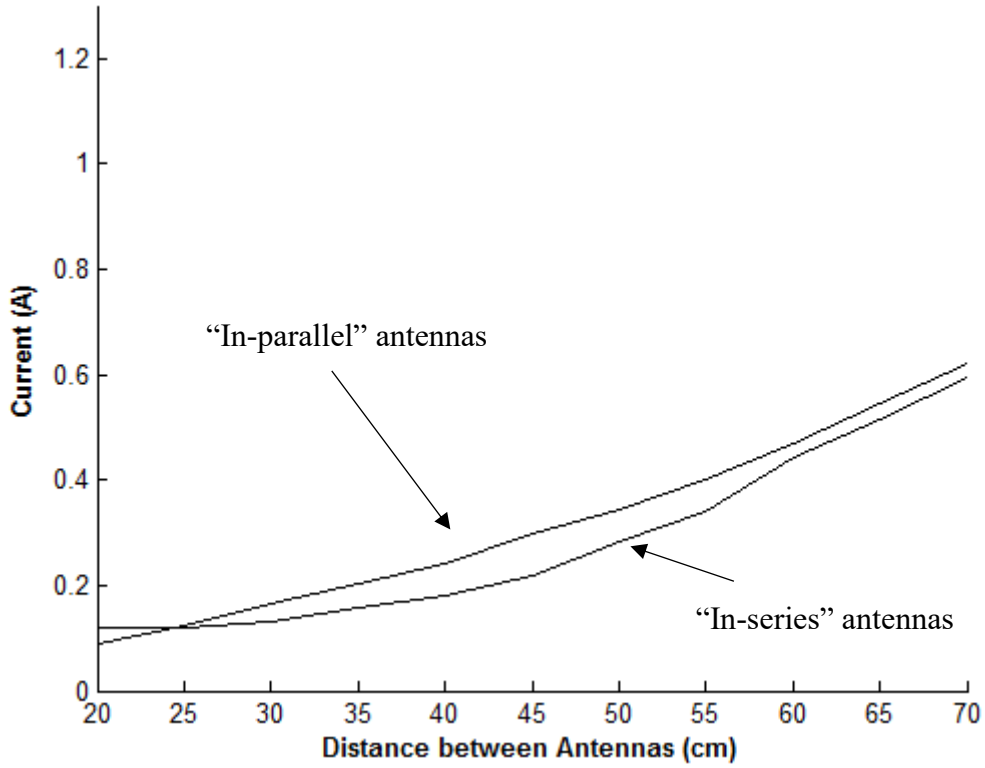

Fig. 4.25 – Comparison of the minimum antenna supply current with the distance between antennas arranged in two configurations, for "in-phase" connection with "in-parallel" antennas and with "in-series" antennas (tags are placed in location **A**).

Figure 4.25 shows that a distance of 70 cm between antennas was achieved for both configurations of antennas with DC supply current values of approximately 0.6 A. Both configurations of antennas only have a maximum difference of 60 mA between them.

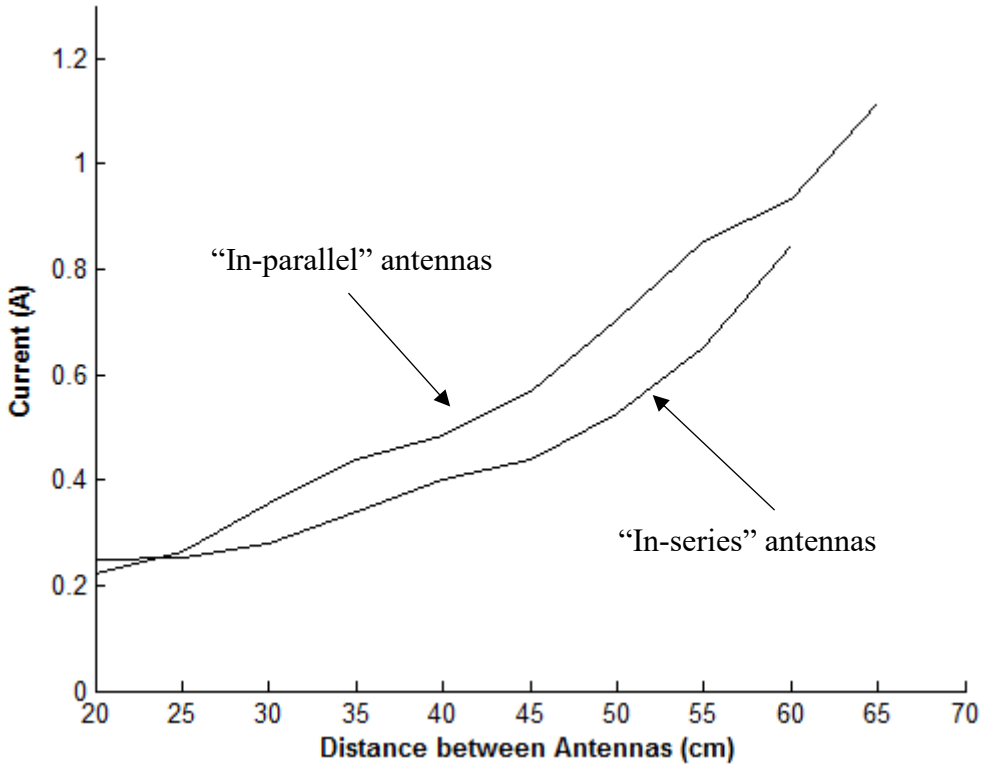

Fig. 4.26 – Comparison of the minimum antenna supply current with the distance between antennas arranged in two configurations, for "in-phase" connection with "in-parallel" antennas and with "in-series" antennas (tags are placed in location **B**).

Figure 4.26 shows that a distance of 65 cm between antennas was achieved for "in-parallel" antennas with DC supply current value of 1.12 A. The "in-series" antennas with DC supply current value of 0.845 A provides a distance of 60 cm between antennas. Both configurations of antennas only have a maximum difference of 100 mA between them. For a specific distance, the tag at location **B** requires higher DC supply current than the tag at location **A**. The "in-series" antennas did not reach 65 cm distance between antennas probably due to capacitive tolerances of the LC circuit.

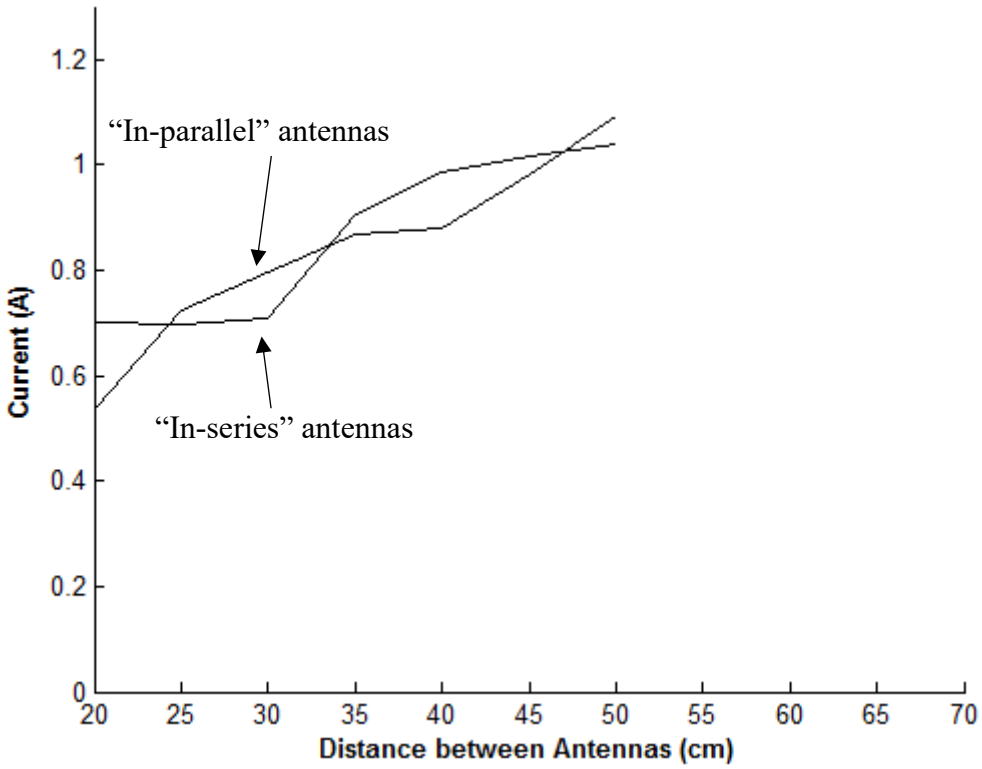

Fig. 4.27 – Comparison of the minimum antenna supply current with the distance between antennas arranged in two configurations, for "in-phase" connection with "in-parallel" antennas and with "in-series" antennas (tags are placed in location **C**).

Figure 4.27 shows that a distance of 50 cm between antennas was achieved for both configurations with DC current value of nearly 1.1 A for "in-parallel" antennas and a DC current value of nearly 1 A for "in-series" antennas. The tag at location **C** requires even higher DC current than the tag at location **B**, decreasing even more the distance between the antennas. For 50 cm, the tag was detected using the maximum performance of the system. Both configurations only have a maximum difference of nearly 160 mA between them. The curves in figure 4.27 are twisted curves for both antenna configurations with a tag at location **C.** It is difficult to determine which configuration of antennas is better. Both configurations cover the entire volume up to 50 cm distance between the antennas for "in-parallel" tags.

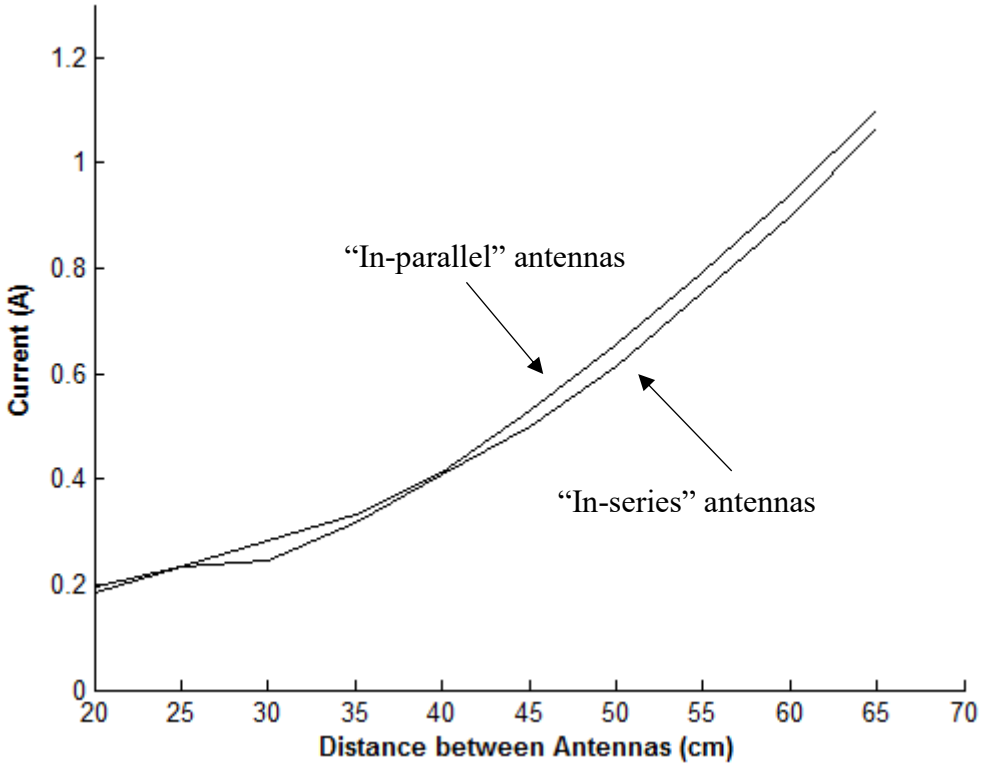

Fig. 4.28 – Comparison of the minimum antenna supply current with the distance between antennas arranged in two configurations, for "out-of-phase" connection with "in-parallel" antennas and with "in-series" antennas (tags are placed in location **B**).

Figure 4.28 shows that a distance of 65 cm between antennas was achieved for both configurations with DC current value of 1.1 A for "in-parallel" antennas and a DC current value of 1.07 A for "in-series" antennas. Both configurations only have a maximum difference of nearly 40 mA between them.

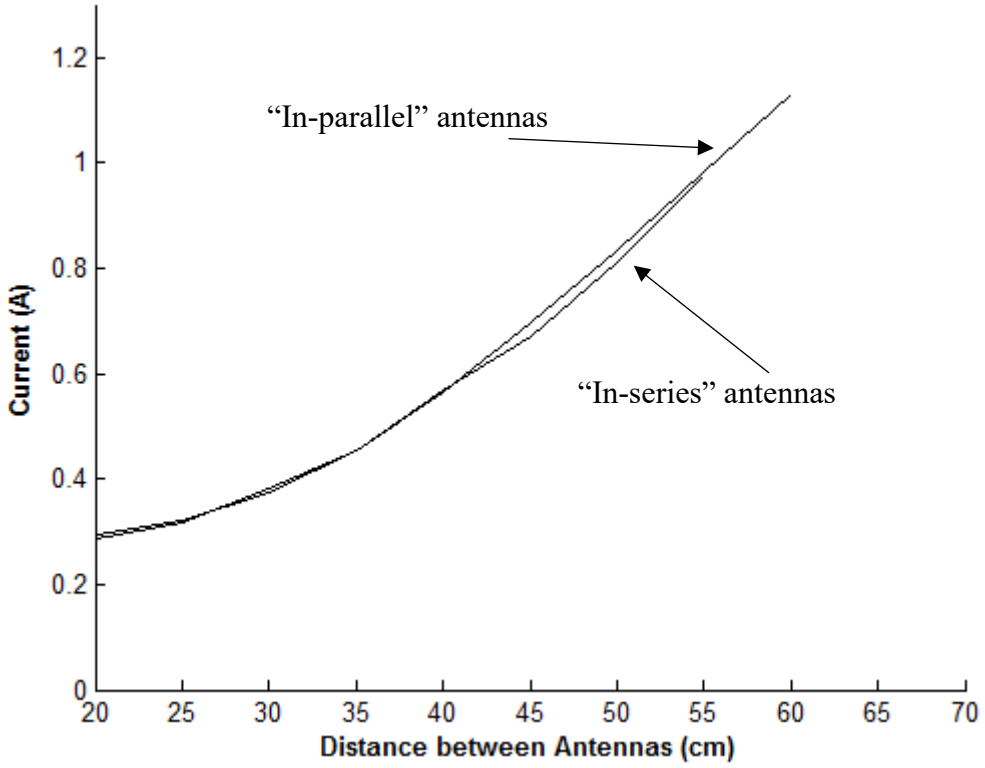

Fig. 4.29 – Comparison of the minimum antenna supply current with the distance between antennas arranged in two configurations, for "out-of-phase" connection with "in-parallel" antennas and with "in-series" antennas (tags are placed in location **C**).

Figure 4.29 shows that a distance of 60 cm between antennas was achieved for "in-parallel" antennas with DC current value of 1.13 A. The "in-series" antennas with DC supply current value of 0.98 A provides a distance of 55 cm between antennas. The tag at location **C** requires higher DC current than the tag at location **B**, decreasing the distance between the antennas. Both configurations only have a maximum difference of 30 mA between them. The "in-series" configuration did not reach 60 cm distance between antennas probably due to capacitive tolerances of the LC circuit.

Comparing figure 4.29 with figure 4.27 relatively to the "in-phase" connection at location **C**, the "out-of-phase" connection is better at detecting the tag to higher distances between the antennas than "in-phase" connection at the corner zones of the volume. The corner zones of the volume is the space containing only location **B** and location **C**, but not location **A** which belongs to the center zone. Therefore, "out-of-phase" connection is better for detecting "in-perpendicular" tags at the corner zones of the volume. However, the "in-perpendicular" tag cannot be detected in location **A** in the center zone at any orientation due to the magnetic field pattern.

4.4.3 **Measurements of the read range in water**

For the measurements of the read range, a water tank of 40 cm width, 70 cm length and 30 cm height was used. The antennas, which have approximately the same height and length of the tank, are placed in contact with the large sides of the tank. The antennas are separated from each other by the width of the tank. The aim is to cover the entire volume of the tank full with water at 40 cm distance between antennas. Figure 4.30 represents the schematic diagram and a photograph of the RFID system mounted.

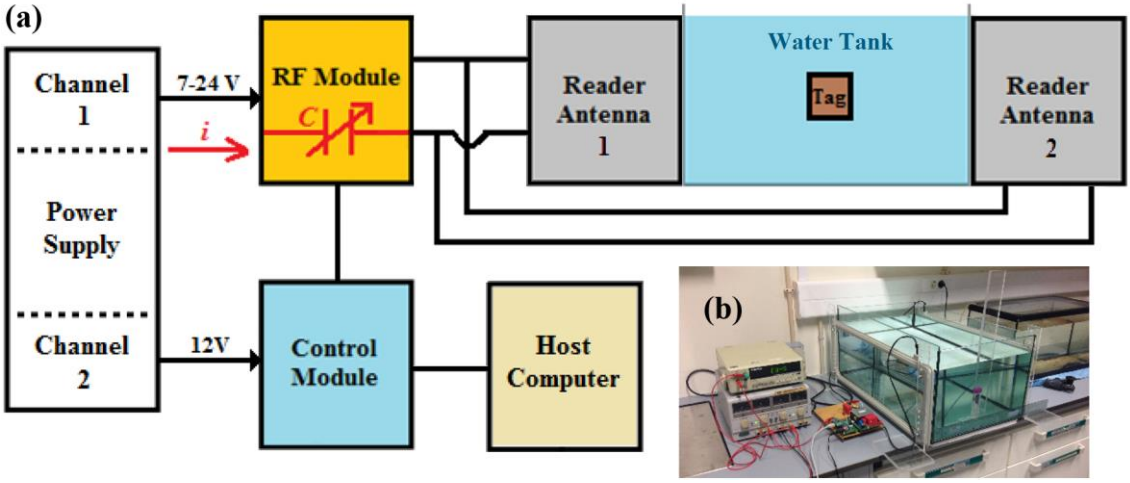

Fig. 4.30 – Implementation of the RFID system to detect tags underwater. (a) Schematic diagram, (b) Photograph taken during measurements in water tank.

Before taking measurements, the best configuration should be used for detecting the tag underwater. Both antennas are used in series and in parallel, since the results of the measurements taken in air were inconclusive about which configuration is better. However, the most suitable connection for the underwater application is “in-phase” connection, because is the only connection which can detect “in-parallel” tags in the entire volume. “Out-of-phase” connection cannot detect “in-perpendicular” tags in the center zone. Therefore, “in-phase” connection is used along with “in-series” and “in-parallel” antennas. The experiments underwater were carried out in similar way as the experiments in air. The minimum DC supply current to detect the tag in the three locations were measured. Also, measurements were made in two types of water, freshwater and seawater. Figure 4.31 provides a comparison between the minimum DC supply current for air, freshwater and seawater, using an “in-series” and “in-parallel” antennas separated by 40 cm, for the three pre-selected locations of the tag.

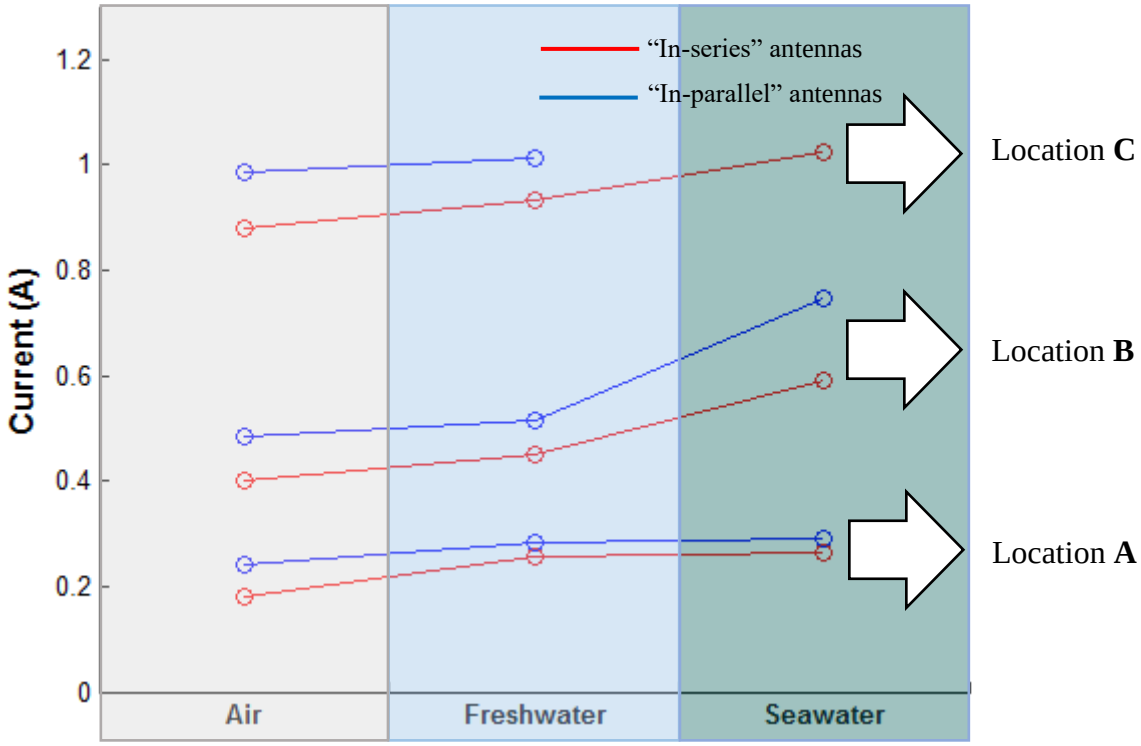

Fig. 4.31 – Comparison between the minimum DC supply current required to detect the tag in air, freshwater and seawater at 40 cm distance between the antennas.

In figure 4.31, for location **A** with "in-series" antennas, the DC current values are 0.18 A for air, 0.26 A for freshwater and 0.27 A for seawater. For location **A** with "in-parallel" antennas, the DC current values are 0.24 A for air, 0.28 A for freshwater and 0.29 for seawater. For location **B** with "in-series" antennas, the DC current values are 0.4 A for air, 0.45 A for freshwater and 0.59 A for seawater. For location **B** with "in-parallel" antennas, the DC current values are 0.48 A for air, 0.51 A for freshwater and 0.75 for seawater. For location **C** with "in-series" antennas, the DC current values are 0.88 A for air, 0.93 A for freshwater and 1.03 A for seawater. For location **C** with "in-parallel" antennas, the DC current values are 0.99 A for air, 1.01 A for freshwater and for seawater the tag was not detected.

Figure 4.31 shows a clear difference between the DC current values in location **A**, **B** and **C**, being the difference between location **B** and **C** greater than the difference between location **A** and **B**. However, the distance between location **A** and **B** is larger than the distance between location **B** and **C**. The straight flux line of the magnetic field which crosses location **A** provides the longest read range and requires less current than the others. The curved flux lines needs much more current to reach location **B** and **C**.

Approximately double current relative to location **A** to reach location **B** and approximately double current relative to location **B** to reach location **C** are needed.

The difference between amount of current required for "in-parallel" and "in-series" antennas configurations is also observed in figure 4.31. For each location, "in-parallel" antennas configurations require higher current than "in-series" antennas configuration and the difference becomes higher in each distant location. For "in-parallel" antennas configuration, there is missing one value for seawater in location **C** because a higher current in location **C** was required which exceeds the peak current provided to the tuned "in-parallel" antennas.

The influence of water conductivity on the read range becomes also clear. Slightly differences between air, freshwater and also seawater are observed, but the differences may not be sufficient to greatly decrease read range. Probably a 40 cm distance is a smaller value compared with the upper bound value of 69 cm defined as the theoretical skin depth value achieved for low frequencies in seawater.

Chapter 5

CONCLUSION

Summary

This chapter summarizes all the relevant results discussed in this thesis. In addition, suggestions for future work are presented.

5.1 Conclusions about the work

The work presents a RFID monitoring system which provides a reasonable read range for monitoring fish underwater. An entire volume of a tank with 40 cm width was covered for "in-parallel" tags using both "in-parallel" and "in-series" reader antennas with "in-phase" connection. The RFID system gives the opportunity to cover a large volume, even in relative high conductive environments (seawater). The "in-perpendicular" tag does not cover all the volume of the tank, mainly in the middle region, where location **A** is. However, "in-perpendicular" tags provide better results in location **B** and **C**, if using "out-of-phase" connection.

Read range can be potentially increased, if some adjustments to the entire system are made. Increasing the antennas size of the reader and tag, increasing input power on reader and keeping tag well oriented (in parallel) relative to the reader antenna. Removal of detrimental elements in the vicinity of the antennas, such as metallic elements, unnecessary additional cables connected to the reader antennas and power sources generating noise are some factors that allow to maximize the read range.

The implementation of an external sensor on the tag was not carried out, neither the tag was attached to a real fish. Instead, the internal temperature sensor presented in the MCU of the tag was used for the demonstration of the capabilities of our system.

5.2 Suggestions for future work

The overall RFID system can be substantially improved, namely in the following aspects:

- To solve the problem of the antennas orientation, a redundancy technique of adding one more antenna on tag can be implemented to cover both “in-parallel” and “in-perpendicular” tags. Basically, two antennas are placed in perpendicular to each other in the tag. Using this strategy, the tag will always be detected. Other option is to increase the number of reader antennas. Also, designing the system in order to obtain “in-phase” and “out-of-phase” connections at alternating intervals would overcome the orientation issue in the corner zones.

- The magnetic field is symmetrically in both sides of the reader antenna. The antenna can be mounted vertically (pass-through or pass-by) or horizontally (pass-over). Pass-by and pass-over antennas, which were used on this thesis, lie on the bottom or on side of a wall, respectively. The arrangement can only use half of the magnetic field since the other half is behind an obstacle, which is unreachable. However, pass-through antenna can cover all the reading area which comes from both sides, doubling the read range, comparing with the other arrangements [64]. Figure 5.1 represents the three arrangements of the antennas.

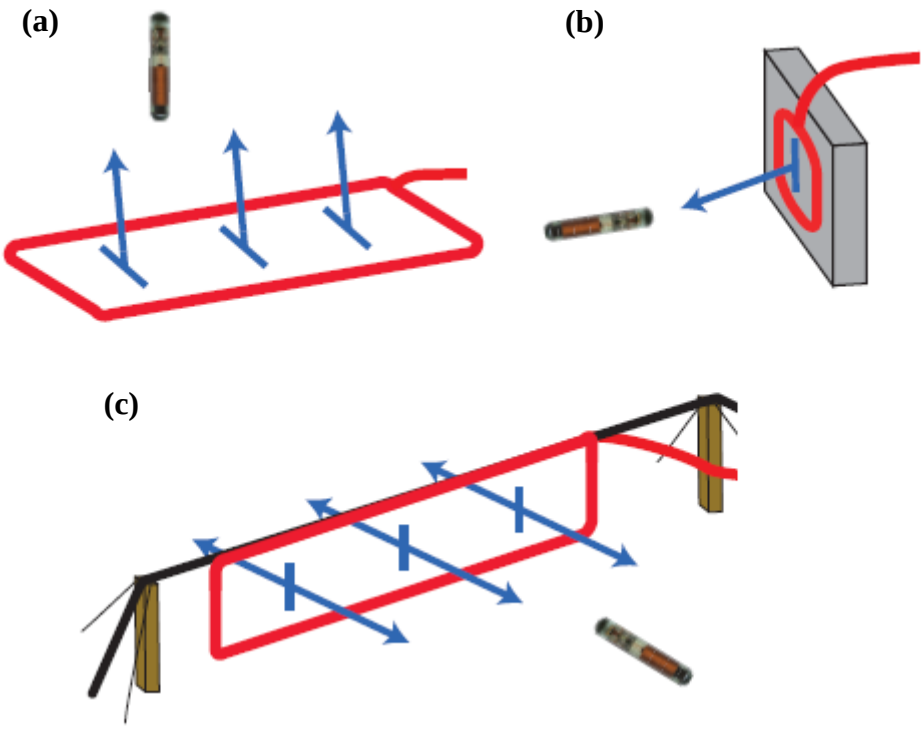

Fig. 5.1 – Mounted antennas arrangement [64]. (a) Pass-over arrangement as if the antenna is placed on the bottom of the tank. (b) Pass-by arrangement as if the antenna is placed on the walls of the tank. (c) Pass-through arrangement as if an antenna is placed in the middle of the tank.

- Re-designing the gate antennas by combining two "in-parallel" loop antennas (one is the primary loop and other is the secondary loop) is a way to improve the distribution of the magnetic field for any orientations, resulting in better read range of the system. The shape of the primary loop is rectangular for generating the magnetic field in the y-axis, whereas the secondary loop is within the primary loop and is optimized for the magnetic fields in x-axis and z-axis being strongly generated. Therefore, the two parallel dual loop antennas are installed as a pass-through gate arrangement of the system. In addition, one gate antenna is shifted against the other to avoid cancellation of magnetic fields between two antennas and also to improve the distribution of magnetic fields in the middle region of the gate. The advantage of the proposed antenna is the possibility to be used for any tag orientation with increased read range. The proposed antenna structure may extend the operating percentage of volume comparing to the standard loop gate antenna. After some measurements in air, the percentages of volume in all principal axis are equal to 100% for a distance between gate antennas equal to 100 cm. Dual loop gate antennas may be used efficiently in the

monitoring of fish underwater [53]. Figure 5.2 represents the arrangement of the dual loop antennas.

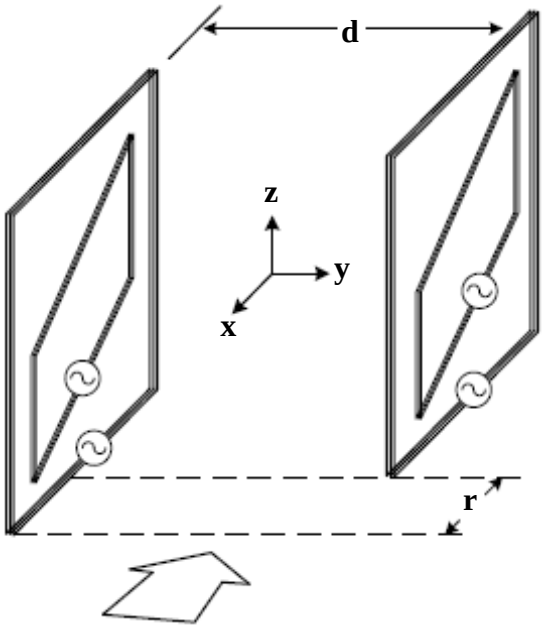

Fig. 5.2 – Dual loop antennas arranged as a shifted gate in the x-axis. The distance *d* is the separation between gate antennas and the distance *r* is the shifted distance in the x-axis (adapted from [53]).

- Apart from these developments on the reading system (reader), there are also some interesting developments that can be explored at the level of sensing (tag). The implementation on the tag of external sensors such as the accelerometer to measure physical activity and ventilation rate of the fish or other sensors measuring other stress indicators shall be tested and placed on the fish swimming freely in the aquaculture tank. The entire platform that interacted with the user needs a substantial improvement. A GUI application with the necessary functions for monitoring fish underwater in real-time shall be developed.

REFERENCES

[1] L. Ababouch, A. A. J. Alder, U. Barg, Bartley, M. Bernal, and G. Bianchi, “The State of World Fisheries and Aquaculture.” Food and Agriculture Organization of the United Nations, p. 200, 2016.

[2] P. J. Ashley, “Fish welfare: Current issues in aquaculture,” *Appl. Anim. Behav. Sci.*, vol. 104, no. 3–4, pp. 199–235, 2007.

[3] F. A. Huntingford, C. Adams, V. A. Braithwaite, S. Kadri, T. G. Pottinger, P. Sandøe, and J. F. Turnbull, “Current issues in fish welfare,” *J. Fish Biol.*, vol. 68, pp. 332–372, 2006.

[4] “Report on the welfare of farmed fish.” Farm Animal Welfare Council, p. 43, 1996.

[5] “European convention for the protection of animals for farming purposes,” *European Treaty Series*, vol. 10, no. 3. Council of Europe, p. 8, 1976.

[6] D. Fraser, D. M. Weary, E. A. Pajor, and B. N. Milligan, “A Scientific Conception of Animal Welfare That Reflects Ethical Concerns,” *Anim. Welf.*, vol. 6, pp. 187–205, 1997.

[7] J. Webster, *Animal Welfare: Limping Towards Eden*. Blackwell, 2005.

[8] *Terrestrial Animal Health Code*, 20th ed., vol. 1. World Organisation for Animal Health, 2011.

[9] “Fish Welfare.” Fisheries Society of the British Isles, p. 21, 2002.

[10] B. A. Barton, “Stress in Fishes: A Diversity of Responses with Particular Reference to Changes in Circulating Corticosteroids.,” *Integr. Comp. Biol.*, vol. 42, pp. 517–525, 2002.

[11] F. A. Huntingford and S. Kadri, “Defining, assessing and promoting the welfare of farmed fish,” *World Organ. Anim. Heal.*, vol. 33, no. 1, pp. 1–17, 2014.

[12] T. Ellis, J. D. James, C. Stewart, and A. P. Scott, “A non-invasive stress assay based upon measurement of free cortisol released into the water by rainbow trout,” *J. Fish Biol.*, vol. 65, pp. 1233–1252, 2004.

[13] S. J. Lupica and J. W. Turner, “Validation of enzyme-linked immunosorbent assay for measurement of faecal cortisol in fish,” *Aquac. Res.*, vol. 40, pp. 437–441, 2009.

[14] T. Ellis, A. P. Scott, and J. James, “A Non-Invasive Stress Assay for Rainbow Trout,” *Cent. Environ. Fish. Aquac. Sci.*, 2002.

[15] E. Höglund, P. H. M. Balm, and S. Winberg, “Behavioural and neuroendocrine effects of environmental background colour and social interaction in Arctic charr (Salvelinus alpinus),” *J. Exp. Biol.*, vol. 205, no. Pt 16, pp. 2535–2543, 2002.

[16] J. Rotllant, L. Tort, D. Montero, M. Pavlidis, M. Martinez, S. E. Wendelaar Bonga, and P. H. M. Balm, “Background colour influence on the stress response in cultured red porgy Pagrus pagrus,” *Aquaculture*, vol. 223, pp. 129–139, 2003.

[17] A. L. Van Der Salm, M. Pavlidis, G. Flik, and S. E. Wendelaar Bonga, “The acute stress response of red porgy, Pagrus pagrus, kept on a red or white background,” *Gen. Comp. Endocrinol.*, vol. 145, pp. 247–253, 2006.

[18] K. I. O’Connor, N. B. Metcalfe, and A. C. Taylor, “Does darkening signal submission in territorial contests between juvenile Atlantic salmon, Salmo salar?,” *Anim. Behav.*, vol. 58, pp. 1269–1276, 1999.

[19] E. M. V. Cruz, M. B. Valdez, R. B. Bolivar, and R. J. Borski, “Duration of Appetite Inhibition Predicts Social ominance in Nile Tilapia, Oreochromis

nicoticus L.," *Better Sci. better fish, better life. Proc. Ninth Int. Symp. Tilapia Aquac.*, pp. 86–94, 2011.

[20] R. H. A. Freitas, C. A. Negrão, A. K. C. Felício, and G. L. Volpato, "Eye darkening as a reliable, easy and inexpensive indicator of stress in fish," *Zoology*, vol. 117, pp. 179–184, 2014.

[21] E. M. V. Cruz and M. P. Tauli, "Eye Color Pattern During Isolation Indicates Stress-Coping Style in Nile Tilapia Oreochromis niloticus L.," *Sci. Res. Knowl.*, vol. 3, no. 7, pp. 181–186, 2015.

[22] O. Folkedal, L. H. Stien, T. Torgersen, F. Oppedal, R. E. Olsen, J. E. Fosseidengen, V. A. Braithwaite, and T. S. Kristiansen, "Food anticipatory behaviour as an indicator of stress response and recovery in Atlantic salmon post-smolt after exposure to acute temperature fluctuation," *Physiol. Behav.*, vol. 105, pp. 350–356, 2012.

[23] J. Delcourt, C. Becco, M. Y. Ylieff, H. Caps, N. Vandewalle, and P. Poncin, "Comparing the EthoVision 2.3 system and a new computerized multitracking prototype system to measure the swimming behavior in fry fish," *Behav. Res. Methods*, vol. 38, no. 4, pp. 704–710, 2006.

[24] J. Cachat, A. Stewart, E. Utterback, P. Hart, S. Gaikwad, K. Wong, E. Kyzar, N. Wu, and A. V. Kalueff, "Three-Dimensional Neurophenotyping of Adult Zebrafish Behavior," *PLoS One*, vol. 6, no. 3, p. 14, 2011.

[25] N. Hafner, J. C. Drazen, and V. M. Lubecke, "Fish Heart Rate Monitoring by Body-Contact Doppler Radar," *IEEE Sens. J.*, vol. 13, no. 1, pp. 408–414, 2013.

[26] P. A. Cotter and K. J. Rodnick, "Fishing for an ECG: a student-directed electrocardiographic laboratory using rainbow trout," *Adv. Physiol. Educ.*, vol. 31, pp. 211–217, 2007.

[27] J. Sherrill, E. S. Weber, G. D. Marty, and S. Hernandez-Divers, "Fish Cardiovascular Physiology and Disease," *Vet. Clin. North Am. - Exot. Anim. Pract.*, vol. 12, pp. 11–38, 2009.

[28] D. J. Milan, I. L. Jones, P. T. Ellinor, and C. A. Macrae, "In vivo recording of adult zebrafish electrocardiogram and assessment of drug-induced QT prolongation.," *Am. J. Physiol. Heart Circ. Physiol.*, vol. 291, pp. 269–273, 2006.

[29] P. Sun, Y. Zhang, F. Yu, E. Parks, A. Lyman, Q. Wu, L. Ai, C. H. Hu, Q. Zhou, K. Shung, C. L. Lien, and T. K. Hsiai, "Micro-electrocardiograms to Study Post-Ventricular Amputation of Zebrafish Heart," *Ann. Biomed. Eng.*, vol. 37, no. 5, pp. 890–901, 2009.

[30] X. Zhang, T. Beebe, Y. Liu, J. Park, T. Hsiai, and Y. Tai, "Wearable Flexible Micro Electrode for Adult Zebrafish Long Term ECGmonitoring," *IEEE Int. Conf. Micro Electro Mech. Syst.*, pp. 690–693, 2015.

[31] M. Martínez-Porchas, L. R. Martínez-Córdova, and R. Ramos-Enriquez, "Cortisol and Glucose: Reliable indicators of fish stress?," *Panam. J. Aquat. Sci.*, vol. 4, no. 2, pp. 158–178, 2009.

[32] R. L. Oswald, "The use of telemetry to study light synchronization with feeding and gill ventilation rates in Salmo trutta," *J. Fish Biol.*, vol. 13, pp. 729–739,

1978.

[33] S. C. Rogers and A. H. Weatherley, “The use of opercular muscle electromyograms as an indicator of the metabolic costs of fish activity in rainbow trout, Salmo gairdneri Richardson, as determined by radiotelemetry,” *J. Fish Biol.*, vol. 23, pp. 535–547, 1983.

[34] P. R. De Almeida, T. J. Pereira, B. R. Quintella, A. Gronningsaeter, M. J. Costa, and J. L. Costa, “Testing a 3-axis accelerometer acoustic transmitter (AccelTag) on the Lusitanian toadfish,” *J. Exp. Mar. Bio. Ecol.*, vol. 449, pp. 230–238, 2013.

[35] F. Broell, T. Noda, S. Wright, P. Domenici, J. F. Steffensen, J.-P. Auclair, and C. T. Taggart, “Accelerometer tags: detecting and identifying activities in fish and the effect of sampling frequency,” *J. Exp. Biol.*, vol. 216, pp. 1255–1264, 2013.

[36] E. B. Thorstad, A. H. Rikardsen, A. Alp, and F. Økland, “The Use of Electronic Tags in Fish Research – An Overview of Fish Telemetry Methods,” *Turkish J. Fish. Aquat. Sci.*, vol. 13, pp. 881–896, 2013.

[37] K. Finkenzeller, *RFID Handbook: Fundamentals and Applications in Contactless Smart Cards, Radio Frequency Identification and Near-Field Communication*, Third. Wiley, 2010.

[38] M. A. El Khaddar, M. Boulmalf, H. Harroud, and M. Elkoutbi, “RFID Middleware Design and Architecture,” in *Designing and Deploying RFID Applications*, C. Turcu, Ed. InTech, 2011, pp. 305–326.

[39] T. J. Zhi, Z. Ibrahim, and H. Aris, “Effective and Efficient Attendance Tracking System Using Secret Code,” in *6th International Conference on Information Technology and Multimedia*, 2014, pp. 109–114.

[40] A. T. Mobashsher, M. T. Islam, and N. Misran, “RFID Technology: Perspectives and Technical Considerations of Microstrip Antennas for Multi-Band RFID Reader Operation,” in *Current Trends and Challenges in RFID*, C. Turcu, Ed. InTech, 2011, pp. 87–112.

[41] J. Wyatt, “PaLFI Range Extend.” Texas Instruments Inc., p. 19, 2010.

[42] “Series 2000 Reader System: High Performance Reader Frequency Module RI-RFM-007B – Reference Guide.” Texas Instruments Inc., p. 49, 2002.

[43] “Series 2000 Reader System: Control Modules RI-CTL-MB2B, RI-CTL-MB6B – Reference Guide.” Texas Instruments Inc., p. 40, 2008.

[44] A. Lozano-Nieto, *RFID Design Fundamentals and Applications*. CRC Press, 2011.

[45] “microID® 125 kHz RFID System Design Guide.” Microchip Technology Inc., p. 204, 2004.

[46] “Series 2000 LF Antenna Design Guide – Application Note.” Texas Instruments Inc., p. 38, 2003.

[47] V. Chawla and D. S. Ha, “An overview of passive RFID,” *IEEE Commun. Mag.*, vol. 45, no. 9, pp. 11–17, 2007.

[48] P. Sorrells, “Optimizing read range in RFID systems,” *Microchip Technol. Inc.*,

pp. 173–184, 2000.

[49] “HDX Technology.” Texas Instruments Inc., p. 3, 2013.

[50] “RFID FAQs.” Texas Instruments Inc., p. 6, 2013.

[51] D. Ciudad, P. C. Arribas, P. Sanchez, and C. Aroca, “RFID in Metal Environments: An Overview on Low (LF) and Ultra-Low (ULF) Frequency Systems,” in *Radio Frequency Identification Fundamentals and Applications*, InTech, 2010, pp. 182–196.

[52] “Antenna – Reference Guide.” Texas Instruments Inc., p. 38, 1996.

[53] S. Kawdungta, C. Phongcharoenpanich, and D. Torrungrueng, “Novel Design of Double Loop Antennas by Using a Shifted Gate for the LF-RFID System.” p. 4, 2007.

[54] C. Mansap, P. Wounchoum, C. Phongcharoenpanich, and D. Torrungrueng, “Trapezoidal Dual Loop Antenna for Radio Frequency Identification (RFID) System at Low Frequency,” in *ECTI International Conference*, 2007, p. 4.

[55] G. Benelli and A. Pozzebon, “RFID Under Water : Technical Issues and Applications,” in *Radio Frequency Identification from System to Applications*, InTech, 2013, pp. 379–396.

[56] “eZ430-TMS37157 Development Tool – User’s Guide.” Texas Instruments Inc., p. 47, 2010.

[57] “Mixed Signal Microcontroller – MSP430F2274-EP Datasheet.” Texas Instruments Inc., p. 80, 2011.

[58] “Passive Low Frequency Interface Device with EEPROM and 134.2 kHz Transponder Interface – TMS37157 Datasheet.” Texas Instruments Inc., p. 49, 2009.

[59] “Controller Entry Device with Integrated DST80 Authentication, EEPROM, and LF Immobilizer Interface – TMS37F158 Datasheet.” Texas Instruments Inc., p. 8, 2012.

[60] “Series 2000 Antennas – RI-ANT-G01E, RI-ANT-G02E, RI-ANT-S01C, RI-ANT-S02C Datasheet.” Texas Instruments Inc., p. 7, 2013.

[61] A. Frantzke, “A Low-Power Battery-Less Wireless Temperature and Humidity Sensor for the TI PaLFI Device – Application Report.” Texas Instruments Inc., p. 21, 2011.

[62] S. Recknagel, “Communicating With the RFID Base Station – Application Report.” Texas Instruments Inc., p. 6, 2011.

[63] “MSP Debuggers – User’s Guide.” Texas Instruments Inc., p. 51, 2015.

[64] “Installation Guide.” Oregon RFID Inc., p. 39, 2009.